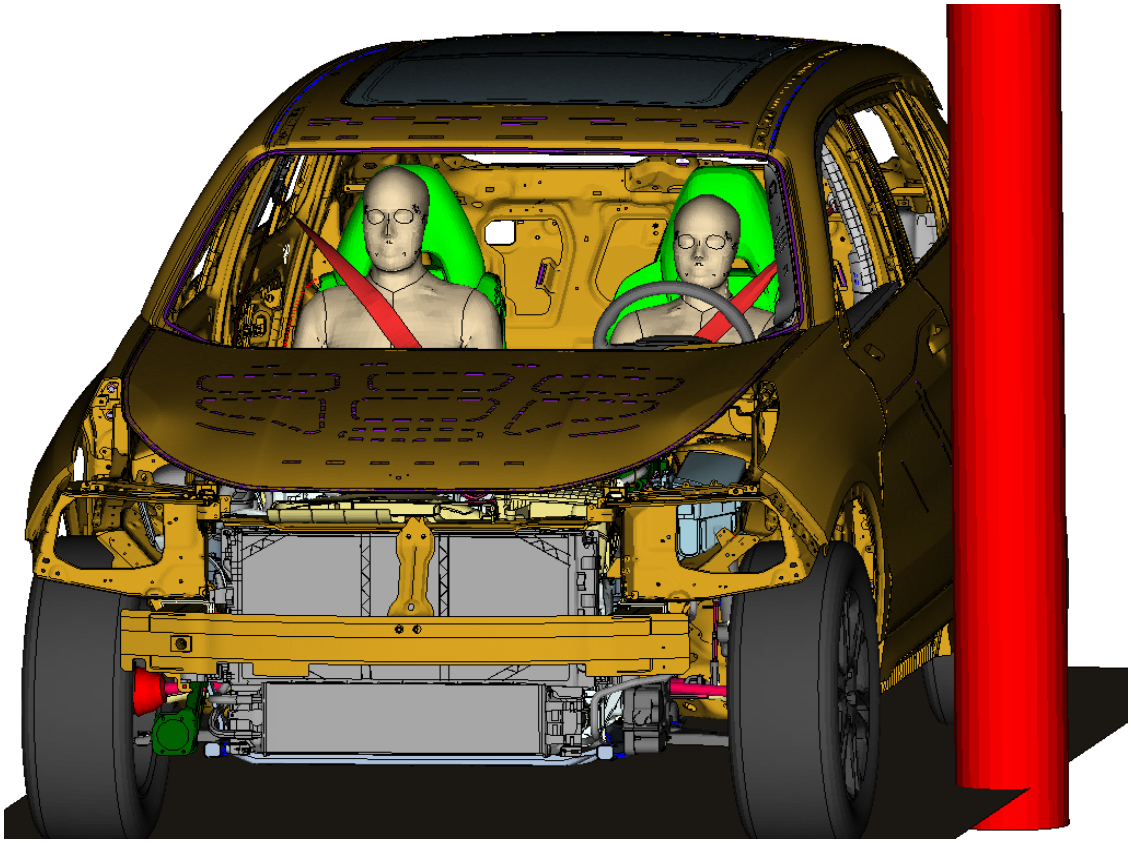

The human body model VIVA+ in far-side collisions

A validation and evaluation study of HBM usage

Master's thesis in Applied Mechanics

Lucas Johansson Sundblad

Philip Wassenius

DEPARTMENT OF MECHANICS AND MARITIME SCIENCES

CHALMERS UNIVERSITY OF TECHNOLOGY

Gothenburg, Sweden 2022

www.chalmers.se

Master's thesis in Applied Mechanics, 2022

The human body model VIVA+ in far-side collisions

A validation and evaluation study of HBM usage

Lucas Johansson Sundblad
Philip Wassenius

CHALMERS
UNIVERSITY OF TECHNOLOGY

Department of Mechanics and Maritime Sciences
Division of Vehicle Safety
Chalmers University of Technology
Gothenburg, Sweden 2022

The human body model VIVA+ in far-side collisions
A validation and evaluation study of HBM usage
Lucas Johansson Sundblad
Philip Wassenius

Supervisor: Dag Thuvesen, CEVT
Examiner: Johan Iraeus, Division of Vehicle Safety, Chalmers University

Master's Thesis 2022:23
Department of Mechanics and Maritime Sciences
Division of Vehicle Safety
Chalmers University of Technology
SE-412 96 Gothenburg
Telephone +46 31 772 1000

Cover: Female VIVA+ HBM driver and male VIVA+ HBM passenger in a Lynk & Co 01 far-side collision setup.

Typeset in LaTeX
Printed by Chalmers Reproservice
Gothenburg, Sweden 2022

The human body model VIVA+ in far-side collisions
A validation and evaluation study of HBM usage
Lucas Johansson Sundblad
Philip Wassenius
Department of Mechanics and Maritime Sciences
Chalmers University of Technology

Abstract

Crash dummies have been used for many years to evaluate occupant safety. However, with more advanced computers, virtual human body models are becoming increasingly useful. With this as a background, this project aims to validate the male VIVA+ model, perform identical simulations using a female version of the VIVA+ human body model and subsequently compare these results with the male model. Then, the male VIVA+ model is compared with the WorldSID model in a virtual car environment. Lastly, the VIVA+ model was used to identify if sex dependant behaviour could be observed in a fully modelled car.

In order to validate the male VIVA+ model, it was positioned in a generic sled rig which is modelled to replicate the physical sled rig used in a previous study from which the real-world data has also been fetched. When using the VIVA+ model in a safety evaluation, two VIVA+ human body models were placed in a far-side collision setup of a Lynk & Co 01. The human body models' responses were compared with the responses of two WorldSID models used in the same setup, retrieved from an analysis made at CEVT. Additionally some comparisons between the human body models themselves, placed in a Lynk & Co 01, were performed.

A conclusion was drawn that the male VIVA+ model was able to predict the kinematics of a Post Mortem Human Subject in the generic sled rig. The average and median kinematic CORA scores were 0.64 and 0.63, respectively, which is indicating a fair but close to good correlation. In the generic sled simulations, it was disclosed that the simulations had problems with that the seat belt slipped off the occupants' shoulder to a larger extent than what the experiments showed. It also was concluded that the male and female VIVA+ models have similar kinematic responses in a far-side collision where the lowest average kinematic CORA score in a configuration was 0.73.

Regarding the evaluation simulations, it was possible to see a resemblance between the male VIVA+ model and the WorldSID model. When comparing the upper body kinematics, Head Injury Criterion values and head acceleration curves between the models, similarities could be seen. Finally, it was concluded that the injuries of the occupants were dependent on their sex. The female VIVA+ model behaved differently compared to the male VIVA+ model when positioned in the driver seat, resulting in lesser injuries for the female model.

Keywords: VIVA+, Human Body Model, Far-side Collision, CORA, Validation, Virtual Testing, WorldSID.

Acknowledgements

This master's thesis has been conducted during the spring of 2022 within the division of Vehicle Safety at the department of Mechanics and Maritime Sciences at Chalmers University of Technology, in collaboration with China Euro Vehicle Technology, CEVT.

Firstly, we would like to express our greatest gratitude towards our supervisor Dag Thuvesen, Team lead CAE Safety at CEVT. He gave us the opportunity to write this master's thesis at CEVT and has provided us support and help throughout the entire project. We would also like to thank our co-supervisor and examiner Johan Iraeus, researcher at the division of Vehicle Safety, who has supported us with his knowledge within bio-mechanics and thereby has given us guidance on how to proceed with the project.

Secondly, we would like to thank CEVT as an organisation, for providing us with a workplace and necessary resources to carry out the project. Furthermore, we want to express our gratitude for the support from the knowledgeable colleagues at CEVT we have received when having encountered problems related to our simulations: Henrik Sundberg, Kim Olander, Peter Appelgren and Henrik Nilsson.

Thirdly we would like to thank Liselotte Rydqvist at Autoliv who provided us with valuable knowledge and clarifications about both previously performed HBM studies and inputs regarding CORA rating.

Lastly, we would like to thank the VIVA+ team for having faith in this master's thesis and allowing us to use the VIVA+ human body model in our simulations. We would also like to acknowledge the THUMS User Community 2 Project, TUC 2 project, for having created the FE model of the validation rig and made it available to use.

Lucas Johansson Sundblad
Philip Wassenius
Gothenburg, July 2022

Contents

List of Acronyms

The acronyms that have been used throughout this thesis are listed below in alphabetical order.

AIS	Abbreviated Injury Scale
CFL	Courant–Friedrichs–Lewy
Euro NCAP	European New Car Assessment Programme
EV	Electric Vehicle
FE	Finite Element
FEM	Finite Element Method
FSAB	Far-Side Airbag
HBM	Human Body Model
HIC_{15}	Head Injury Criterion (impact during maximum of 15 milliseconds)
HIC_{36}	Head Injury Criterion (impact during maximum of 36 milliseconds)
MDB	Mobile Deformable Barrier
MPP	Massively Parallel Processing
PDE	Partial Differential Equation
PMHS	Post Mortem Human Subjects
PSIS	Posterior Superior Iliac Spine
WorldSID-50M	Worldwide Harmonized Side Impact Dummy 50 Percentile Male

List of Figures

List of Tables

1

Introduction

The automotive industry is undoubtedly one of the largest manufacturing industries in the world. This is particularly noticeable today with the increasing production of electric vehicles, EVs [1], [2]. The EVs have innovative technologies which will replace or erase the existing internal combustion engines used today. The main reason for this is that big structural changes are made, such as e.g. fitting a battery into a car, creating new opportunities and posing new challenges for the car manufacturers.

One of the most important areas to investigate during the development of new vehicles is safety, which is seen as a key area since it cannot be neglected. Driving a vehicle is the everyday life for many people, for example when going to work, leaving the children at school, or going grocery shopping. Hence, a lot of time is spent on the road, time when occupants want to feel safe.

1.1 Background

Today the safety of occupants in a vehicle is evaluated with the use of physical crash dummies. The dummies are available in various sizes and represent different human beings, such as a large man, an average man, and a small woman etc. The dummies have accelerometers, force gauges and displacement sensors at specific positions to measure these quantities [3]. The acceleration data have boundaries for what is deemed to be safe, and therefore have limits for what is acceptable [4]. In parallel to these physical dummies, there also exist Finite Element models, FE-models, of the different dummies. The virtual dummies are used by the automotive industry to evaluate the safety of their vehicles virtually instead of physically, which saves them both time and money.

With an increase in computer performance, the possibilities of virtual testing are increasing. In the beginning of the 2000's a new type of FE-model was released [5]. These new models are known as Human Body Models, HBMs. They are not intended to represent a physical crash dummy, instead it is representing an actual human of a specific size, for example a 50th percentile male. Some advantages of using an HBM instead of a dummy is that the HBMs do not have the design constraint of the crash tests dummies, where the dummies have to be robust and not break. Further,

the biofidelity is much more advanced in an HBM, which means that injuries may be evaluated more accurately, though this requires a validated FE-model. Another useful property of the HBM is that it is omni-directional. This means that it can take up loads and have biofidelic kinematics in any direction, whereas the dummies are designed for special load cases only e.g. frontal impacts or side impacts.

The European New Car Assessment Program, Euro NCAP, is an organisation which evaluates the safety of new cars. Today Euro NCAP only use physical tests in the evaluation of car safety characteristics. The crash tests that are used in the evaluation of the adult's safety can be divided into three bigger areas, frontal, lateral and rear impacts [6]. All these tests are set up in a real environment with either the whole car or a part of it. Today, no virtual testing is included in the evaluation of the occupant's safety. However, there are some indications that HBMs will be introduced in the future to evaluate injuries of occupants [7].

1.2 Unprioritised Areas in Safety Testing

There are several types of crash testing done when evaluating the safety of vehicles. Some of the common ones are frontal impacts, rear impacts, and lateral impacts where the latter have focused on near-sided collisions, i.e. a collision where the oncoming object or vehicle is colliding with the side where the occupant is stationed. It is only in recent years, that one has started to be more interested in far-side collisions, i.e. the impact appears on the opposite side of the occupant position, when assessing the safety of vehicles, see figure 1.1 for a visual explanation of far-side. It has been shown that a large proportion, 35%, of injuries on occupants sustained in side impacts are of far-side nature [8].

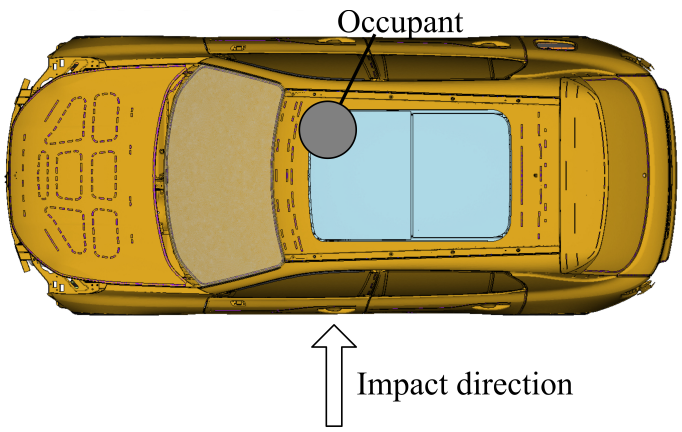

Figure 1.1: Visual explanation of a far-side collision

The HBM that is used in this thesis is the open-source VIVA+ [9]. This model can take the form of both a 50th percentile male and a 50th percentile female. The VIVA+ model has been validated in other crash scenarios but has yet to be validated in a far-side collision. An average female HBM is a new implementation in

the HBM field. In fact, there have not been many investigations on crash scenarios where the occupants are female. The main reason for this is the lack of will of using females in safety testing [10]. Another reason is that experimental data is not easily obtained since these are collected from Post Mortem Human Subjects, PMHS, i.e. human cadavers, where females are a minority [11]. Extensive PMHS tests are needed during validation processes and are thus both time-consuming and quite cumbersome to perform, not to mention the ethical part of performing such tests.

1.3 Purpose

The first purpose of this study was to validate the VIVA+ HBM representing an average male occupant to published PMHS responses in far side collisions [12]. The validation is essential since otherwise the results from simulations using the VIVA+ HBMs cannot be trusted. The second purpose was to compare the kinematics of the average female VIVA+ HBM to the average male VIVA+ HBM in the far side load case. The third purpose was to evaluate the two VIVA+ HBMs in a production vehicle model, and to compare the kinematic and injury risk results to results based on traditional crash test dummies.

1.4 Research Questions

From the recently stated purpose the following research questions are established which intends to clarify the purpose of the thesis. The first two are connected to the validation phase while the last two are clarifying the purpose of the evaluation phase.

- How similar are the kinematics of the male VIVA+ model compared to the cadavers in the PMHS study [12]?
- How does the female VIVA+ HBM relate kinematically to the male VIVA+ HBM?
- Is the response of the male VIVA+ model similar to the response of the World-wide Harmonized Side Impact Dummy 50 Percentile Male, WorldSID-50M, in a simulation environment of a far-side crash?
- Do the injury risks of the occupants depend on the sex?

1.5 Scope

This thesis was limited in time to 20 weeks which required simplifications and limitations of the work, see the list below.

- During the validation, only far-side collisions using 60° oblique impacts and 90° pure lateral impacts, measured from the front of the setup, were investigated.

- From the 36 experiment setups used in [12], only 12 were used during the validation in this project.
- Only used predefined models.
- Did not investigate all combinations of sex of the occupants in the evaluation phase.
- Was only altering one parameter of the fully modelled car's safety equipment.
- Was only investigating one position of occupants in the evaluation.

1.6 Thesis Outline

The thesis starts with a small overview of some important literature connected to this thesis, followed by an introduction to important theories which has been used throughout the project. When all basic knowledge has been established the methodology is described. The method chapter is divided into a validation section and an evaluation section for which different methods have been needed to be used. Thereafter, the results are connected to the different phases presented in form of snapshots from the simulations together with 2D plots and tables. The results are then discussed in the following chapter and the findings are at last summarised in the conclusion chapter at the end.

2

Theory

In the following chapter, a brief literature study is presented where the report that composed the experimental data is summarised. Additionally two validation studies performed on other HBMs are introduced. Further, some of the most important theories used in this thesis are presented and explained.

2.1 Literature Study

To consider the VIVA+ HBM as valid the kinematics must be similar to the kinematics of a human, i.e. mimic the movements of a human body relatively well. The real-world data in this thesis is represented by the PMHS study [12]. The PMHS that were used in the study were six different men of varying stature and had ages ranging from 44 to 70. These test subjects were placed in the seat of a simple sled setup and had their exact position recorded with respect to some points of the sled. An acceleration pulse was then applied to the system to replicate a collision. There were four different types of pulses used in the study in total, a high and low severity pulse applied 60° and 90° from the front of the sled setup.

A total of 36 different tests were conducted where the following parameters were changed: Pulse severity, pulse direction, belt angle, belt pretensioning, and adding a plate to block the movement of the pelvis. One thing worth noting is that some tests kept the same configuration regarding the sled and only changed the PMHS used [12]. Sensors were placed on the PMHS and seat belt to measure the accelerations and forces. In parallel to the sensors the tests were recorded via VICON, a tracking system to capture the kinematics of the PMHS.

The PMHS study mentioned above has been used before to validate the kinematics of two other human body models, one using the THUMS HBM and one using the SAFER HBM [8], [13]. The study with the THUMS model was beyond validating the HBM also looking into the benefits of using an airbag between the seats. However, this part was evaluated using a WorldSID-50M dummy. The study performed on the SAFER HBM was also evaluating the use of a far-side airbag but with an HBM instead of a dummy.

In both studies with the THUMS and the SAFER HBM, only 12 of the total 36 tests from the PMHS study were used to create six different configurations. The HBMs were placed into these configurations in an attempt to validate the respective model. Each of the six configurations was defined by a specific setup and was used for one or more tests but with different PMHS. For the setups, a pre-developed model with some modifications was used. The difference between the original model and the one used in the HBM studies was mainly the seat belt, where an own developed belt model created at Autoliv was used.

To validate the HBMs, 20 different quantities were used. These were the X-, Y- and Z-movements of the head, T1 vertebra, left and right acromion and pelvis. From these were also the lateral lean and torso twist quantities calculated. The belt forces were measured at three different locations, above the shoulder, above the belt buckle and lastly at the seat belt's anchoring point to the sled [8]. For all these 20 quantities, corridors were created out of the data captured by the PMHS. From the corridors, CORA scores were calculated to get a measurable value on how well the HBMs captured the behaviours of the PMHS.

In both of Pipkorn's papers it was concluded that both HBMs assessed in the different studies were valid [8], [13]. He did point out that there were some configurations that did not capture the kinematics completely. One source of error that Pipkorn brings up is that the belt slips off the shoulder in the simulations while this was not the case for the PMHS [13]. Furthermore, Pipkorn is a bit sceptical about the tape which held the head, arms, and legs into place. Forman, who conducted the physical tests, implies that the tape will break at such a low load since it was nicked and would not affect the kinematics of the PMHS [12]. Pipkorn however, is reluctant to this [13].

2.2 Far-Side Safety Evaluation

In the background 1.1, it was mentioned that Euro NCAP performs several different tests when evaluating a car's safety. During Euro NCAP's far-side evaluation, two different tests are used. In one test, a mobile deformable barrier, MDB, impacts the car purely lateral, i.e. 90° measured from the car's front. In the other test a 75° oblique impact is performed where the car crashes into a rigid pole [4]. In both tests, the occupant's safety is evaluated using a WorldSID-50M. With the WorldSID some relevant variables are checked and graded. Euro NCAP's rating is divided into three parts of the body: the head's acceleration, the force and moment in the neck and the deflection of the chest/abdomen. One last thing that influence the grade is the lateral displacement of the head [4].

2.3 Finite Element Method

The kinematics of a car crash can be described by partial differential equations, PDEs. These differential equations may be solved by using computers together with

the finite element method, FEM. The idea behind FEM is to discretise a continuous system or body into finitely small elements, which are assigned certain material properties. These elements may have applied loads on them, which come in different forms, e.g. stresses or temperatures. The combination of geometry, material and loading of an element can in an equation then describe the element's response which for an example may be a displacement.

2.3.1 Implicit and Explicit Time Integration

The solution process of FE problems can be divided into two groups, implicit and explicit solutions, where the two methods are desirable for different kinds of problems. If a problem is of a static or quasi-static nature the implicit method is favourable, mainly because of its unconditionally stable time steps. This means that large time steps, and therefore fewer steps to find the solution, can be used and are not limited by the model as it is for the explicit solution. These time steps can however, become highly computationally expensive when solving large non-linear and dynamic problems due to costly matrix inversions [14]. Such problems are where the explicit method is the preferred solution strategy, and a car crash is very much a dynamic problem. Therefore, an explicit method is used in this thesis.

The explicit method makes it possible to calculate the next time step directly since it purely builds upon known quantities. Contrary to the implicit method where also a later state is included in the equations that need to be solved, which also means additional calculations [14]. For example, the equation of motion defined in equation 2.1 can describe the response of a mechanical system which depends on the state variable $\boldsymbol{x}$. Depending on if the implicit or explicit solution method is used, the update of the state variable will be defined differently as seen in equation 2.2, where the implicit needs additional information.

$$\boldsymbol{M}\ddot{\boldsymbol{x}} + \boldsymbol{C}\dot{\boldsymbol{x}} + \boldsymbol{K}\boldsymbol{x} = \boldsymbol{f}(\boldsymbol{t}) \tag{2.1}$$

$$\begin{aligned} \boldsymbol{x}_{known} &= \{\ddot{\boldsymbol{x}}^n, \dot{\boldsymbol{x}}^n, \boldsymbol{x}^n, \ddot{\boldsymbol{x}}^{n-1}, \dot{\boldsymbol{x}}^{n-1}, ...\} \\ \text{Explicit} : \boldsymbol{x}^{n+1} &= f(\boldsymbol{x}_{known}) \\ \text{Implicit} : x^{n+1} &= f(\boldsymbol{x}_{known}, \ddot{\boldsymbol{x}}^{n+1}, \dot{\boldsymbol{x}}^{n+1}) \end{aligned} \tag{2.2}$$

However, the advantage of the explicit method regarding updating the state variable comes at a cost. Unlike the implicit method, the time steps are not unconditionally stable. They are bound by the Courant–Friedrichs–Lewy, CFL, condition. This condition is shown in equation 2.3 and shows how the size of the time steps are limited by element dimensions and material properties [15], [16].

$$\Delta t_{min} = \frac{l}{c} \qquad c = \sqrt{\frac{E(1-\nu)}{(1+\nu)(1-2\nu)\rho}} \tag{2.3}$$

Where l is the element length and c represent wave propagation velocity in 3D-continuum of that element. In short, the condition involves that no information should propagate through more than one element during one time step. To summarise, the implicit solutions may use few but costly time steps which are unconditionally stable while the explicit ones require many small cheap time steps due to the CFL condition.

2.3.2 Mass Scaling

An intuitive way to make a simulation run faster is to increase the size of the time steps used. However, this simple idea is constrained by the CFL condition mentioned above, where the time step size is limited by an element's size and material properties. By increasing the density ρ in equation 2.3 one can then achieve larger critical time steps Δt_{min} which are stable, this is known as mass scaling. When altering the density of an element one also affects the inertia properties of the model. Therefore, one must be careful in simulations where inertia effects are non-negligible i.e. dynamic systems. Too much mass scaling can influence the response of the system. It is therefore common practice to allow a maximum of 5% increase of added mass, preferably in each part, in dynamic systems [17], [18].

2.3.3 Hourglass Energy

A material routine is used to find the material response of each element in a system. This material routine uses the integration points of the elements when evaluating the responses, one time for each integration point [19]. When using a single integration point it is placed in the middle of an element, while if several integration points were to be used, they are evenly distributed within the element. The advantage of using just one integration point is that the material routine just have to be solved once for each element and thereby requires less computational time. However, if just one integration point is used the zero-energy mode must be regulated by the hourglass energy control. The zero-energy is created by the hourglass control algorithm which prevents the element to deform inaccurately. This might happen if just one integration point is used since then it is possible to deform the element without creating any strains within the element, see figure 2.1 for a visual explanation of how this might occur [20].

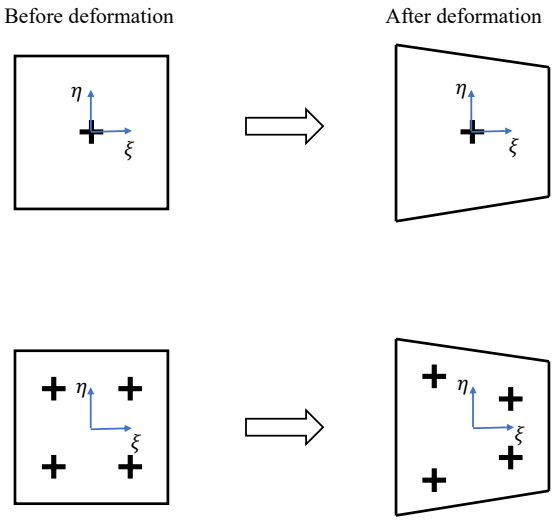

Figure 2.1: 2D elements before and after deformation with either one or four integration points. The top right element will not register any strain because the single integration point's position has not changed. While the lower right element has had its integration points moved and will therefore experience strain

The hourglass energy should not exceed more than 10 %, preferably on part level, of the total energy in the system [21], which is hard for very soft materials that deform easily. If this is the case the number of integration points must increase, to obtain a so-called fully integrated element, though such elements will "crash" after rather small strains. In this thesis the limit is checked by the ratio, hourglass energy divided by total energy, also known as hourglass ratio in this report.

2.3.4 Energy Balance

When checking if FE simulations are accurate or not, the energy balance often is checked. According to the first law of thermodynamics, energy cannot be created nor destroyed. Therefore, the initial potential energy that is available can be transformed into for example kinetic energy [22]. The energy balance can be controlled with the ratio, total energy divided by initial energy and external work, defined in this thesis as the energy balance ratio. Ideally, this ratio should be equal to one. However, a margin of 5 % is within what is assumed to be negligible [21]. Another thing to investigate is any sudden changes in the total energy level. If there are sudden changes, there probably is some energy that is lost or created in a non-physical order.

2.4 Human Body Models

An HBM's purpose is to model a human being as close to reality as possible. To do this, the right geometry and material properties need to be used to get an accurate representation. Thus, this requires extensive testing, simulation, and validation

work. The female version is the baseline model from which the male version is a derivative. This is achieved by morphing node positions and changing a sex parameter which controls other parameters [23].

The three major differences,in addition to overall geometry, between the male and the female VIVA+ HBMs are the head mass and its inertia properties, the density of soft tissues and the length of a couple of larger muscles and ligaments. The first two differences are used to match the mass of the models. The length of the ligaments in the knees are changed to have the unstretched ligament length as close to reality as possible. The same procedure has been done for the quadriceps muscle as well [23].

The VIVA+ model has various levels of detail at different parts of the body. The inside of the head is not modelled. Instead, there are six different discrete mass elements added to give the head its correct head mass and inertia. The stomach is not detailed, there are no internal organs in the model. It has just been given an overall density and stiffness to mimic the the organs. However, much of the skeletal parts such as the ribs and spine of the VIVA+ model are modelled in detail.

2.5 Injury Theory

To evaluate the injuries caused by a collision it is necessary to have the correct properties of each material in the body. The material properties of a human are not constant and vary between different individuals. However, the VIVA+ model is, as of today, only available with one set of material properties, and represent an average 50-year-old human [24]. The age of the model is of particular interest since the density and the ductility of the bones are decreasing throughout the life of a human. In a study, it was shown that the Young's modulus of the bone has its peak between the years 25-30 and then it starts to decrease [25]. One additional important property of the bone is the maximum strain. This is also dependent on the age [26]. In figure 2.2 the risk of rib fracture is plotted as a function of true strain [26].

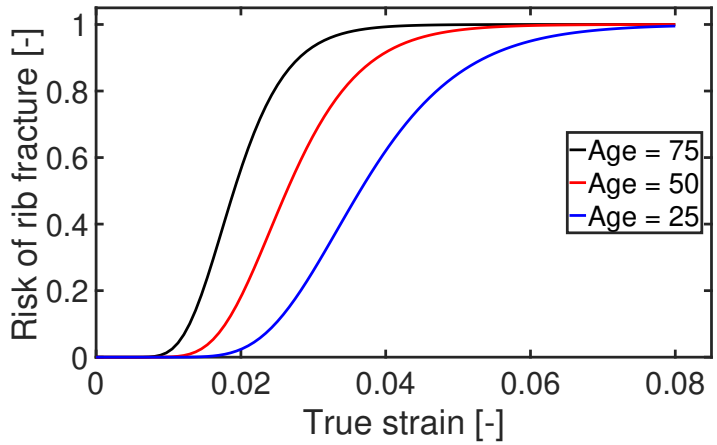

Figure 2.2: The relation between true strain and risk for rib fracture for humans of age 25, 50 and 75 [26]

As seen in the figure, a fracture is definite at 0.04 true strain for a 75-year-old human, while it is definite at 0.055 for a 50-year-old and almost at 0.075 for a 25-year-old. There are in total 24 ribs in a human body, and in a car crash they are often at risk for fracture. Therefore, it is important to find the risk of fracture for each rib. This can be obtained by reading the strain in each rib and then use figure 2.2 to evaluate the risk.

Since there are only two outcomes of a fracture risk i.e. either the rib will break, or it will not. A binomial distribution can be used to evaluate the total number of rib fractures. However, the risk is not the same for each rib and therefore a Poisson binomial distribution must be used to evaluate the total number of fractures. The difference between Poisson binomial and ordinary binomial distribution is the fact that the probability for each outcome can vary from trial to trial [27]. Using this distribution, the probability that two or more fractures will occur, can be calculated. This can then easily be translated to the Abbreviated Injury Scale, AIS, which is used to get an objective and comparable value of injuries [28]. This is given on a scale from 1 to 5 which is describing how severely injured the victim is. For the case of chest wall injuries, which is looked at in this thesis, AIS2+ is translated into two or more rib fractures [28].

One additional quantity commonly investigated in car crashes is head acceleration. The head acceleration is evaluated through Head Injury Criterion, HIC, values. The HIC value is calculated as an integral of the head acceleration during maximum 15 ms or 36 ms resulting in HIC_{15} respectively HIC_{36}, see equation 2.4 where d represents the period over which the HIC value is captured [29].

$$HIC = d\left(\frac{1}{d}\int_{t}^{t+d} a(\tau)\,d\tau\right)^{2.5} \tag{2.4}$$

The limit for when a car gets zero points in the HIC evaluation by Euro NCAP is

drawn at a HIC_{15} value over 700. For maximum points, a HIC_{15} value less than 500 is required [4].

2.6 Correlation Analysis

An objective and quantitative way of comparing time-history data curves with each other is to use the Correlation and Analysis, CORA, method. This method measures similarities between at least two different data signals, often an experimental data signal and a simulation data signal, which calculates a score between 0 and 1 where 1 signifies a perfect match. The total CORA rating consists of two sub-metrics, a cross-correlation rating and a corridor rating. The cross correlation rating compares the phase, size, and shape of the two signals. The corridor rating computes the differences between the two signals with respect to an established data corridor. The corridor data consists of an "inner" and "outer" limit. The signal gets a rating of 0 if it stays outside the outer corridor, and it gets a 1 if it is located inside the inner corridor. If a line is in between these corridors the rating gets interpolated between 0 and 1. Each rating from the cross correlation and corridor method then gets weighted and summed up into the total CORA rating which is a comparable quantity, figure 2.3.

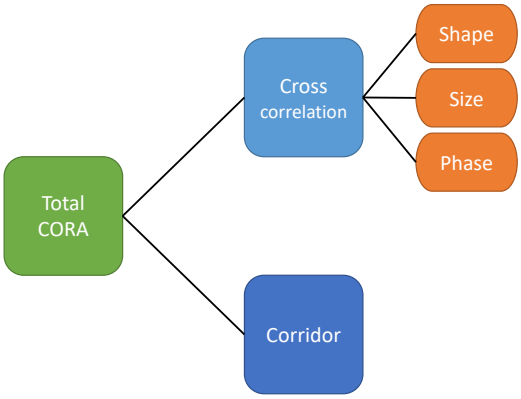

Figure 2.3: Overview of the components in the total CORA rating

In the SAFER HBM study, it was assumed that a good CORA rating for an HBM is 0.65 or above [13]. This is based on the ISO/TR 9790 standard which defines lateral impact response requirements on crash dummies to assess biofidelity. The standard uses a scale of 0 to 10, where 10 is excellent biofidelity [30]. The different levels of biofidelity can be seen in table 2.1. The biofidelity levels are easily translated into the CORA rating scale which ranges from 0 to 1 as stated above.

Table 2.1: The different limits of biofidelity defined in ISO/TR 9790 [30]

Excellent	$8.6 \leq Rating < 10.0$
Good	$6.5 \leq Rating < 8.6$
Fair	$4.4 \leq Rating < 6.5$
Marginal	$2.6 \leq Rating < 4.4$
Unacceptable	$0.0 \leq Rating < 2.6$

2.7 The Function of a Seat Belt

A 3-point seat belt consists of a fabric or webbing whose task is to enclose the occupant in the seat in the event of an accident. The belt starts in a fixed anchoring point where it is connected to the vehicle, then travels over the lap of the occupant and passes through the belt buckle located by the centre console. From there it spans diagonally over the chest of the occupant and goes through the D-ring which is positioned a bit above the shoulder. Finally, the belt makes its way down into a coil which can retract or feed out the belt when released or pulled, thus making it possible to fit occupants of different sizes. The coil also includes important safety features such as a retractor and a pretensioner. The retractor is sensitive to speed which will lock the webbing if it is pulled too hard but let loose if the force is released. In the event of a collision the pretensioner will pull the belt, and thereby reduce the slack in the seat belt, in order to collide with the airbag in a correct way and reduce the relative velocity between the occupant and the vehicle. The belt webbing will then be locked until a load limiter is activated, to reduce the risk of damaging the occupant [31].

3

Methods

In this chapter, the general workflow and approach, i.e. how some of the theories stated in the previous chapter were implemented, is presented to the reader. Simulation models and different configurations of these are also defined here. The pre- and post-processing suite from BETA CAE Systems, ANSA v22.0.2 and META v22.0.2 respectively, were used for both the validation and the evaluation simulations. The FE simulations were conducted using LS-Dyna R9.3.1 MPP.

3.1 HBM Validation in Sled Environment

The VIVA+ models were placed in six different configurations of the generic sled rig from the PMHS study [12]. They followed the same name and setup convention seen in the study of the THUMS HBM [8]. All six configurations were used with both a male and a female version of the VIVA+ model. The setups are summarised in table 3.1. Two things can be pointed out. Firstly, in the last two configurations the impact direction is completely lateral, C5 at low severity and C6 at high severity. Secondly, the first three configurations together with the last all have the same D-ring position.

Table 3.1: Set up of the different configurations. Configuration numbering follows the one used in Pipkorn's 2018 study [8]

	C1	**C2**	**C3**	**C4**	**C5**	**C6**
ΔV [km/h]	34	16	16	16	16	34
Impact direction [°]	60	60	60	60	90	90
D-ring position	Middle	Middle	Middle	Back	Forward	Middle
Pretensioning	Yes	No	Yes	Yes	Yes	Yes
Pelvis blocked	No	No	No	Yes	No	No
PMHS ID	591 602	591 602 608	591 602 608	587	551 559	559
Test ID	S0124 S0135	S0122 S0133 S0136	S0123 S0134 S0137	S0129	S0083 S0088	S0091
Simulation time [ms]	550					

3.1.1 Modifications of the Test Rig

The test rig used during the validation was downloaded from THUMS USER COMMUNITY, TUC. The TUC is a project, which has the aim: "The aim of TUC is to setup of a framework and harmonise general and administrative requirements for the implementation of FE Human Body Models (HBMs) in vehicle and traffic safety applications. Therefore, the project partners work closely together to achieve these goals." [32]. It is an incomplete setup of the test, where a model of an occupant is missing and needs to be inserted [33]. Figure 3.1 shows the TUC setup together with the VIVA+ model. The coordinate system is defined by the SAE J211 [34], which implies that X is in the anterior direction, Y is defined as to the right of the occupant and Z is the downward direction.

In the model from TUC, a belt model was included which controlled the retractor and the pretensioner. The retractor was pulling the belt with 20 N to make the belt fit well to the occupant. The pretensioner pulled with a force of 2.5 kN, 10 ms after the pulse was applied to mimic the delay in a real car crash. The friction coefficient between the seat and the VIVA+ model as well as between the seat belt and the VIVA+ model was defined as 0.5, similar to previous studies [35], [36].

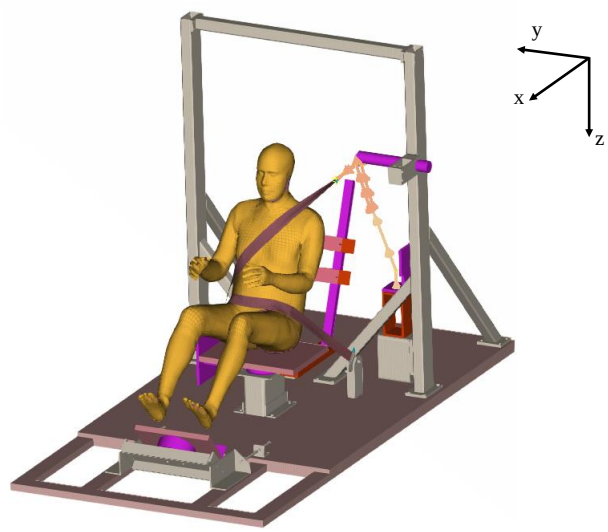

Figure 3.1: The sled setup used in the validation simulations. Notice how the coordinate system is oriented according J211 [34]

The defined configurations differ in both impact severity as well as the impact direction. Therefore, these parameters had to be able to be changed. However, in the test rig downloaded from TUC, only the 60° high severity pulse was included. The PMHS tests that was to be replicated used both 60° and 90° pulses of both high and low severity, 14 g respective 6.6 g. To obtain the lower magnitude the supplied pulse data was used and scaled with the factor $6.6/14 = 0.47$. In figure 3.2 the simulation pulse data is plotted together with the experimental pulse data retrieved from the PMHS study [12].

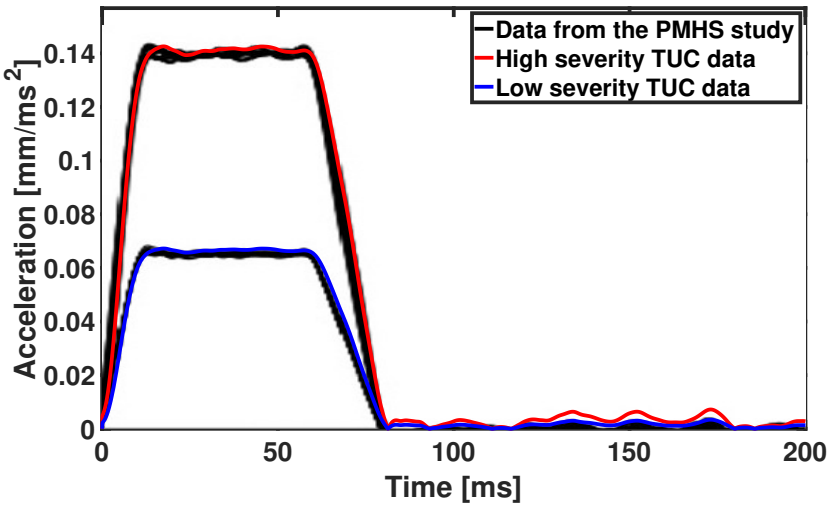

Figure 3.2: The supplied pulse data (High severity TUC data), together with a scaled load curve (Low severity TUC data) and the load curves from the experiments in the PMHS study [12]

As seen in the figure the pulse data retrieved from TUC match very well with the experimental data. The scaled curve is also close to the actual data from the experiment. Because of this, it was deemed accurate enough to be used in the low severity load cases. To change the load pulse from only acting in one direction the acceleration load curve was split into an X and a Y component by multiplying with either $\cos 60°$ or $\sin 60°$ respectively.

3.1.2 Positioning of the HBM

The six chosen load cases can be split up into three groups depending on the position of the D-ring. The first group covers configurations 1, 2, 3, and 6 which all had the D-ring in the "middle" position, called Configuration A. For configurations 4 and 5, the D-ring were in a "back" and "forward" position respectively, which defines the last two groups. The initial positions of the tests are reported in the PMHS study and for each group, a mean value and a standard deviation were calculated [12]. In table 3.2 the mean and the standard deviation for each group and measurement are presented.

All measurements were not considered equally important. The kinematics of the legs were hard to capture because of the differences between the virtual sled model and the physical test setup, where such as foam blocks and tape between the legs were omitted in the virtual model [13]. Therefore, the leg angles were assumed to be the least important. The belt angle is affected by the position of the D-ring. Therefore, a compensation had to be made on which parameter was to be prioritised. Because the belt angle has a direct impact on the interaction between the seat belt and the occupant it was seen as more important than the D-ring's exact position. Table 3.2 is ordered to have the measurements with the highest priority at the top of the table and the lowest priority at the bottom. The three in the top are though equally important since they directly affect the position of the VIVA+ HBM.

Table 3.2: Target positioning measurements. **St. dev. missing, used average St. dev. of Config A and 5. **St. dev. missing, used St. dev. of Config A*

	Config. A		**Config. 4**		**Config. 5**	
	Mean	**St. dev.**	**Mean**	**St. dev.**	**Mean**	**St. dev.**
Torso angle [°]	80	1	83	1*	78	1
Belt angle [°]	41	1	35	1*	45	1
H-pt. to seat edge [mm]	127	9	179	8*	184	7
D-ring to seat edge [mm]	515	7	700	7**	510	7**
D-ring lateral [mm]	299	5	307	6*	298	7
D-ring height [mm]	783	17	801	13*	765	8
Femur angle [°]	12	2	14	1	14	2
Tibia angle [°]	41	2	45	6	41	1

The goal was to have the same initial position of the VIVA+ HBM as the mean for each configuration, the criterion for when it was assumed to be good enough

was within one standard deviation of the PMHS positions for both the female and the male version. Note in table 3.2 that for Configuration 4 the standard deviation was inherited as the mean of Configuration A and 5 since there is only one test that defined Configuration 4. The same goes for the D-ring to seat edge value in Configuration 5 where the two tests had the exact same value and therefore would have given a standard deviation of zero. A reason why an exact position was not possible to achieve is that the VIVA+ model and the PMHS are not of the same sizes, see appendix A for a comparison between age, height, and weight between the two VIVA+ models and the cadavers used in the PMHS study [12].

As of today, spring 2022, the VIVA+ model is not supported by ANSA's *Human Body Model Articulation* tool which allows manipulation of the model joints in order to position it. Therefore, all movements of the HBM's body parts were done by using the manikin method. Where discrete spring elements pulls a node of the VIVA+ HBM to a desired location and then the associated nodes and elements will follow.

There are two different approaches when doing this positioning with springs. Either simulate the positioning of the HBM and then use the coordinates from the final state as the initial position in the main simulation, or extend the simulation and do the positioning in the same simulation as where the pulse will be applied. The first approach would lead to that the elements would have a new position, but the elements would have no strains which is not completely accurate and might therefore affect the result. Therefore, the second approach was used where the positioning and applying load case is done in one simulation. This would make the entire simulation span over 550 ms, 350 ms of positioning and 200 ms of the main simulation where the pulse is applied.

Depending on which of the configurations it was aimed to mimic the HBM was moved using these discrete spring elements or rotated around the X-, Y- or Z-axis as a rigid body. The foot plate and the D-ring were also moved to the correct position in order to match the values of table 3.2 above. For Configuration 5 and 6, the upper backrest was rotated and the radius of its edge increased since it was creating contact problems in the model. The contact problem was caused by a node on the back of the HBM got stuck in the sharp edge of the backrest.

3.1.3 Defining the Quantities of Interest

To validate the male VIVA+ model against the real-world data, corridor data was used to define a range which is used in the CORA method, as described in chapter 2.6. The actual calculation of each sub-metric and total score was done using the software CORA v3.6.1 [37], which used the settings seen in appendix B. The corridor data used in this thesis for the male validation was gathered from Pipkorn's paper from 2021 which used the mean and standard deviation from the PMHS data to create the corridors [13]. The male VIVA+ HBM was compared to the PMHS for the measured quantities presented in table 3.3. The same quantities, see table 3.3, were also used to compare the female version of the VIVA+ HBM with the male

version. Also for this comparison, the CORA method described in 2.6 was used and calculated in the software CORA v3.6.1 [37]. One difference to the male versus PMHS comparison is that the corridor was not the same. Instead, the corridors were calculated automatically by the CORA software using the male VIVA+ HBM response.

Table 3.3: The different quantities of interest that was used to validate the male VIVA+ HBM

	Component		
Head [mm]	X	Y	Z
Pelvis [mm]	X	Y	Z
T1 [mm]	X	Y	Z
Left acromion [mm]	X	Y	Z
Right acromion [mm]	X	Y	Z
Belt forces [N]	Shoulder	Lap	Side
Thorax [°]	Lateral lean	Torso twist	-

The Torso twist is defined as the difference in forward translation between the left and right acromion. The Lateral lean is defined as the difference between the translation in the Y-direction of the pelvis and T1. One thing to point out is that the pelvis quantity is a virtual point located in the middle of the left and right Posterior Superior Iliac Spine, PSIS. All these positions of the body are visualised in figure 3.3.

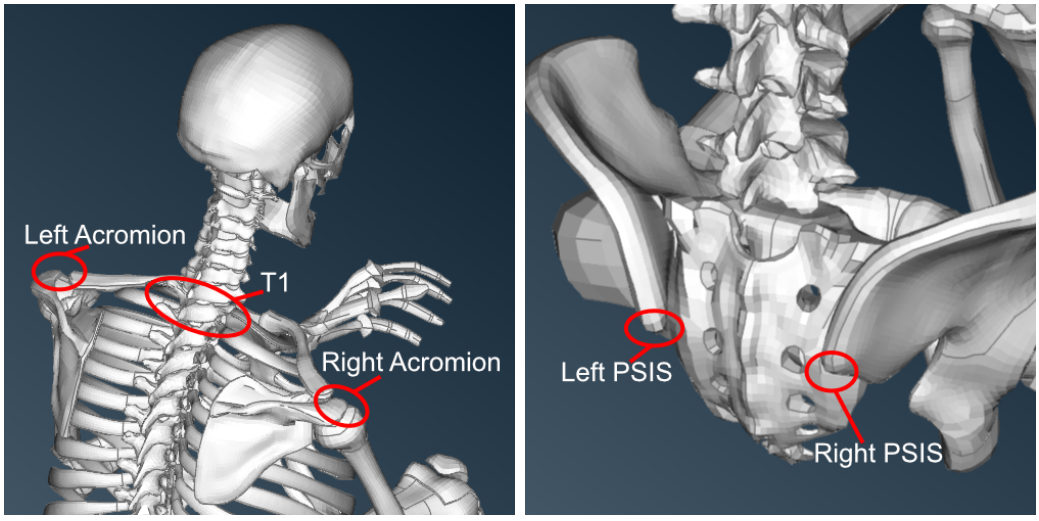

Figure 3.3: Visual clarification of acromion, T1 and PSIS points

The belt forces were captured at three separate locations, above the shoulder (Shoulder), above the belt buckle (Lap) and at the anchor of the belt (Side), see figure 3.4.

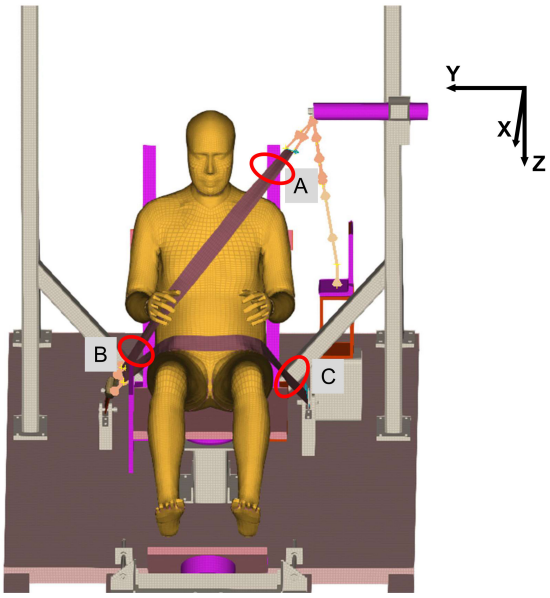

Figure 3.4: The positions where the belt forces were captured. A, B and C represent above shoulder, above belt buckle and anchor of the belt, respectively

3.2 HBM Evaluation in Full Vehicle Environment

For the second part of the project the VIVA+ model was placed in a fully modelled car and not in the generic sled which was used during the validation. The setup that was used had previously contained WorldSID models, which for this study were replaced by VIVA+ models.

In a previous analysis performed at CEVT the fully modelled car, of model Lynk & Co 01, was given an initial velocity of 32 km/h applied in 75° from the driving direction, see figure 3.5. This created a far-side collision for the passenger and a near-side collision for the driver.

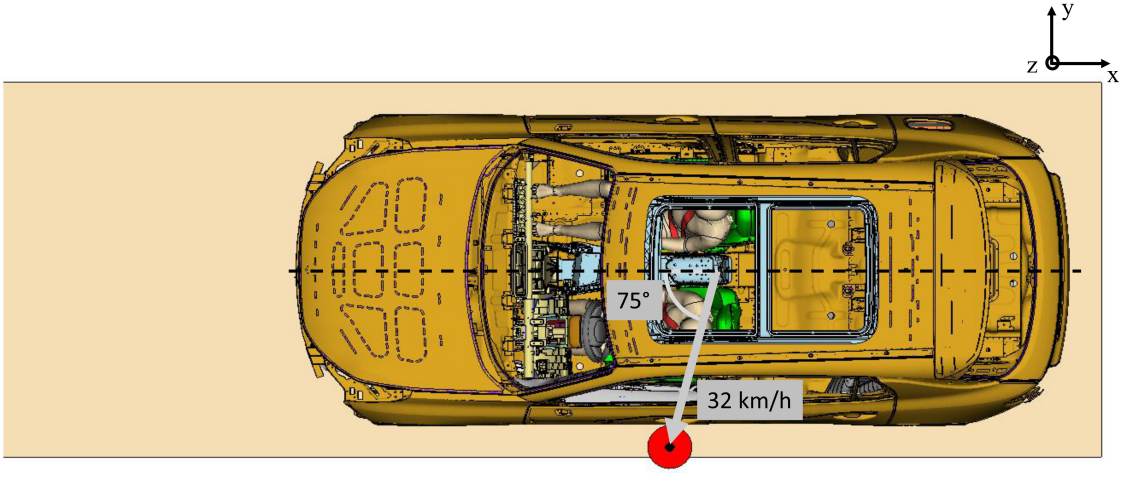

Figure 3.5: Visualisation of the load case applied in the evaluation simulations

3.2.1 The Configurations' Setup

The positions of the HBM models were aimed to visually match the positions of the WorldSIDs from the analysis performed at CEVT. No extremities were moved during the positioning, contrary to the sled setups. The whole HBM was imported in a seated position and was only moved into the seat by translation and rotation of the whole model. The VIVA+ models were placed in their initial position directly using so-called "null shells". These null shells are exact copies of the outer geometry on the occupant models which "instantly" are pushed down into the foam of the seat and create a force equilibrium between the occupant and seat to avoid clipping problems. The null shells are deactivated, i.e. all contacts are removed after 4 ms and the HBMs take their place instead. Whereas the total evaluation simulation spans over 150 ms.

In total, six different evaluation simulations were run. These were divided into two groups. Group 1 contained three simulations where only the occupants were switched from WorldSIDs into VIVA+ HBMs. These simulations are defined as: male driver and passenger, female driver and male passenger, male driver and female passenger. The occupant setup of Group 2 was the same as for Group 1. Instead, a modified FSAB was used, where the pressure inside the airbag was lowered by 25%. An overview of these simulations is presented in table 3.4 below. An E is added to the names of the configurations to avoid confusion with the setups defined in the validation phase.

Table 3.4: An overview of the different setups for the evaluation configurations

	Group 1			**Group 2**		
Config	C1-E	C2-E	C3-E	C4-E	C5-E	C6-E
Driver	Male	Female	Male	Male	Female	Male
Passenger	Male	Male	Female	Male	Male	Female
Airbag pressure [% of original]	100	100	100	75	75	75
Simulation time [ms]	150					

3.2.2 Specifying the Quantities of Interest

For each simulation, the HIC_{15}-values and the maximum principal strain in each rib were extracted, as well as the largest minimum distance between the heads of the occupants. The HIC-values were compared to the criterion in Euro NCAP's test procedure [4]. The maximum first principal strains in each rib were used to evaluate the risk of an AIS2+ injury using the method described in chapter 2.5. The Poisson Binomial distribution was calculated using Comprehensive R Archive Network, CRAN, which is a compiler for the programming language R commonly used in statistics [38]. To get the probability density function the predefined function *dpoibin* was used. From this function the probability of zero and one rib fracture

was subtracted from one, i.e. 100%, to obtain the risk of two or more fractures. The minimum head-to-head distances, hereby also known as Head2Head distance, were obtained using the post-processor META's tool *iHistory Part2Part*, which plots the minimum distance between two parts during the entire simulation. Additionally to these measurable quantities, the kinematic of the HBMs, such as the upper body movements, were also evaluated visually to see if the HBMs behaved differently depending on the sex of the occupants or the airbag pressure.

4

Results

This chapter will present a comparison between the kinematics of PMHS and the VIVA+ models from the generic sled simulations. There will also be results from the fully modelled vehicle presenting injury predictions on the VIVA+ model as well as a comparison between the VIVA+ model and the WorldSID model.

4.1 HBM Validation in Sled Environment

In the following section results from the simulations with the generic test rig are presented. Before any result is presented the energies were checked to see that the simulations could be trusted.

4.1.1 The Energy Ratios

The energy ratios and the mass scaling were controlled to see that the simulations had worked as they should. There were no unexpected energy peaks or unreasonable amounts of mass scaling. In figure 4.1 the hourglass ratio is plotted next to the energy balance ratio for the male simulations. Due to that the energy balance ratio had two larger peaks, a closed-up variant was created to get a better estimate of the values close to one.

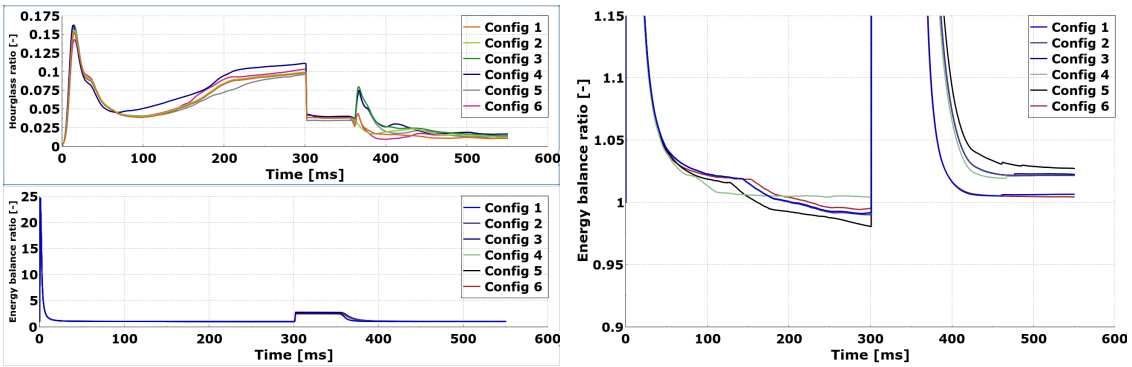

Figure 4.1: Hourglass ratio and energy balance ratio for the male validation simulations

The same procedure was done for the simulations with the female version of the VIVA+ model. However, since the energy balance ratios were similar between the two VIVA+ HBM versions the closed-up variant was moved to appendix C. The hourglass ratios were different and can be seen in figure 4.2 where the complete energy balance is also shown. The mass scaling was consistently around 0.05 % for all male configurations and approximately 0.07 % for all female configurations.

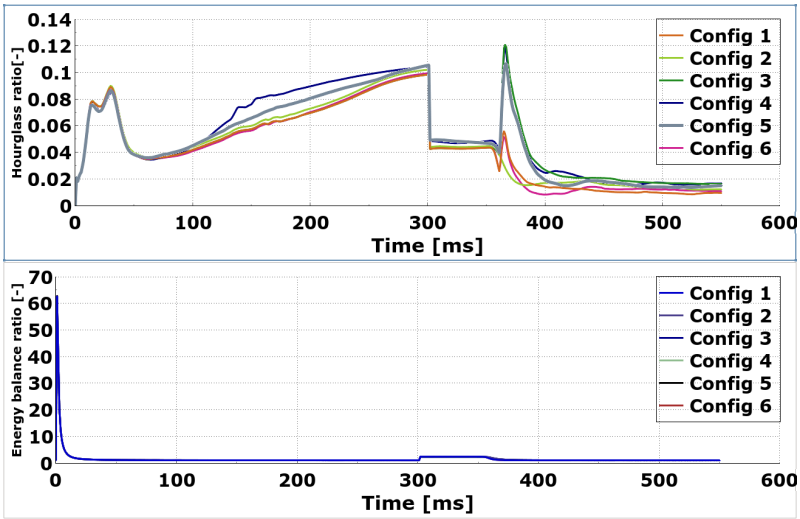

Figure 4.2: Hourglass ratio and energy balance ratio for the female sled simulations

4.1.2 The CORA Scores

The six configurations from the validation phase yielded data curves on the quantities defined in table 3.3 which made it possible to achieve the CORA scores. A detailed table containing all CORA scores for the male VIVA+ HBM can be seen in table 4.1. These values were used to calculate the average values seen in the bottom three rows. Where the Kinematics category is the average of all quantities except Belt Force Shoulder, Belt Force Side, and Belt Force Lap. The belt forces need to have high CORA scores in order to validate the male VIVA+ model. Since otherwise the belt forces will have a too large impact on the outcome, which makes it impossible to know if it is the VIVA+ model or the seat belt that is modelled inaccurately.

Table 4.1: All CORA scores for the male VIVA+ HBM

	C1	C2	C3	C4	C5	C6
Head X	0.68	0.94	0.87	0.41	0.76	0.87
Head Y	0.79	0.91	0.75	0.88	0.52	0.73
Head Z	0.52	0.50	0.61	0.80	0.61	0.54
Pelvis X	0.90	0.54	0.87	0.41	0.42	0.61
Pelvis Y	0.71	0.63	0.65	0.89	0.98	0.92
Pelvis Z	0.58	0.50	0.53	0.26	0.11	0.48
Belt Force Shoulder	0.76	0.85	0.87	0.80	0.77	0.85
Belt Force Side	0.96	0.84	0.95	0.74	0.87	0.99
Belt Force Lap	0.82	0.89	0.90	0.89	0.77	0.91
Left Acromion X	0.64	0.37	0.19	0.44	0.73	0.77
Left Acromion Y	0.73	0.93	0.82	0.82	0.42	0.63
Left Acromion Z	0.62	0.78	0.68	0.56	0.45	0.75
T1 X	0.89	0.60	0.41	0.47	0.55	0.69
T1 Y	0.89	0.95	0.79	0.76	0.42	0.61
T1 Z	0.58	0.82	0.55	0.54	0.34	0.73
Right Acromion X	0.68	0.64	0.88	0.70	0.53	0.58
Right Acromion Y	0.98	0.99	0.88	0.92	0.45	0.80
Right Acromion Z	0.56	0.38	0.42	0.57	0.20	0.68
Lateral Lean	0.58	0.84	0.71	0.94	0.45	0.61
Torso Twist	0.32	0.41	0.47	0.38	0.40	0.30
Average						
Belt forces	0.84	0.86	0.91	0.81	0.81	0.91
Kinematics	0.68	0.69	0.65	0.63	0.49	0.66
Total	0.71	0.71	0.69	0.66	0.54	0.7

The quantity that was best captured in total was the right acromion in Y-direction. All the configurations except the fifth configuration got a CORA score above 0.8. The fifth configuration had a poor accuracy but in figure 4.3 one can see that the shape of the curve is similar to corridor data albeit with an offset. The configuration that is capturing the right acromion best is configuration 2. In figure 4.3 it is possible to see that the curve is well within the corridor and has a similar shape. One important thing that should be highlighted here is that the data curves from the validation simulations are gathered during the interval 350 ms to 550 ms, i.e. the main simulation time, since the first 350 ms are purely a positioning phase and not of interest when calculating the CORA scores and comparing to the PMHS corridor data.

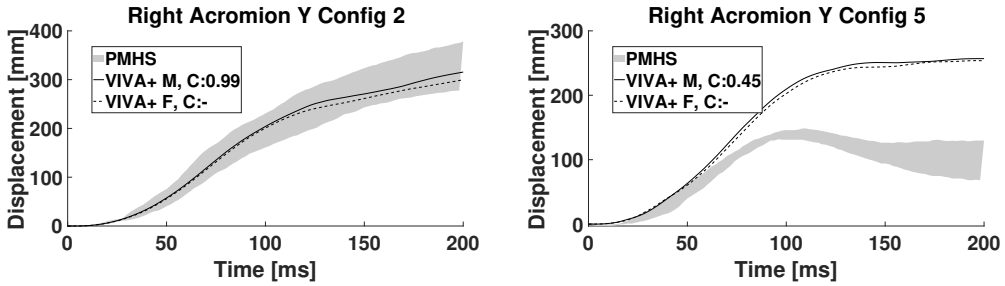

Figure 4.3: The right acromion's movement in Y-direction for the second and the fifth configuration. M = Male response, F = Female response

One more thing to point out from table 4.1 is that the accuracy for the torso twist is poor. In figure 4.4 the torso twist for the third and sixth configuration is shown, i.e. the best and the worst accuracy with respect to torso twist.

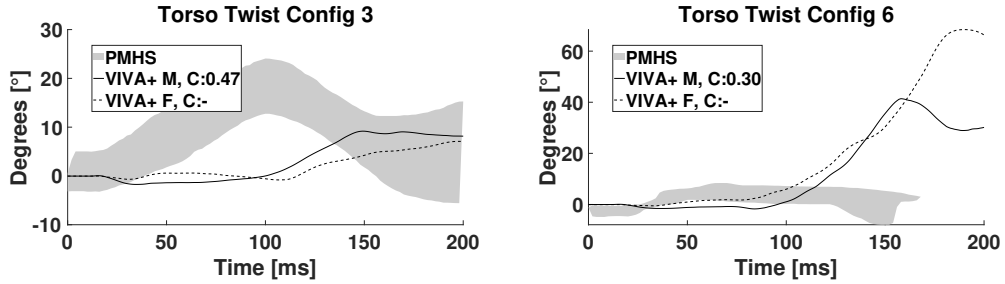

Figure 4.4: The torso twist for the third and the sixth configuration. M = Male response, F = Female response

An interesting observation could be made for the fifth configuration where the pelvis movements are similar to the corridor data in the Y-direction, while it is very poor accuracy for the X- and Z-movements of the pelvis. In figure 4.5 the pelvis movements in all directions are plotted.

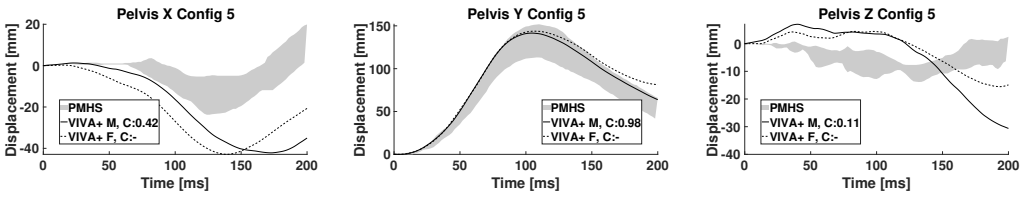

Figure 4.5: The pelvis movements for the fifth configuration. The movements in X- and Z-direction are captured poorly while the movement in Y-direction is accurate

As one can notice, the CORA scores for the female VIVA+ model are not disclosed in the figures 4.3, 4.4 and 4.5 above. This is since the female VIVA+ model would be

an inappropriate comparison to the PMHS test data which used cadavers of the male sex. Instead, it was of interest in this project to conduct a comparison between the male and female VIVA+ HBM, to see if there are any significant differences between the two sexes. In table 4.2 below, all CORA scores computed on the female versus male VIVA+ HBM are presented.

Table 4.2: All CORA scores for the female VIVA+ HBM

	C1	**C2**	**C3**	**C4**	**C5**	**C6**
Head X	0.85	0.96	0.93	0.78	0.26	0.75
Head Y	0.92	0.99	0.97	0.99	0.99	0.92
Head Z	0.98	0.96	0.98	0.98	0.89	0.92
Pelvis X	0.44	0.74	0.58	0.76	0.73	0.48
Pelvis Y	0.69	0.79	0.77	0.77	0.98	0.80
Pelvis Z	0.54	0.92	0.83	0.31	0.78	0.51
Belt Force Shoulder	0.88	0.86	0.87	0.83	0.85	0.91
Belt Force Side	0.80	0.86	0.83	0.86	0.83	0.82
Belt Force Lap	0.83	0.82	0.80	0.80	0.97	0.92
Left Acromion X	0.68	0.76	0.63	0.41	0.55	0.74
Left Acromion Y	0.94	0.99	0.93	0.98	0.99	0.91
Left Acromion Z	0.65	0.97	0.90	0.46	0.88	0.56
T1 X	0.89	0.88	0.85	0.75	0.51	0.82
T1 Y	0.90	0.99	0.95	0.99	0.99	0.90
T1 Z	0.99	0.91	0.83	0.77	0.42	0.97
Right Acromion X	0.93	0.92	0.57	0.63	0.49	0.74
Right Acromion Y	0.89	0.99	0.96	0.99	0.99	0.87
Right Acromion Z	0.99	0.82	0.72	0.77	0.77	0.92
Lateral Lean	0.85	0.98	0.92	0.99	0.99	0.69
Torso Twist	0.63	0.88	0.53	0.76	0.68	0.62
Average						
Belt forces	0.84	0.85	0.83	0.83	0.88	0.88
Kinematics	0.81	0.91	0.81	0.73	0.76	0.77
Total	0.81	0.90	0.82	0.78	0.78	0.79

From table 4.2 a couple of things can be noted. Firstly, the head movements in the Y- and Z-direction are captured very well. Where the lowest accuracy of these is the head's Z-movement for the fifth configuration with a CORA score of 0.89. The highest CORA score is found for the Y-movement of the head for configurations 2, 4 and 5 with a value of 0.99. In figure 4.6 the head's Z-movement for the fifth configuration as well as the head's Y-movement for the second configuration is plotted together with the automatically calculated corridor.

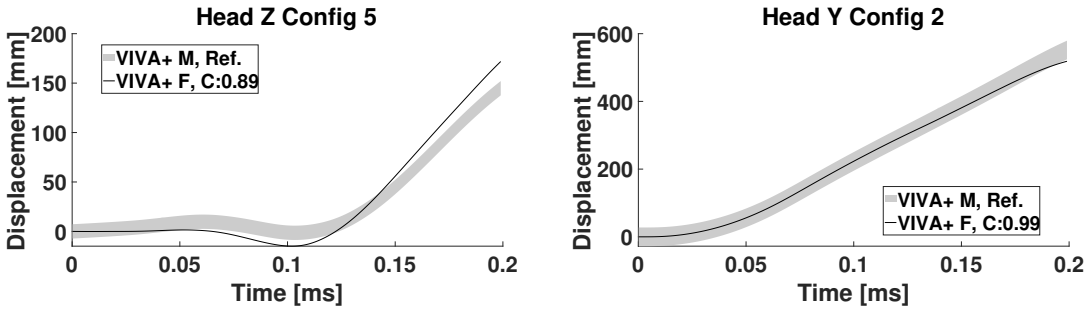

Figure 4.6: The worst and the best performing quantity in terms of CORA score found in the female sled simulations. Where the worst is seen to the left, Head Z Config 5, and the best to the right, Head Y Config 2

The pelvis movements are the quantities that are the least similar between the female and male VIVA+ HBMs. For the first configuration, the pelvis movements in X-direction achieve a score of 0.44 which implies that the correlation between the two versions is not optimal. From figure 4.7 can it be seen that the low CORA score comes from the difference in size, i.e. the female version has a smaller magnitude than the male version. However, from the phase and shape metrics, similarities can be spotted.

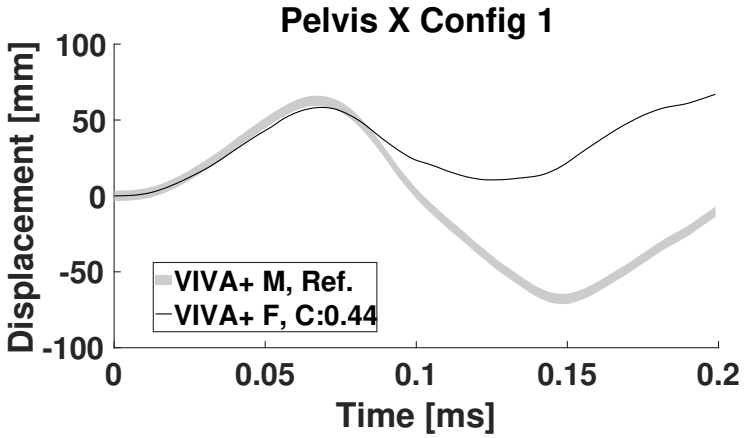

Figure 4.7: The female VIVA+ HBM correlation to the male VIVA+ HBM for the pelvis movements in X-direction

The total kinematic CORA scores for each configuration are indicating that the female and male version are similar since all kinematic CORA scores are above 0.73 and several of the configurations are even above 0.8. All the data curves corresponding to a CORA score, like figures 4.5 and 4.6, can be found in appendix D.

One thing all the configurations had in common was that the seat belt slipped off the shoulder and was only stopped when it was caught by the bend of the arm, no matter if a male or female VIVA+ HBM was used. In figure 4.8 an example of

this is shown, where two snapshots are taken from Configuration 1, one before the belt has slipped off the shoulder and one after. In appendix E all the other sled configurations, which show belt slip, are presented.

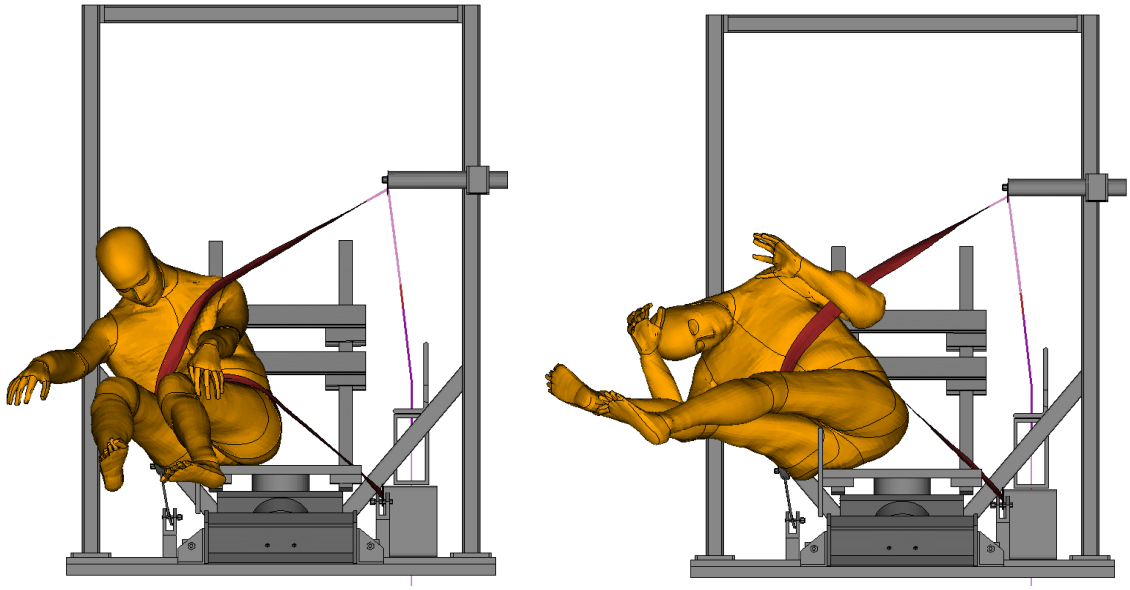

Figure 4.8: Snapshot of a male VIVA+ HBM in Configuration 1, just before and after the seat belt has slipped off. Taken at 100 ms and 150 ms respectively, after the pulse was applied

The forces in the belt for the first configuration can be seen in figure 4.9 below.

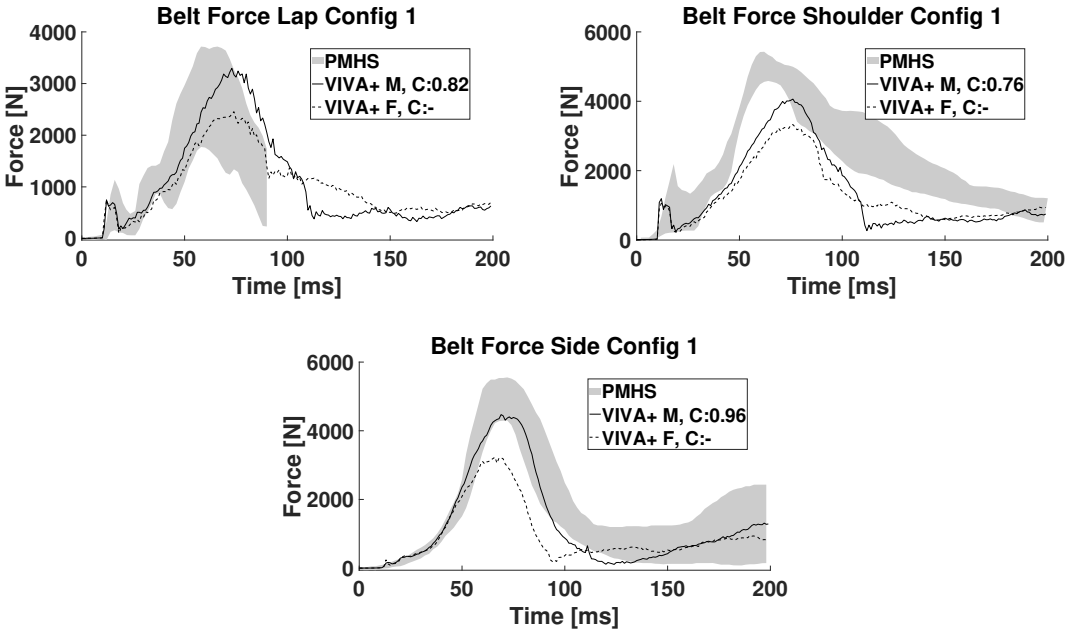

Figure 4.9: Belt forces from Configuration 1. Using a male VIVA+ HBM

From figure 4.9 and table 4.1 it can be determined that the CORA scores for the seat belt sections are indicating good correlation between simulation data and physical test data.

4.2 HBM Evaluation in Full Vehicle Environment

The evaluation section follows the validation structure where the energy ratios are examined to begin with to ensure credibility. This is then followed by presenting the values of the quantities of interest that was captured.

4.2.1 Energy Relations

In the same way as for the validation part, both the hourglass ratio as well as the energy balance ratios were plotted which can be seen in figure 4.10.

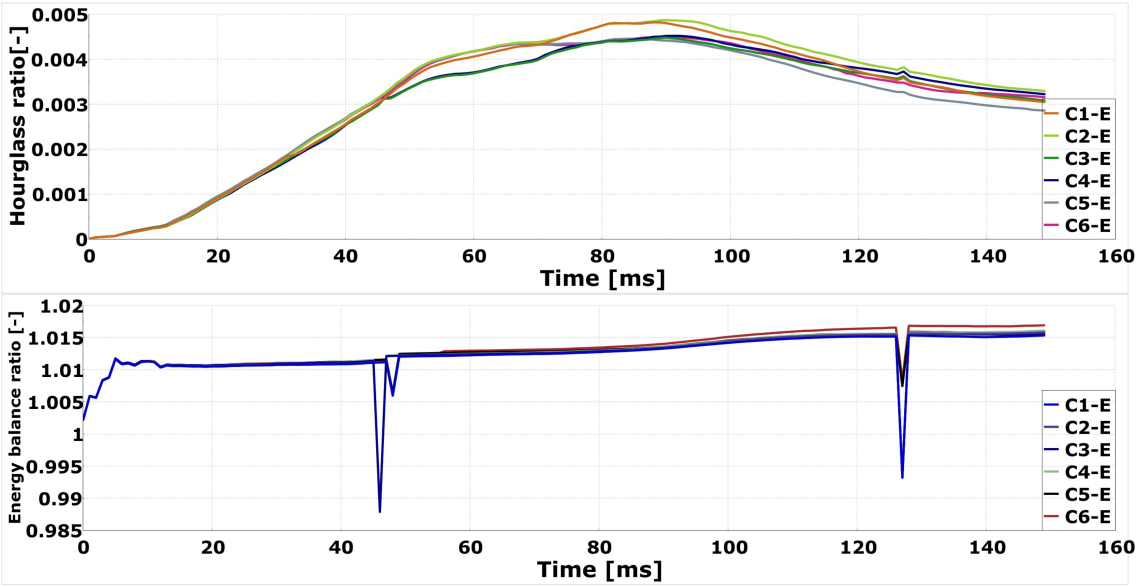

Figure 4.10: Hourglass ratio and energy balance ratio of the simulations in the evaluation phase

The distribution between the different curves for the hourglass ratio as well as for the energy balance ratio is narrow. The spread among mass scaling is also slim, the largest mass scaling is 2.31e-3 % and the smallest mass scaling is 2.28e-3 %.

4.2.2 Head Acceleration and Risk of Rib Fractures

The three quantities of interest, HIC_{15}, AIS2+ and Head2Head distance, of the evaluation simulations are presented in the following section. In figure 4.11 the quantities of interest are presented for the respective load cases with the two different airbag pressures.

In figure 4.11 the quantities of interest are presented for the respective load cases with the two different airbag pressures.

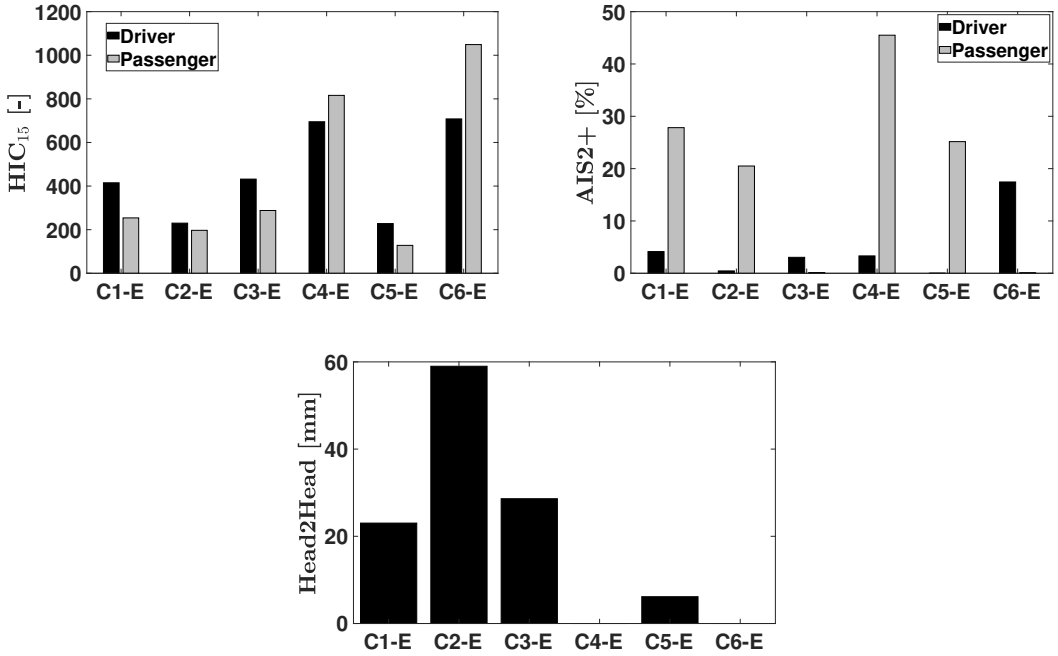

Figure 4.11: The evaluation configurations' values of HIC_{15}, risk for AIS2+ and Head2Head distance. The Head2Head distance of zero for C4-E and C6-E indicate a head collision

An example of the data curves that were used to calculate the HIC_{15} values can be seen in figure 4.12 which shows the magnitude of acceleration of the heads of the occupants as well as the HIC_{15} values in configuration C1-E. Note that the driver is the occupant that experiences the greatest acceleration value during the intrusion phase.

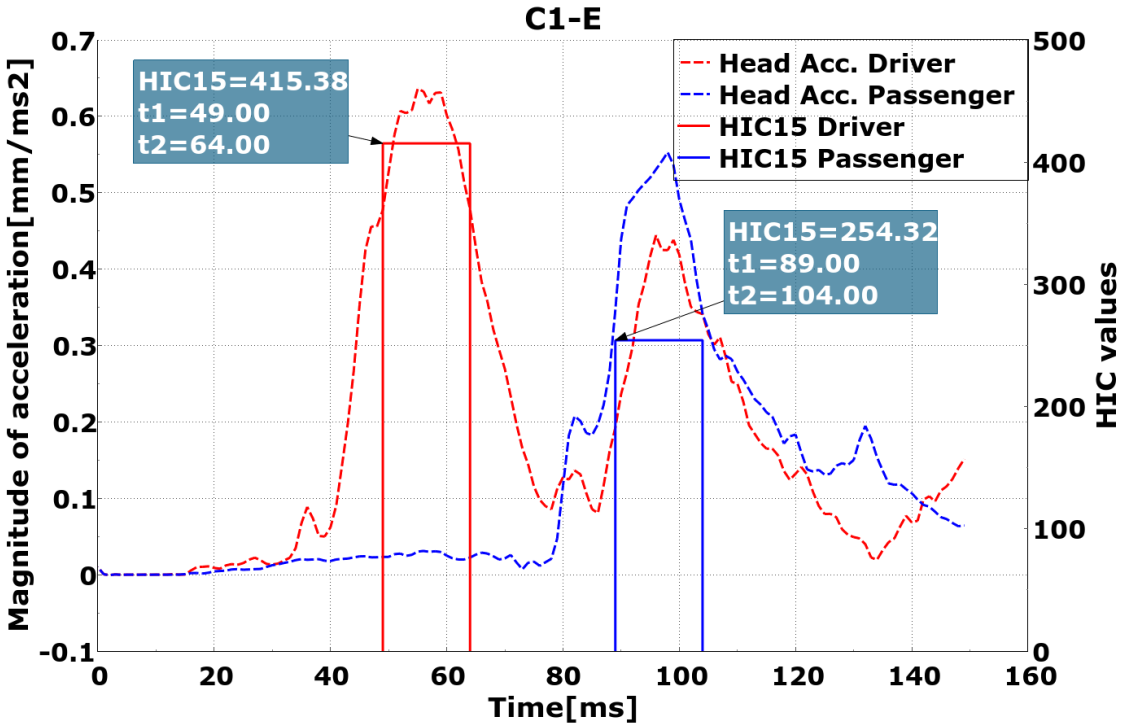

Figure 4.12: Head acceleration and HIC_{15} values of the occupants in configuration C1-E

In table 4.3 the quantities from the analysis made at CEVT using the WorldSID as occupants are displayed. CEVT's analysis did not present any quantities needed to calculate the AIS2+ probability, which is why it is missing in the table below.

Table 4.3: Comparable quantities from a WorldSID analysis performed at CEVT.

	WorldSID
HIC_{15} Driver [-]	330
HIC_{15} Passenger [-]	440
Min. dist. Head2Head [mm]	6

To get an idea of the shape, size and magnitude of the WorldSID models' head accelerations compared to the male VIVA+ HBMs one can examine figure 4.13. There one can see that the passenger dummy will experience the largest acceleration of the two occupants according to the WorldSID model, while the VIVA+ HBM show the opposite.

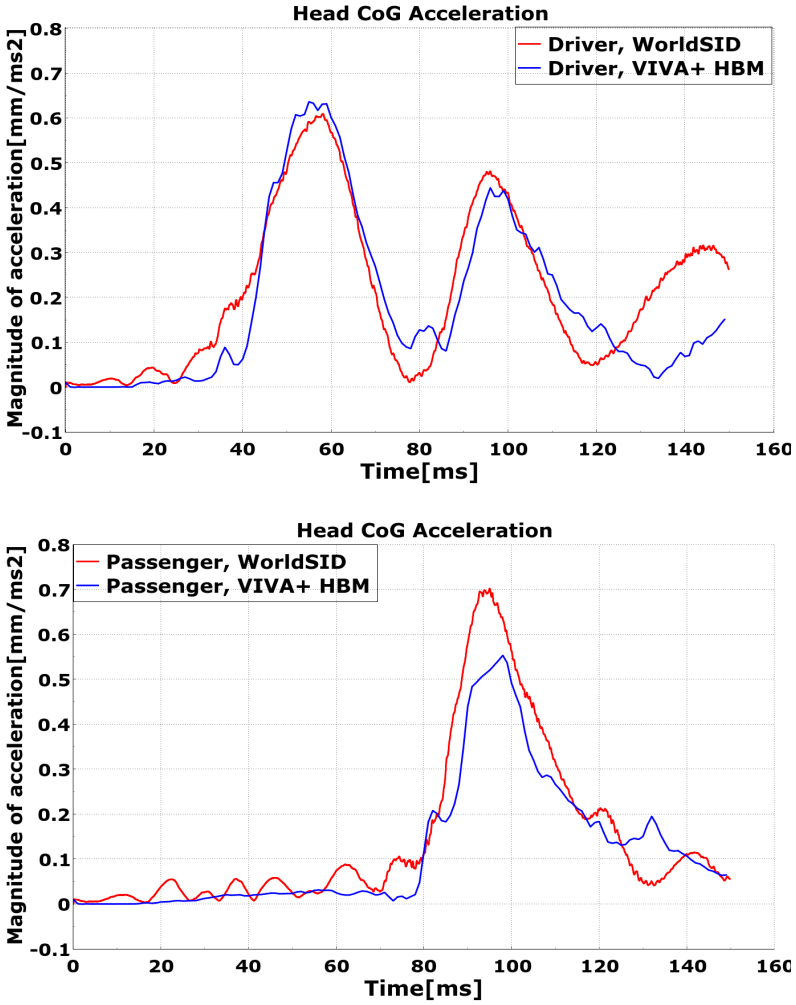

Figure 4.13: Head accelerations of male VIVA+ HBMs versus WorldSID models. Top plot shows the response of the male VIVA+ HBM versus the WorldSID model as driving occupants. Bottom plot shows the response of the male VIVA+ HBM versus the WorldSID model as passenger occupants.

4.2.3 The Occupants' Movements

In addition to the measurable quantities, some visual results were also investigated. From figure 4.11 above it is observable that the simulations predict head collisions in configurations C4-E and C6-E, which both have a lowered airbag pressure. One can also note that the last configuration using the lowered airbag pressure, C5-E, is very close to a collision compared to the unmodified airbags. In figure 4.14 below a snapshot of the head collision in configuration C4-E is shown, where the airbag is transparent to increase visibility.

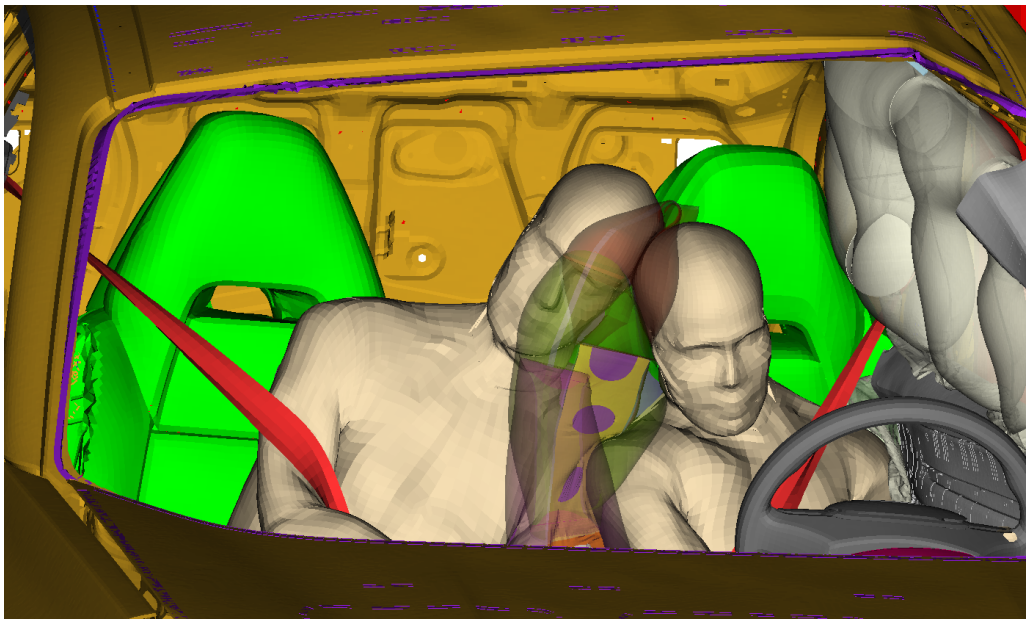

Figure 4.14: A snapshot at 102 ms of the Head2Head distance in configuration C4-E. Notice that there is a collision between the heads

Comparatively is the largest distance, which occur in C2-E, seen in figure 4.15. This distance is almost twice the length of the other unmodified airbag simulations.

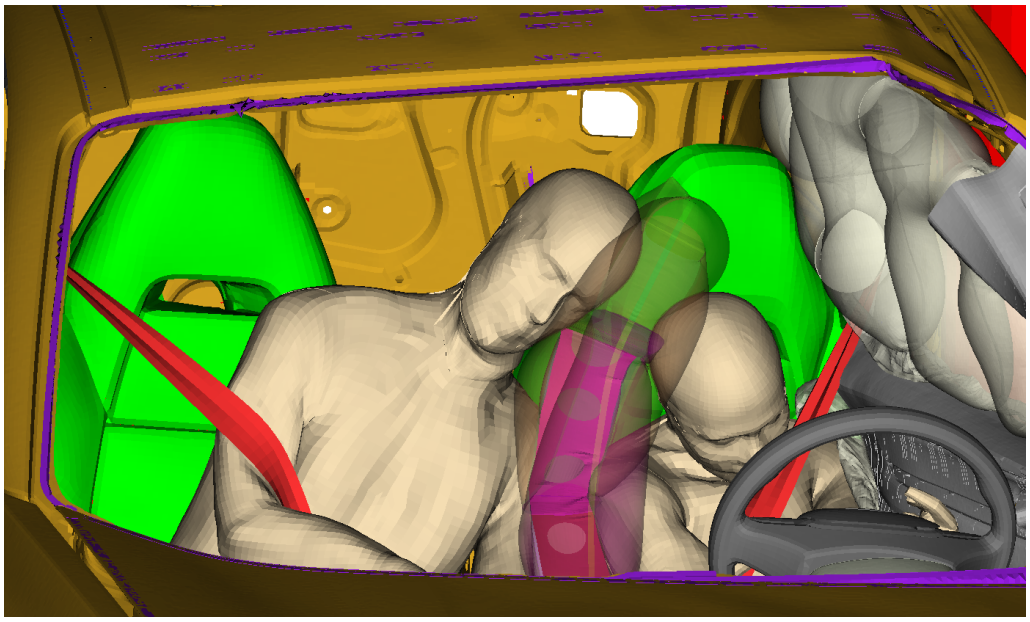

Figure 4.15: A snapshot at 107 ms of the Head2Head distance in configuration C2-E

The head acceleration curves from which the HIC_{15} has been calculated, all individual rib strain data and the rest of the snapshots showing the minimum Head2Head distance are included in appendices F, G and H, respectively.

5

Discussion

In this chapter, the results found in the previous chapter are analysed and discussed. Starting with the results obtained in the validation phase and ending by examining the results from the evaluation phase.

5.1 HBM Validation in Sled Environment

The following section discusses the energy ratios of the simulations in the validation phase, and then continues with analysing and discussing the belt slip. After that it ends with an explanation of the male VIVA+ HBM's movements with respect to the PMHS data, as well as a comparison between the female and male VIVA+ model.

5.1.1 The Simulations are Reliable

To begin with, one can start by asking if the simulation results can be relied on. This is done by looking to the energy plots seen in the results chapter. As found for both the female and the male simulations, the energies within the system are similar. The hourglass ratio for each male configuration have all similar shape and behaviour, and all curves manage to stay below the 10 % limit except for the start of the simulations and for Configuration 4 where the 10 % limit is breached between 200 and 300 ms. The first peak is caused by the large deformations of the soft tissue in the buttocks during the positioning. The hourglass energy decreases when the VIVA+ model settles in. The drop in the hourglass ratio is explained by that the pulse is applied and therefore the hourglass energy becomes a smaller part of the total energy. The second peak is caused by the deformation of the soft tissues around the breasts. Therefore, the second peak is higher for the female version than the male VIVA+ HBM. The female version is modelled with larger breasts of a material with low stiffness and therefore a larger part of the body is deformed due to the pretension of the seat belt.

The energy balance should ideally always be equal to one. However, one usually allows a difference of max 5% as stated in the chapter 2.3.4. This is almost always the case as seen in figure 4.1. The first peak can be explained due to the small total energy in the system, when the total energy is increased the minor differences

become more negligible. The second peak can be explained by that the discrete spring elements that position the HBM are removed at this time. The discrete spring elements builds up more negative energy the closer the end node is to the desired location. When this negative energy is removed the total energy is increased while the initial energy and external work remains constant which makes the ratio increase. When the pulse is applied at 350 ms the external work and total energy increase and thereby the energy difference caused by the discrete spring elements is negligible. The sled simulations were assumed to be okay, however, the energy balance ratio might not be the most useful method to investigate this. One reason for this is that a lot of energy is added to the system in the form of the acceleration pulse, as well as removing energy by deleting the discrete spring elements.

5.1.2 The Belt Slip Problem

All the validation simulations consistently had the seat belt slip off the shoulder. This was not the case for the physical tests in the PMHS study where most of the seat belts successfully retained the occupants [12]. This might be one of the reasons why the CORA score is not higher. For example, by examining figure 4.3 one can see how the PMHS corridor and the VIVA+ HBM follow each other until 50 ms. After this, the curve for the VIVA+ model continues to increase while the PMHS corridor starts to level out. Since the belt slips off the shoulder the VIVA+ HBM can move in Y-direction until the belt has come to the bend of the arm, which restricts further movement of the body. In fact, many of the data signals seen in appendix D wanders off from the PMHS corridor in this fashion and may be explained by this effect. In an attempt to reduce the slippage some increased friction coefficients between the seat belt and the VIVA+ model were tested. However, no signs of improvement could be spotted. One additional investigation was done, specifically on the shoulder stiffness to see if this could affect the belt slip. There was not enough time to study this in detail and therefore it is recommended to start here in a future study.

Although belt slip occurred the CORA values for the belt forces in each configuration indicate a good correlation where the lowest CORA score was 0.77 and several of the belt forces achieved a CORA score above 0.8. By looking at the plots in figure 4.9 it can be seen that the force in Belt Force Shoulder for Configuration 1 is a bit lower than the psychical test. This is a recurring response of this quantity when looking at the other configurations in D. If this behaviour is causing the belt slip or merely an effect of it is not investigated in this report and is a possible area to investigate in future studies.

The force in the pretensioner, which is represented by the lower peak of the belt force plots, is smaller in the simulations than what the cadaver tests, performed by Forman [12], showed. This was not seen in the previous studies when using the THUMS HBM and the SAFER HBM [8], [13]. There, larger pretensioner forces can be observed. This difference may also be one of the reasons the sled simulations in this thesis predicts seat belt slip to a greater extent.

5.1.3 Interpretation of the CORA Scores

The kinematics of the male VIVA+ HBM have an average CORA score of 0.64 and a median of 0.63. Both values are thus within the biofidelity level, fair. However, it is very close to being within the good range, when considering the scale that is described in chapter 2.6. With this, it can be stated that the male VIVA+ HBM has a fair but very close to good correlation to the PMHS tests that were conducted in Forman's studies [12]. It should be highlighted that by looking at table 4.1 one can see that Configuration 5 is quite hard to capture compared to the other configurations, which is why its CORA score is significantly lower. If this configuration would have been omitted, the biofidelity of the male VIVA+ HBM would have received the rating, good. The belt slip is however something the validation simulations predicts to a larger extent than for the PMHS, thus making it overpredict lateral displacement of the head.

Three interesting things should be noted from table 4.1. Firstly, the torso twist is below the limit for fair accuracy in all male configurations. This might have to do with the fact that this quantity builds upon two other measures. Since neither the left nor the right acromion is 100% accurate these small errors will become larger when adding them together. This might also be explained by the belt slip that occurs in the simulations. When the seat belt is slipping rather than gripping onto the HBM the seat belt will not affect the thorax which would make the upper body rotate. One can see hints of this in the torso twist plots, where the rotation is delayed compared to the PMHS corridors. The sudden increase of rotation near the end of the curves may be explained by that the seat belt gets caught by the bend of the arm, which restricts the seat belt to slip further.

Secondly, the fifth configuration has a total kinematic CORA score below the limit of fair accuracy. One reason for this is probably that the combination of a pure lateral pulse together with a D-ring in the forward position will make the HBM easily slip out of the belt. Interesting is that for Configuration 6 the VIVA+ model is valid even though this has a high pulse instead of the low pulse used in Configuration 5. The saviour might be that in Configuration 6 the D-ring is in a middle position which increases the contact between the belt and the VIVA+ model and restricts the occupant's movement more than the fifth configuration. Interestingly the physical tests on which configuration 5 is based, tests S0083 and S0088, manage to keep the seat belt on the shoulder of the PMHS and show no sign of having the belt slip [13], contrary to what was seen for the simulation of Configuration 5 in this thesis.

Thirdly it is intriguing to see that the pelvis movements are accurate in Y-direction while they are quite poor for the other two directions. For example, when specifically looking at Configuration 5 in figure 4.5 where the insufficient correlation in X- and Z-direction can be explained by that the belt slips. The belt slip allows the torso to lean further in Y-direction than for a case where the seat belt stays on. The increased leaning movement of the torso was also seen to affect the pelvis movement in Z-direction. The pelvis travelled upwards in a negative Z-direction because of its

rotation around the right buttock. Another type of rotation of the torso created by the loss of retention caused the pelvis to move differently in X-direction. However, similarities between the male VIVA+ HBM and the PMHS can be spotted in the X-direction while in the Z-direction it is difficult to see any similarities.

A choice was made in the beginning of the project to place the female version so that the angles and distances would match the male PMHS according to table 3.2. This was a decision which made it easy to compare the male and female versions. It would therefore be interesting to see how the different versions of VIVA+ HBM would react if the sled used for the male version would be used without changing any positions for the female version. However, this is left for future studies.

The CORA scores for the female version are not part of the validation study since it would compare simulation models using female occupants against experimental data which consists of male PMHS. A set of female PMHS tests would have been needed to complete an accurate validation of these. The female simulations were completed to see how they differed from the male configurations.

By studying table 4.2 it can be seen that the CORA scores representing the correlation between the female and male VIVA+ model are overall high. This indicates that there is a correlation between the two models. For example, the head movements of the two models are more or less the same where the CORA scores indicate an excellent correlation for several quantities. However, there are some quantities where there are some differences, such as the pelvis in the X-direction where the female is following the same trajectory but with a lower magnitude. It is reasonable that there are some differences in response between the two models since the size and inertia properties are not modelled the same. The female is shorter and has a lower mass than the male version which should affect the response in some way.

5.2 HBM Evaluation in Full Vehicle Environment

This section of the discussion concerns the analysis of the results from the evaluation simulations of the fully modelled vehicle. Opening with a short analysis of the energy ratios in the systems.

5.2.1 Energy Ratios Show Trustworthiness

Unlike the validation simulations, no unexpected peaks were found for the hourglass ratio nor the energy balance ratio. The hourglass ratio was always below 1% which probably is an effect of that the simulation that was used has already been checked for energy imbalances and that the differences between the WorldSID model and the VIVA+ HBM are negligible since the total energy in the system is much larger.

5.2.2 Analysis of the Quantities of Interest

The quantities that were analysed in the fully modelled vehicle simulations were highly inspired by a previously performed study at CEVT where WorldSID models were used in the same load case. Therefore, it was reasonable to start from there when analysing the VIVA+ model in this simulation environment. By comparing C1-E from figure 4.11 with CEVT's analysis in table 4.3 some interesting things can be spotted. Firstly, the passenger has a higher HIC_{15} value than the driver in the simulations where WorldSIDs were used while the VIVA+ models predicts the opposite. However, by looking at the head acceleration curves in figure 4.13 some similarities can be seen between the two occupant setups. The peaks and the valleys of the curves, the magnitudes of the driving occupants, as well as the incline and decline coincide quite well. Thus, having very similar curve characteristics. The significant difference between them is that the peak for the passenger is higher for the WorldSID than for the VIVA+ model. Secondly one can compare the Head2Head distances between the occupant setups of the male VIVA+ HBM and the WorldSID, in figure 4.11 and table 4.3 respectively. The bar plot of the Head2Head distance for configuration C1-E presents a value of approximately 20 mm while the WorldSID analysis produced a Head2Head distance of 6 mm. Thus, the WorldSID model predicts a larger intrusion of the FSAB, which is probably caused by the stiffer nature of a WorldSID crash dummy [39].

Parallel to the comparison between the different occupant models, i.e. WorldSIDs and VIVA+ models, a comparison between the simulations and Euro NCAP's requirements, mentioned in chapter 3.2.2, was carried out. To get the top score, i.e. five stars, with respect to preventing head injuries, a HIC_{15} value below 500 is required, while HIC_{15} values above 700 receive zero stars. For the simulations that were using the original airbag pressure, all three responses with the VIVA+ model were below 500. However, when the pressure in the airbag was reduced to 75% of the original airbag, the configurations with a male VIVA+ HBM driver, C4-E and C6-E, received zero stars. Thus, the female driver and a male passenger defied this pattern and received full scores for both airbag setups. This circumstance may be explained by the collision between the female driver and the inflatable curtain, situated by the driver's door. The female driver's head got a different trajectory than the male driver's head. This happened because the female model collided with the bottom part of the inflatable curtain, since the female model is shorter than the male model. As a result, the female driver got sent forward while the male passenger sat up straight when hitting the FSAB which increased the distance between the heads. By analysing figure 4.14 and 4.15 one can clearly see this. The passenger occupant had a similar impact area on the FSAB no matter if a male or female model was used. However, this was not the case for the driver occupant, which have different impact zones depending on if a male or female model was used. It may be that even without an airbag appearing above the centre console the heads would miss each other. This would most likely cause a larger risk for AIS2+ rib fractures since the passenger could travel into the centre console without anything to absorb the kinetic energy as the FSAB would have done. It can therefore be concluded that the FSAB may be important to reduce or avoid more than just head injuries.

Beyond the HIC values, it is of interest to see if there is a risk for rib fractures. By looking at figure 4.11 the risk for two or more rib fractures varies between close to zero up to 45 %. Some interesting things should be noted. Firstly, it can be seen that the risk is dependent on the sex of the occupant. For example, in the simulation with the male driver and male passenger it will yield a higher risk for the passenger than the driver. If a male driver instead is placed with a female passenger, it is the driver who has the highest risk of rib fracture. In fact, for all cases where the occupants are of different sex the highest risk is always found for the male occupant, and if there are two males the passenger will have the highest risk.

6

Conclusion

By using the CORA scores obtained in this project, it is possible to conclude that the male VIVA+ HBM shows a fair, but close to a good correlation to the PMHS tests. The mean and median kinematic CORA scores of the male VIVA+ model were 0.64 and 0.63, respectively, where the fair and good biofidelity limit was drawn at 0.44 and 0.65 respectively. It can then be stated that the male VIVA+ model and the PMHS used in the physical tests are similar to a fair level, and should be seen as acceptable to use in far-side safety testing.

The kinematic CORA score for the female simulations showed that the female and male VIVA+ models have a very similar behaviour, where the lowest scoring configuration achieved 0.73 in the average Kinematics category. This is something one easily could have guessed since they are practically the same model, with some slight changes to differentiate between male and female human physical properties. The male model was seen to behave as a human body on a fair level in a far-side sled setup. Whereas, without any female PMHS data, the same cannot be concluded for the female version of the VIVA+ HBM.

The comparison between the WorldSID and the VIVA+ HBM showed that the two different models show similar behaviour in the fully modelled vehicle. The upper body kinematics of both models highly resembles each other. The characteristics of the head acceleration curves follow each other closely. Although there are some differences such as the magnitude of the passengers' head acceleration. Since the VIVA+ HBM comparison with the PMHS showed a fair but close to good correlation could the VIVA+ be used to investigate the robustness of safety systems such as airbags. This is not the case for the WorldSID since this is just available in one size for one sex.

Furthermore it was found that the sex of the occupants may impact the outcome of sustained injuries. When a female HBM was placed in the driver seat, a deviation was detected in the trend of the HIC values and head kinematics. The female HBM, which is shorter compared to the male HBM, gets a different head movement path because the impact with the near side airbag occurs at the lower, rounded, corner of the airbag, while the male driver collides with the main flat area and gets a straighter trajectory into the FSAB.

6.1 Future Work

The belt slip is a recurring problem and something that has been an issue for both Forman's PMHS study and Pipkorn's studies using HBMs [12], [13]. However, these studies identified fewer configurations that encountered belt slip compared to the configurations in this study. In this study, it was shown that the VIVA+ model consistently had the seat belt slipping off the shoulder in all generic sled simulations. Therefore, it is advised that the main focus in a future study using the VIVA+ model should be on how the seat belt slip can be decreased or eliminated.

During the project, the question arose whether the CORA method was a good validation method since it yielded that the majority of the human body models had an acceptable biofidelity even though the seat belt slipped off the occupants' shoulders in all the configurations. Following this, it could be interesting to investigate the possibility to use another correlation analysis tool which takes the belt interaction more into account.

As some finalising words to this thesis, it should be said that even though there are some areas that need to be investigated further, e.g. seat belt slip and female validation, the VIVA+ HBM should be a sufficient tool that has potential to be used in far-side safety evaluations of vehicles in the future.

Bibliography

[1] BizVibe. *Top 10 Largest Manufacturing Companies in the World 2020, Global Manufacturing Industry Factsheet*. 2020. URL: https://blog.bizvibe.com/blog/largest-manufacturing-companies (visited on 02/09/2022).

[2] International Energy Agency. *Global EV Outlook 2020*. 2020. URL: https://www.iea.org/reports/global-ev-outlook-2020 (visited on 02/09/2022).

[3] Humanetics. *Anthropomorphic Test Devices (ATD)*. n.d. URL: https://humanetics.humaneticsgroup.com/products/anthropomorphic-test-devices (visited on 02/14/2022).

[4] Euro NCAP. *FAR SIDE OCCUPANT TEST ASSESSMENT PROCEDURE*. Tech. rep. V2.1.1. Leuven, Belgium: Euro NCAP, 2021. URL: https://cdn.euroncap.com/media/67256/euro-ncap-far-side-test-and-assessment-protocol-v211.pdf (visited on 05/24/2022).

[5] Toyota. *Toyota Offers Free Access to THUMS Virtual Human Body Model Software*. 2020. URL: https://global.toyota/en/newsroom/corporate/32665896.html (visited on 02/14/2022).

[6] Euro NCAP. *Adult Occupant Protection*. n.d. URL: https://www.euroncap.com/en/vehicle-safety/the-ratings-explained/adult-occupant-protection/ (visited on 02/14/2022).

[7] VIRTUAL. "Watch now: Progress in Virtual Testing for automotive applications". In: 2020. URL: https://projectvirtual.eu/2020/09/11/watch-now-progress-in-virtual-testing-for-automotive-applications/ (visited on 05/28/2022).

[8] B. Pipkorn et al. "Occupant protection in far-side impacts". In: *Proceedings of IRCOBI conference*. Athens, Greece, 2018, pp. 125–127.

[9] J. John et al. "Hello, World! VIVA+: A Human Body Model lineup to evaluate Sex-Differences in Crash Protection". In: *Frontiers in bioengineering and biotechnology* (2022). In Press.

[10] A. Linder and W. Svedberg. "Review of average sized male and female occupant models in European regulatory safety assessment tests and European laws: Gaps and bridging suggestions". In: *Accident Analysis Prevention* vol. 127 (2019), pp. 156–162. DOI: https://doi.org/10.1016/j.aap.2019.02.030.

[11] G. R. Booth, P. A. Cripton, and G. P. Siegmund. "The Lack of Sex, Age, and Anthropometric Diversity in Neck Biomechanical Data". In: *Frontiers in*

Bioengineering and Biotechnology vol. 9 (Aug. 2021). DOI: 10.3389/fbioe.2021.684217.

[12] J.L. Forman et al. "Occupant Kinematics and Shoulder Belt Retention in Far-Side Lateral and Oblique Collisions: A Parametric Study". In: *Stapp Car Crash Journal* 57 (Nov. 2013), pp. 343–385. DOI: 10.4271/2013-22-0014.

[13] B. Pipkorn et al. "Validation of the SAFER Human Body Model Kinematics in Far-Side Impacts." In: *Proceedings of IRCOBI conference*. held online, 2021, pp. 444–476.

[14] A. Harish. *Implicit vs Explicit Finite Element Method (FEM): What Is the Difference?* SimScale. Nov. 29, 2020. URL: https://www.simscale.com/blog/2019/01/implicit-vs-explicit-fem/ (visited on 05/09/2022).

[15] Dynamore. *Time step size*. n.d. URL: https://www.dynasupport.com/tutorial/ls-dyna-users-guide/time-step-size (visited on 05/09/2022).

[16] A.M. Prior. "Applications of implicit and explicit finite element techniques to metal forming". In: *Journal of Materials Processing Technology* 45.1-4 (Sep. 1994), pp. 649–656. DOI: https://doi.org/10.1016/0924-0136(94)90413-8.

[17] S. Bala. *Overview of Mass-Scaling in LS-DYNA*. d3VIEW. Oct. 2, 2006. URL: https://www.d3view.com/overview-of-mass-scaling/ (visited on 05/10/2022).

[18] LS-Dyna. *Mass scaling*. n.d. URL: https://www.dynasupport.com/howtos/general/mass-scaling (visited on 05/10/2022).

[19] A. Harish. *How to Calculate Stress and Strain with FEM Software?* SimScale. Jun. 24, 2021. URL: https://www.simscale.com/blog/2017/04/stress-and-strain/ (visited on 06/16/2022).

[20] Livermore Software Technology Corporation. *LS DYNA Theory Manual*. 2006. URL: https://www.lstc.com/pdf/ls-dyna_theory_manual_2006.pdf (visited on 05/12/2022).

[21] T. A. Burkhart, D. M. Andrews, and C. E. Dunning. "Finite element modeling mesh quality, energy balance and validation methods: A review with recommendations associated with the modeling of bone tissue". In: *Journal of Biomechanics* vol. 46.9 (May, 2013), pp. 1477–1488. DOI: https://doi.org/10.1016/j.jbiomech.2013.03.022.

[22] Y. Haseli. "Entropy Analysis in Thermal Engineering Systems". In: Cambridge, USA: Academic Press, 2020.

[23] VIVA+ Team. *VIVA+ Models*. 2022. URL: https://vivaplus.readthedocs.io/en/latest/model/intro/ (visited on 02/22/2022).

[24] VIVA+ Team. *Anthropometry*. 2022. URL: https://vivaplus.readthedocs.io/en/latest/model/anthro/ (visited on 05/17/2022).

[25] A.N. Natali and E.A. Meroi. "A review of the biomechanical properties of bone as a material". In: *Journal of Biomedical Engineering* vol. 11.4 (Jul. 1989), pp. 266–276. DOI: https://doi.org/10.1016/0141-5425(89)90058-7.

[26] K.J. Larsson et al. "Rib Cortical Bone Fracture Risk as a Function of Age and Rib Strain: Updated Injury Prediction Using Finite Element Human Body Models". In: *Frontiers in Bioengineering and Biotechnology* vol. 9 (May, 2021). DOI: 10.3389/fbioe.2021.677768.

[27] R. Wicklin. *The Poisson-binomial distribution*. SAS System. Sep. 28, 2020. URL: https://blogs.sas.com/content/iml/2020/09/28/poisson-binomial-distribution.html (visited on 05/17/2022).

[28] J.E. Baker et al. "Does chest wall Organ Injury Scale (OIS) or Abbreviated Injury Scale (AIS) predict outcomes? An analysis of 16,000 consecutive rib fractures". In: *Surgery* vol. 168.1 (Jul. 2020), pp. 198–204. DOI: https://doi.org/10.1016/j.surg.2020.04.032.

[29] H-W. Henn. "Crash Tests and the Head Injury Criterion". In: *Teaching Mathematics and its Applications: An International Journal of the IMA* vol. 17.4 (Dec. Dec. 1998), pp. 162–170. ISSN: 0268-3679. DOI: 10.1093/teamat/17.4.162.

[30] Road vehicles - Anthropomorphic side impact dummy - Lateral impact response requirements to assess the biofidelity of the dummy ISO/TR 9790. *ISO*. Geneva, Switzerland, 1999. URL: https://www.sis.se/en/produkter/road-vehicles-engineering/diagnostic-maintenance-and-test-equipment/isotr9790/ (visited on 12/06/2018).

[31] Y. Håland. "The evolution of the three point seat belt from yesterday to tomorrow". In: *IRCOBI Conference*. Madrid, Spain, 2006, pp. 3–15.

[32] THUMS User Community. *General*. n.d. URL: https://tuc-project.org/about-tuc/ (visited on 06/06/2022).

[33] THUMS User Community. *FAR-SIDE LOAD CASE*. n.d. URL: https://tuc-project.org/far-side-load-case/ (visited on 02/24/2022).

[34] Safety Test Instrumentation Standards Committee. *Instrumentation for Impact Test - Part 1 - Electronic Instrumentation*. Mar. 2014. DOI: https://doi.org/10.4271/J211/1_201403. URL: https://doi.org/10.4271/J211/1_201403 (visited on 05/16/2022).

[35] M. Katagiri et al. "Comparison of whole-body kinematic behaviour of the GHBMC occupant model to PMHS in far-side sled tests". In: *Proceedings of IRCOBI Conference*. Malaga, Spain, 2016, pp. 679–693.

[36] D. Perez-Rapela et al. "Comparison of the simplified GHBMC to PMHS kinematics in far-side impact". In: *Proceeding of IRCOBI Conference*. Florence, Italy, 2019, pp. 260–281.

[37] Partnership for Dummy Technology and Biomechanics. *CORA*. n.d. URL: https://www.pdb-org.com/en/information/18-cora-download.html (visited on 06/06/2022).

[38] R-Project. *The R Project for Statistical Computing*. n.d. URL: https://www.r-project.org/ (visited on 05/24/2022).

[39] D. Perez-Rapela et al. "Occupant restraint in far-side impacts: cadaveric and WorldSID responses to a far-side airbag". In: *Annals of biomedical engineering* vol .49.2 (Feb. 2021), pp. 802–811.

A

PMHS Vs VIVA+ HBM Physical Properties

Table A.1: A table comparing the height, weight, and age between the PMHS and the VIVA+ model

		C1	**C2**	**C3**	**C4**	**C5**	**C6**
Average height [cm]	**PMHS**	180	177,33	177,33	180	173	175
	VIVA+ Male	175,3					
	VIVA+ Female	161,6					
Average weight [kg]	**PMHS**	82,5	81,33	81,33	91	78	73
	VIVA+ Male	76,83					
	VIVA+ Female	62,67					
Average age [year]	**PMHS**	52,5	53,67	53,67	70	63,5	60
	VIVA+ Male	50					
	VIVA+ Female	50					

B

CORA Settings

Table B.1: The settings used when producing the CORA values from the validation results

	Parameter	Setting	Explanation
Time Interval Settings	A_THRES	0.03	Used to calculate the start time of the interval of evaluation
	B_THRES	0.075	Used to calculate the end time of the interval of evaluation
	A_EVAL	0.01	Extend the interval of evaluation
	B_DELTA_END	0.001	Used to shorten the interval of evaluation
	T_MIN/T_MAX	auto/auto	Defines starting and end point of the interval of evaluation
Corridor Method	K	2	Exponent factor used in the calculation of the corridor rating
	G_1	0.5	Weighting factor of the corridor rating
	a_0/b_0	0.05/0.5	Relative width of inner and outer corridor

Cross-Correlation Method	D_MIN	0.01	Limits allowed phase shift for phase shift rating
	D_MAX	0.12	Limits allowed phase shift for phase shift rating
	INT_MIN	0.8	Defines minimum overlap of the interval
	K_V	10	Exponent factor used in the calculation of the progression rating
	K_G	1	Exponent factor used in the calculation of the size rating
	K_P	1	Exponent factor used in the calculation of the phase shift rating
	G_V	0.5	Weighting factor of the progression rating
	G_G	0.25	Weighting factor of the size rating
	G_P	0.25	Weighting factor of the phase shift rating
	G_2	0.5	Weighting factor of the cross-correlation rating

C

Energy Balance

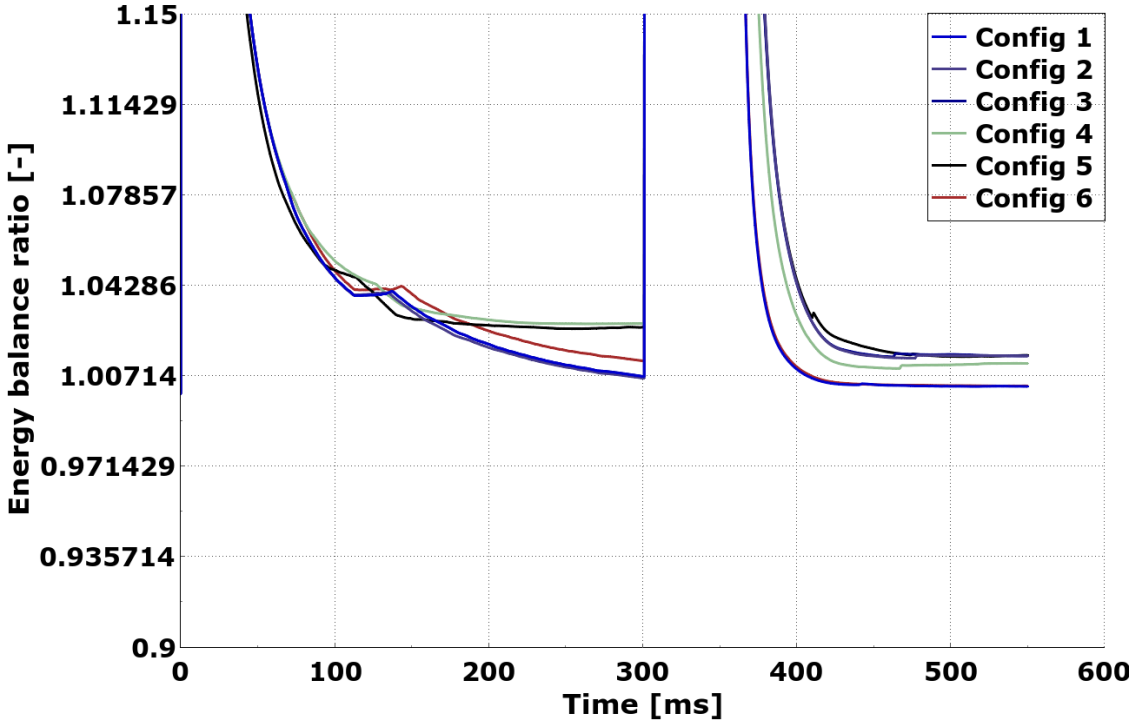

Figure C.1: A closeup of the energy balance ratio for the female sled simulations

D

CORA Plots

D.1 Male VIVA+ HBM Comparison With PMHS

D.1.1 Configuration 1

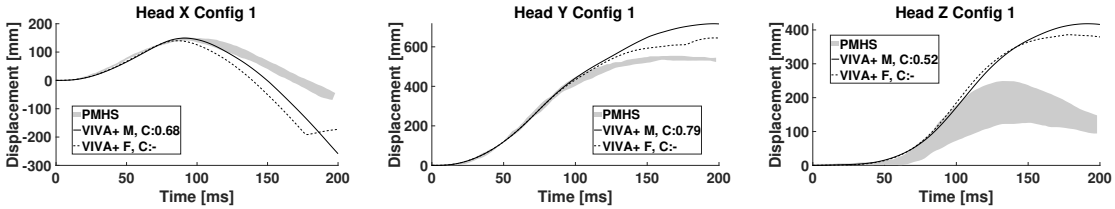

Figure D.1: Displacement of head, Configuration 1

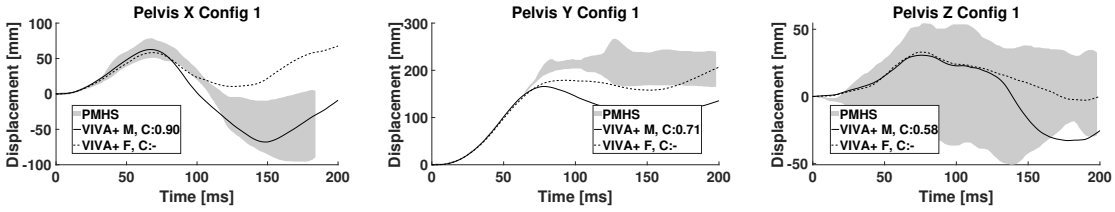

Figure D.2: Displacement of pelvis, Configuration 1

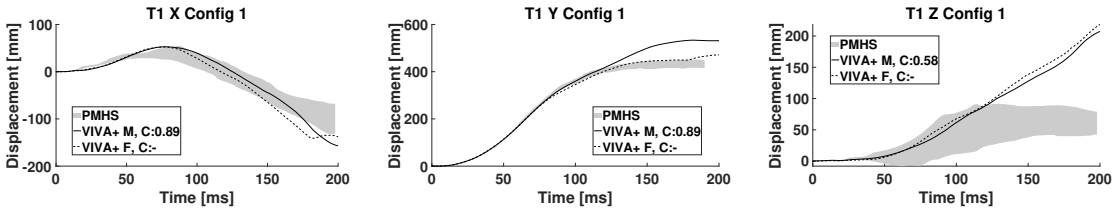

Figure D.3: Displacement of T1, Configuration 1

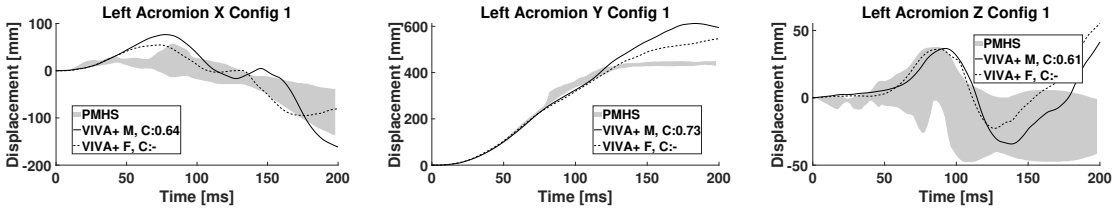

Figure D.4: Displacement of left acromion, Configuration 1

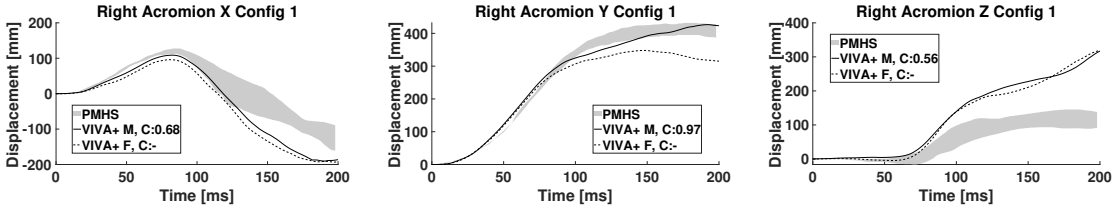

Figure D.5: Displacement of right acromion, Configuration 1

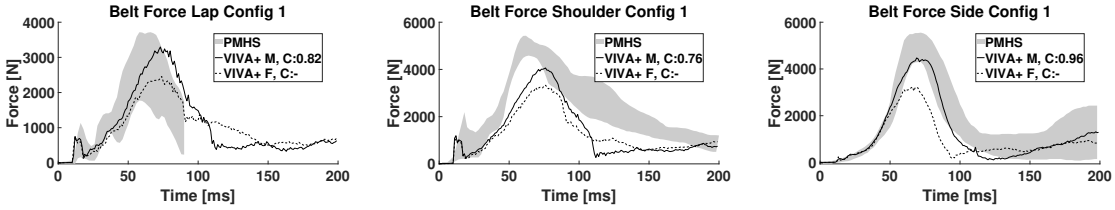

Figure D.6: Belt forces, Configuration 1

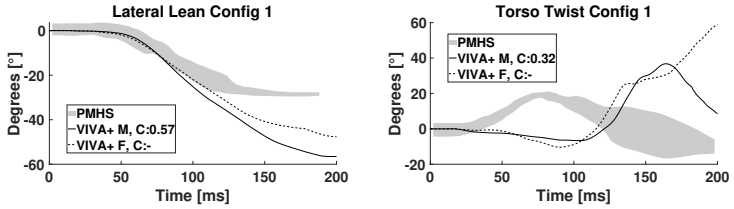

Figure D.7: Motion of thorax, Configuration 1

D.1.2 Configuration 2

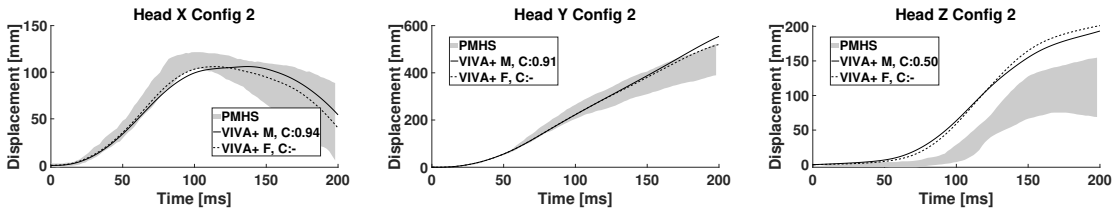

Figure D.8: Displacement of head, Configuration 2

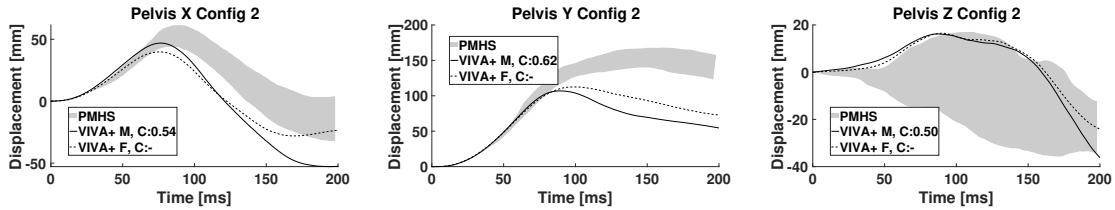

Figure D.9: Displacement of pelvis, Configuration 2

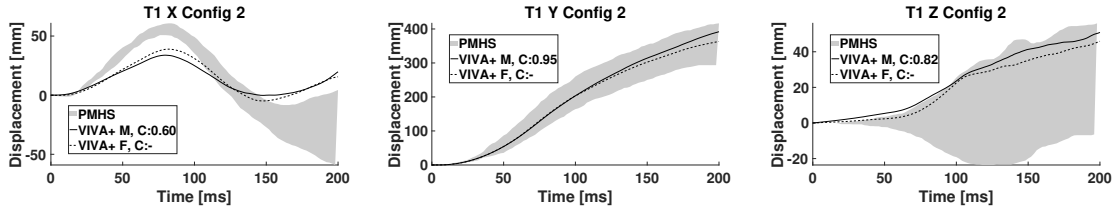

Figure D.10: Displacement of T1, Configuration 2

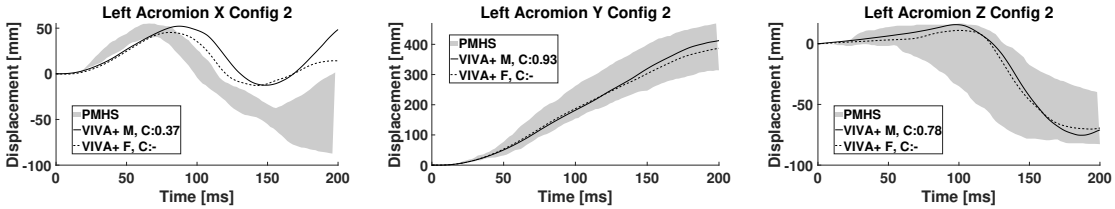

Figure D.11: Displacement of left acromion, Configuration 2

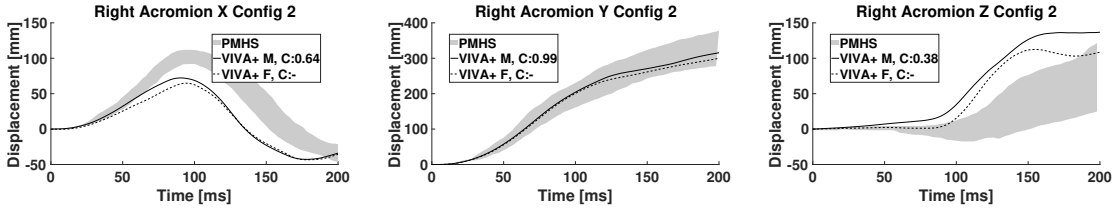

Figure D.12: Displacement of right acromion, Configuration 2

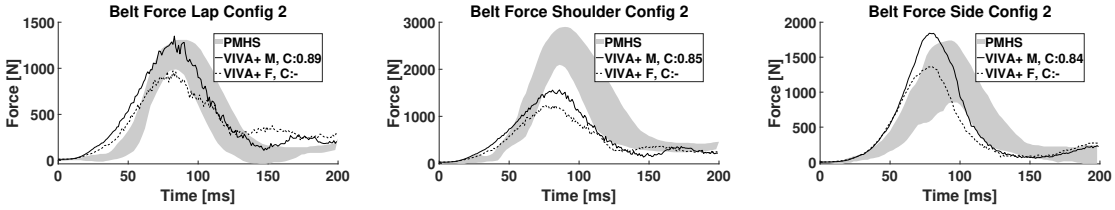

Figure D.13: Belt forces, Configuration 2

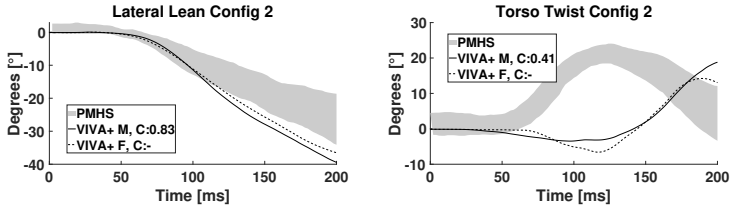

Figure D.14: Motion of thorax, Configuration 2

D.1.3 Configuration 3

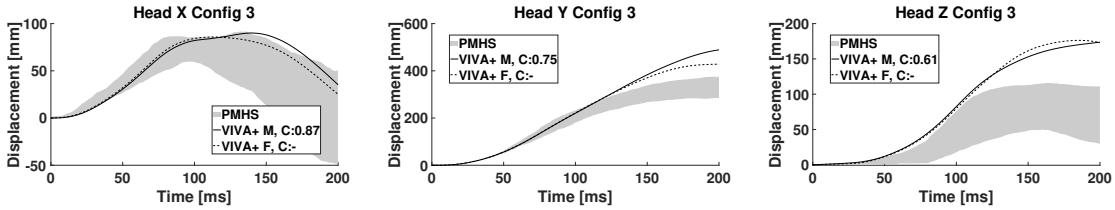

Figure D.15: Displacement of head, Configuration 3

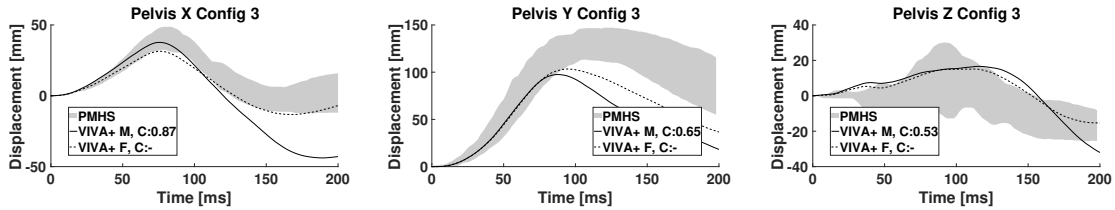

Figure D.16: Displacement of pelvis, Configuration 3

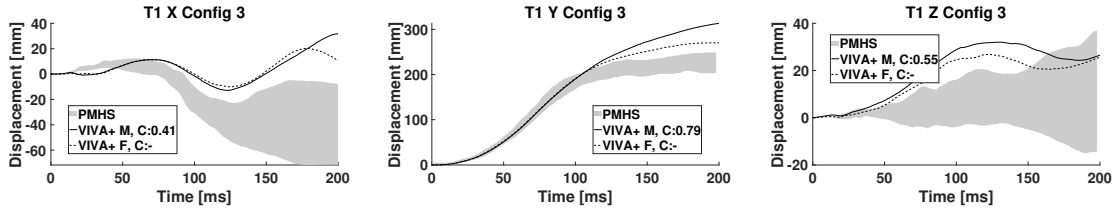

Figure D.17: Displacement of T1, Configuration 3

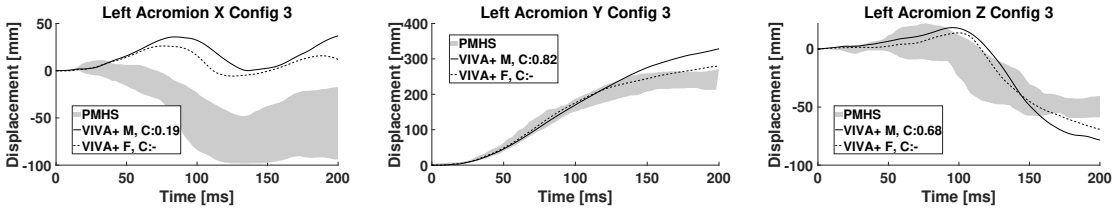

Figure D.18: Displacement of left acromion, Configuration 3

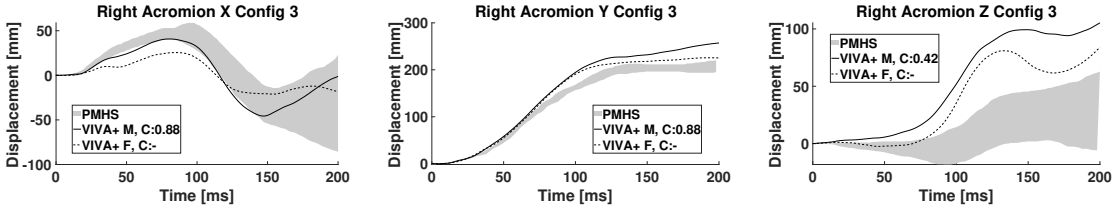

Figure D.19: Displacement of right acromion, Configuration 3

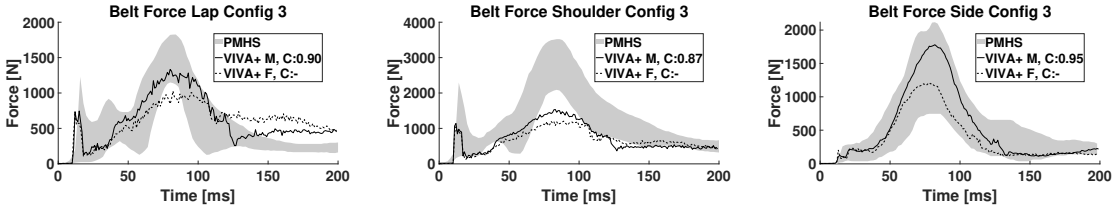

Figure D.20: Belt forces, Configuration 3

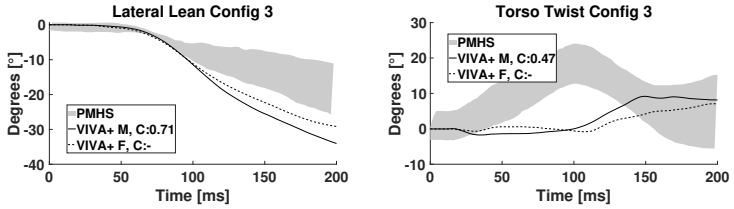

Figure D.21: Motion of thorax, Configuration 3

D.1.4 Configuration 4

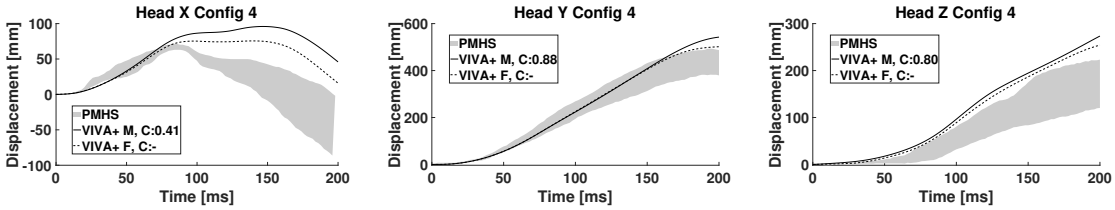

Figure D.22: Displacement of head, Configuration 4

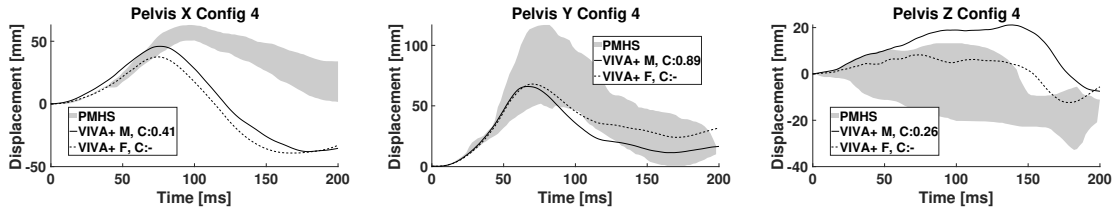

Figure D.23: Displacement of pelvis, Configuration 4

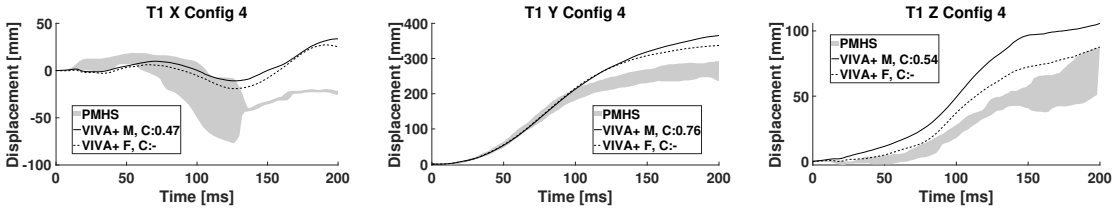

Figure D.24: Displacement of T1, Configuration 4

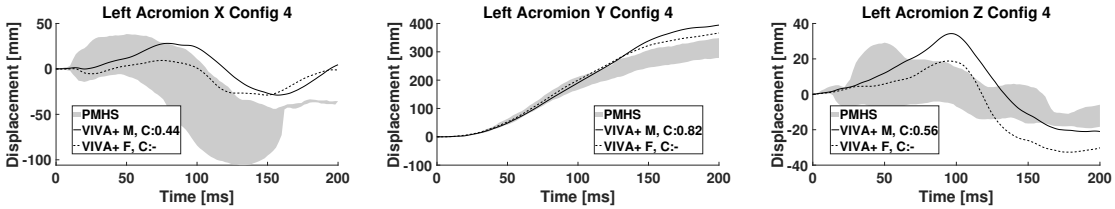

Figure D.25: Displacement of left acromion, Configuration 4

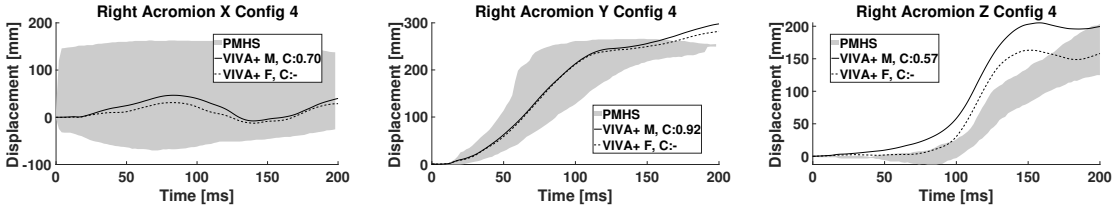

Figure D.26: Displacement of right acromion, Configuration 4

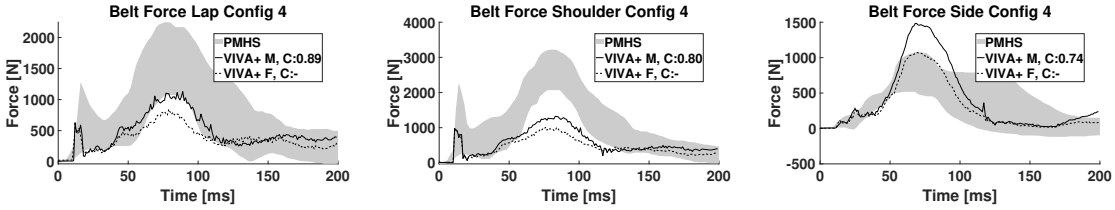

Figure D.27: Belt forces, Configuration 4

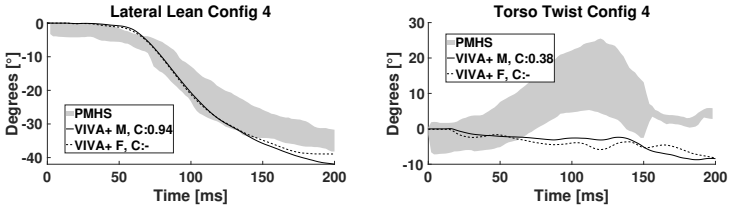

Figure D.28: Motion of thorax, Configuration 4

D.1.5 Configuration 5

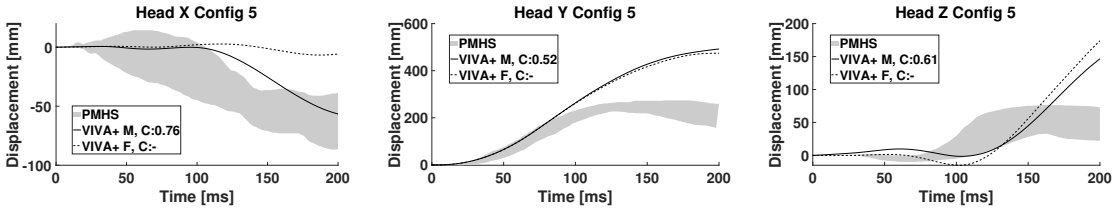

Figure D.29: Displacement of head, Configuration 5

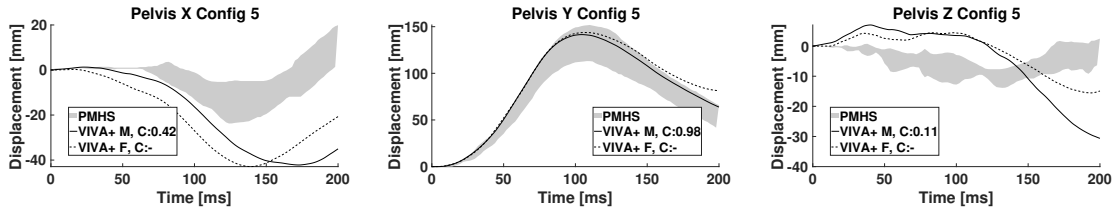

Figure D.30: Displacement of pelvis, Configuration 5

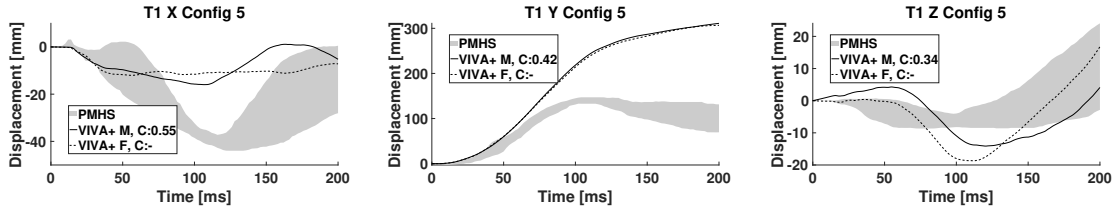

Figure D.31: Displacement of T1, Configuration 5

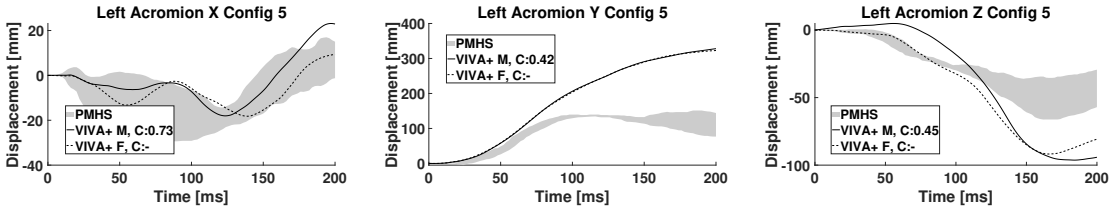

Figure D.32: Displacement of left acromion, Configuration 5

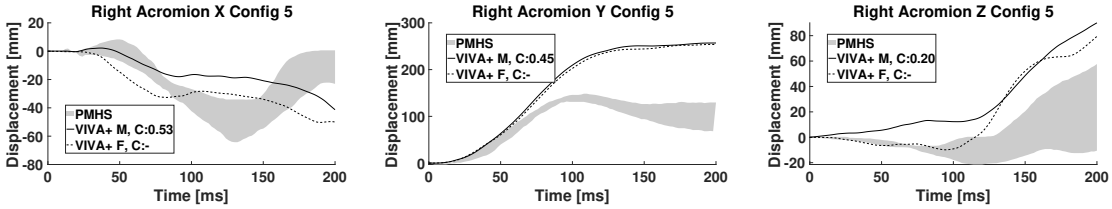

Figure D.33: Displacement of right acromion, Configuration 5

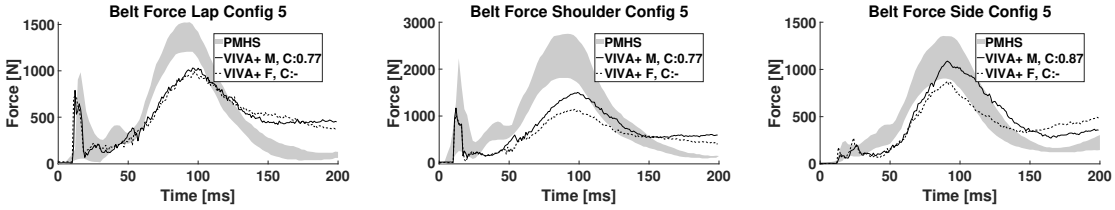

Figure D.34: Belt forces, Configuration 5

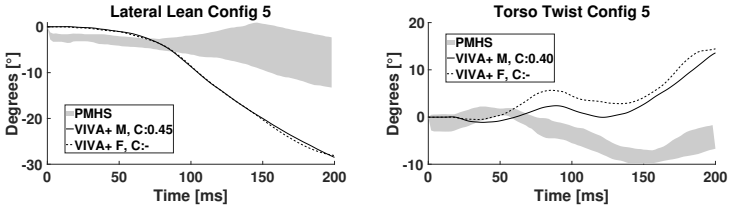

Figure D.35: Motion of thorax, Configuration 5

D.1.6 Configuration 6

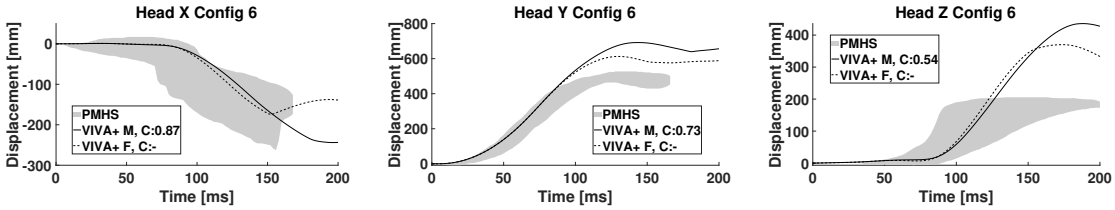

Figure D.36: Displacement of head, Configuration 6

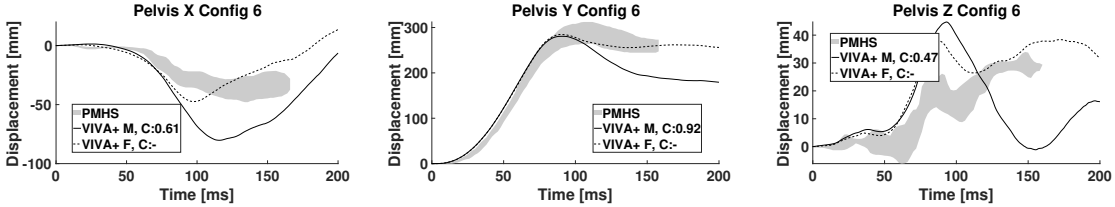

Figure D.37: Displacement of pelvis, Configuration 6

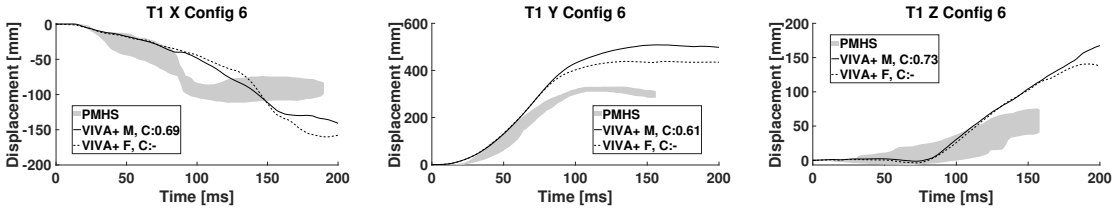

Figure D.38: Displacement of T1, Configuration 6

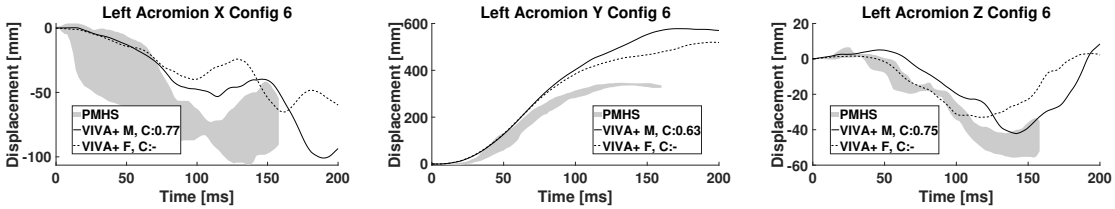

Figure D.39: Displacement of left acromion, Configuration 6

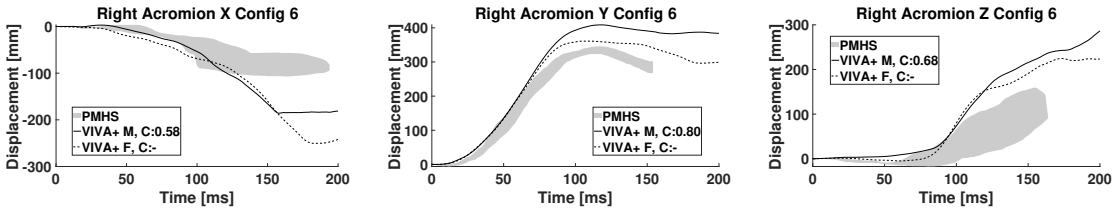

Figure D.40: Displacement of right acromion, Configuration 6

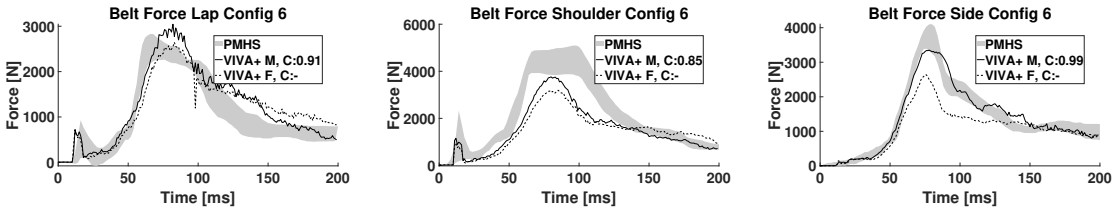

Figure D.41: Belt forces, Configuration 6

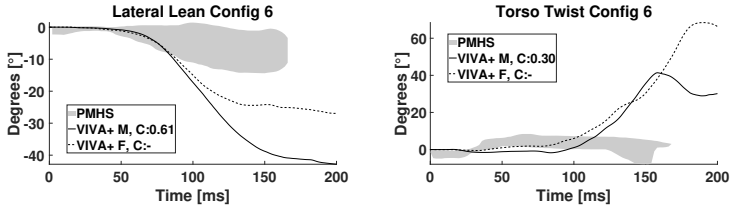

Figure D.42: Motion of thorax, Configuration 6

D.2 Female VIVA+ HBM Comparison With Male VIVA+ HBM

D.2.1 Configuration 1

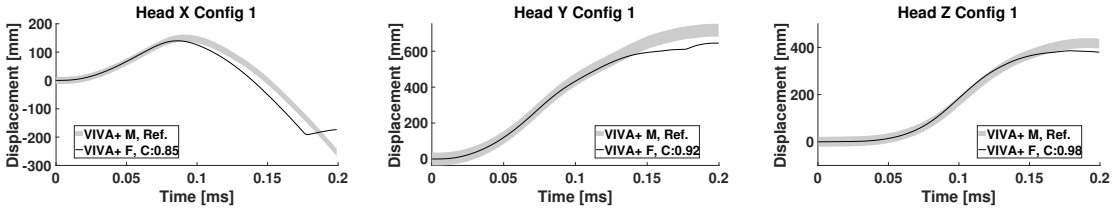

Figure D.43: Displacement of head, Configuration 1

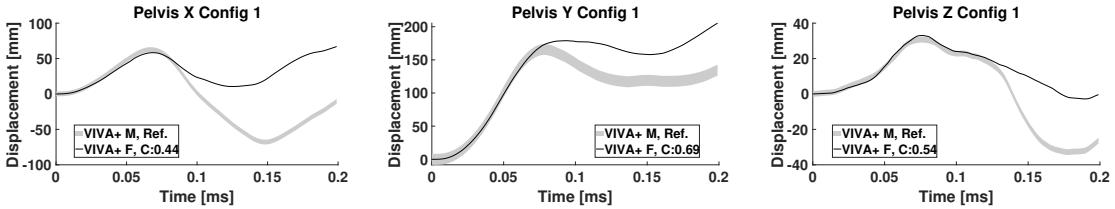

Figure D.44: Displacement of pelvis, Configuration 1

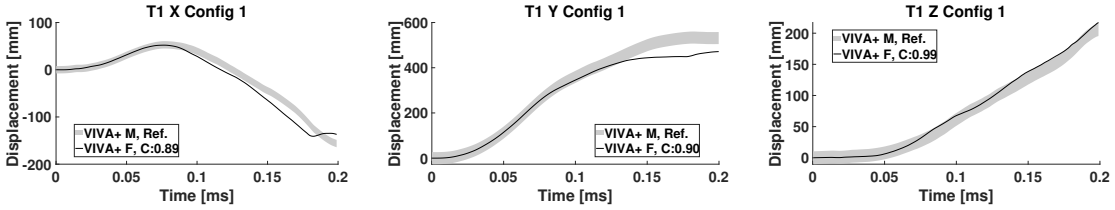

Figure D.45: Displacement of T1, Configuration 1

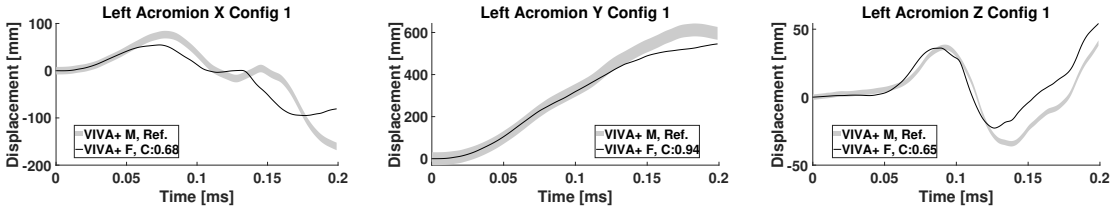

Figure D.46: Displacement of left acromion, Configuration 1

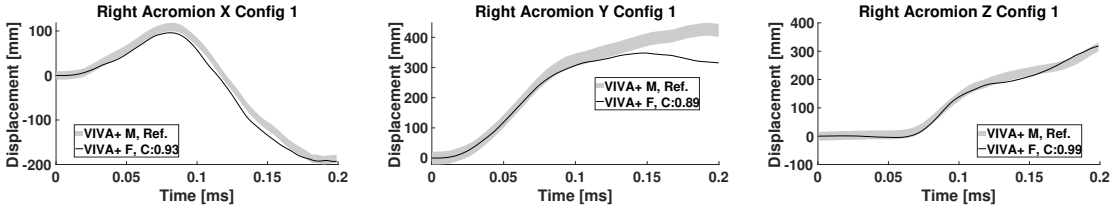

Figure D.47: Displacement of right acromion, Configuration 1

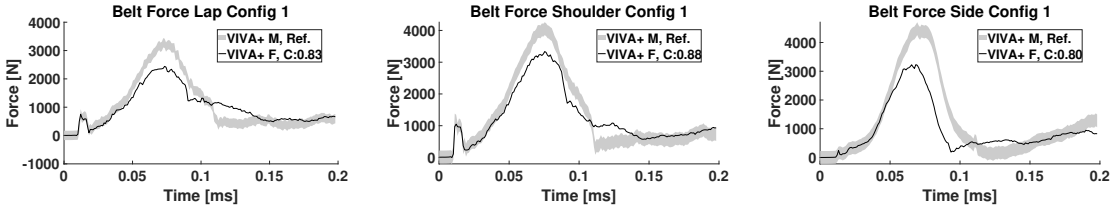

Figure D.48: Belt forces, Configuration 1

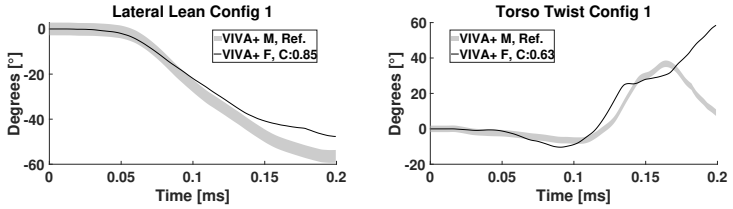

Figure D.49: Motion of thorax, Configuration 1

D.2.2 Configuration 2

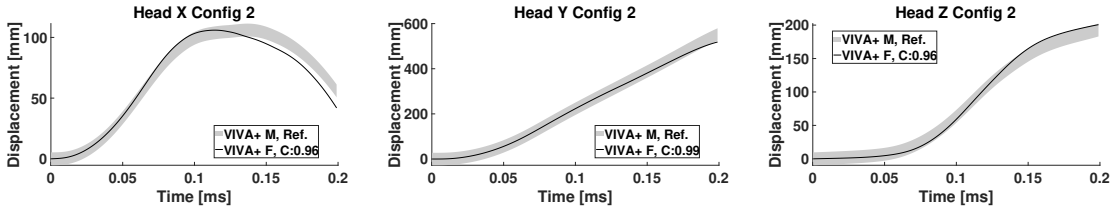

Figure D.50: Displacement of head, Configuration 2

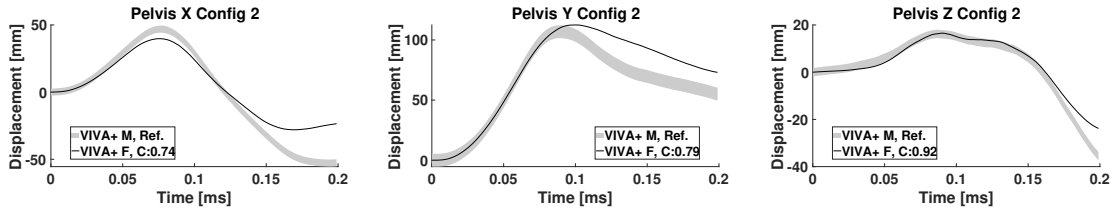

Figure D.51: Displacement of pelvis, Configuration 2

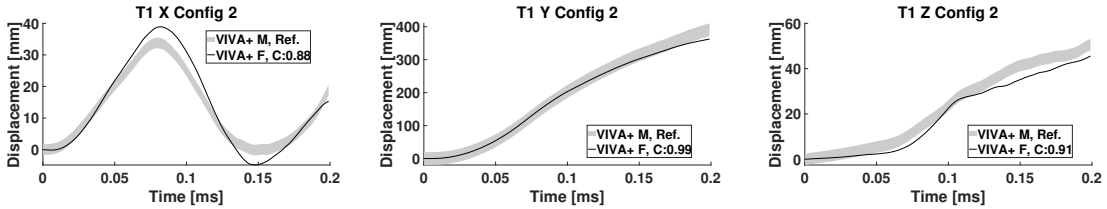

Figure D.52: Displacement of T1, Configuration 2

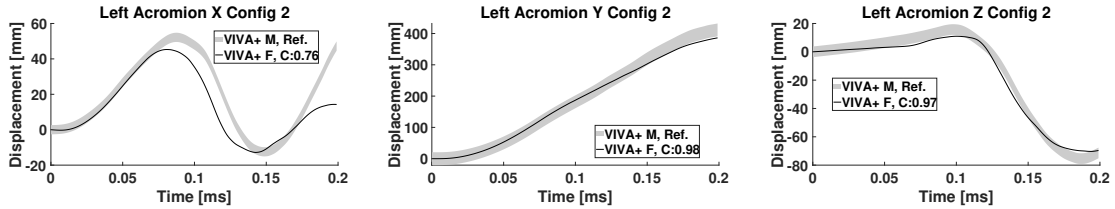

Figure D.53: Displacement of left acromion, Configuration 2

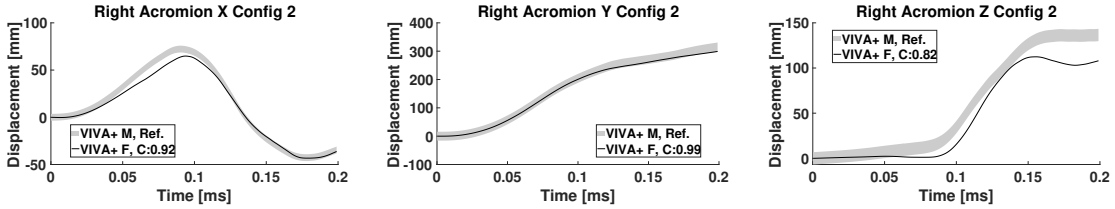

Figure D.54: Displacement of right acromion, Configuration 2

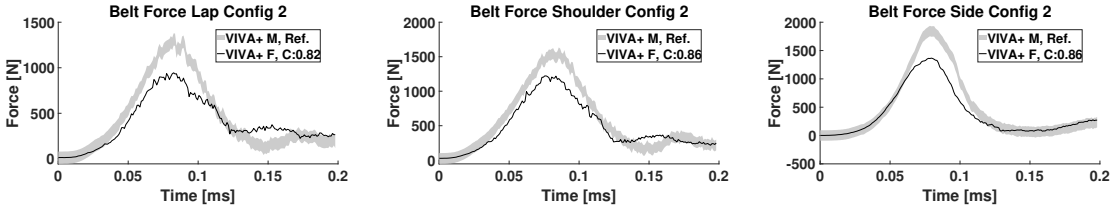

Figure D.55: Belt forces, Configuration 2

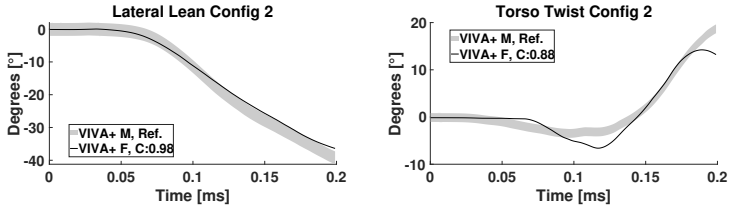

Figure D.56: Motion of thorax, Configuration 2

D.2.3 Configuration 3

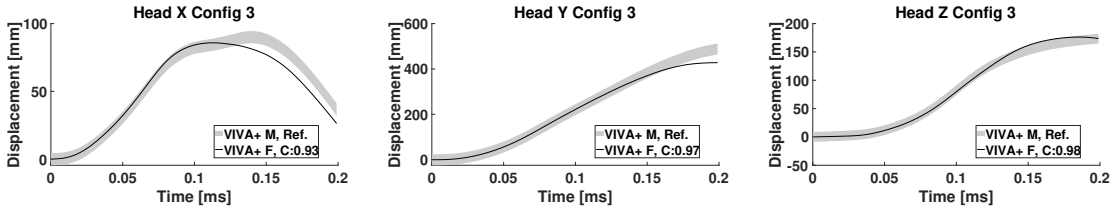

Figure D.57: Displacement of head, Configuration 3

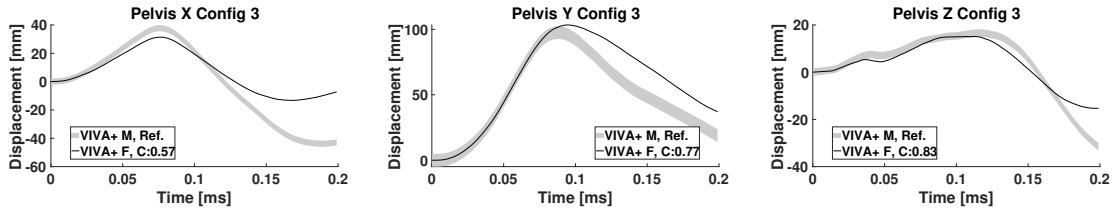

Figure D.58: Displacement of pelvis, Configuration 3

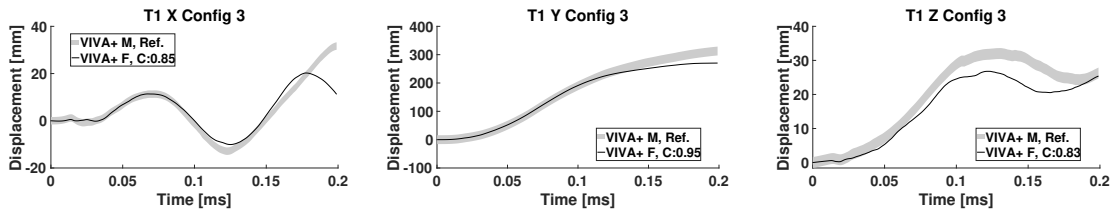

Figure D.59: Displacement of T1, Configuration 3

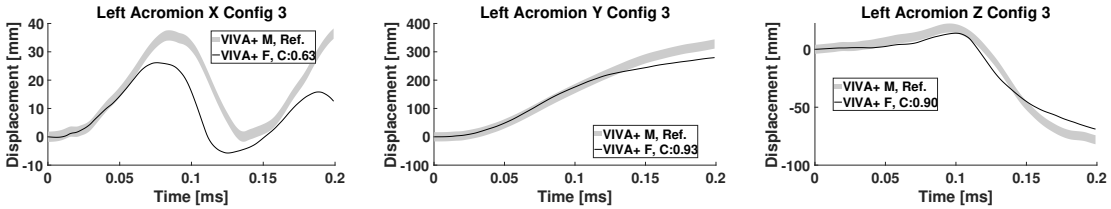

Figure D.60: Displacement of left acromion, Configuration 3

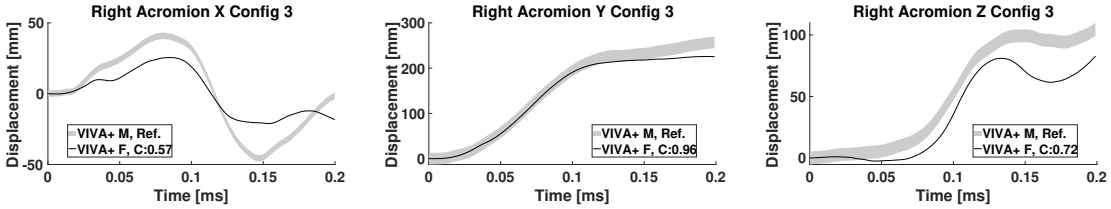

Figure D.61: Displacement of right acromion, Configuration 3

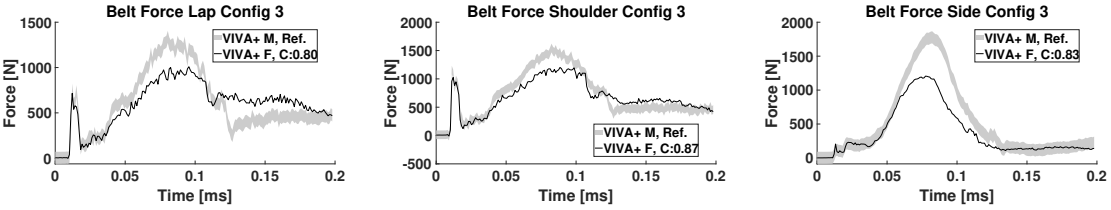

Figure D.62: Belt forces, Configuration 3

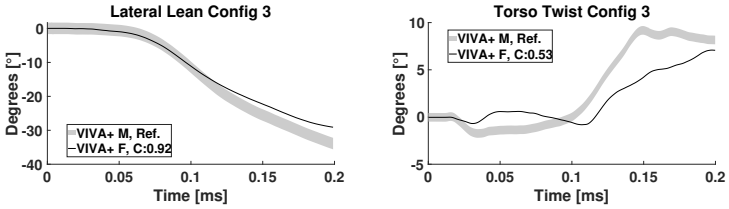

Figure D.63: Motion of thorax, Configuration 3

D.2.4 Configuration 4

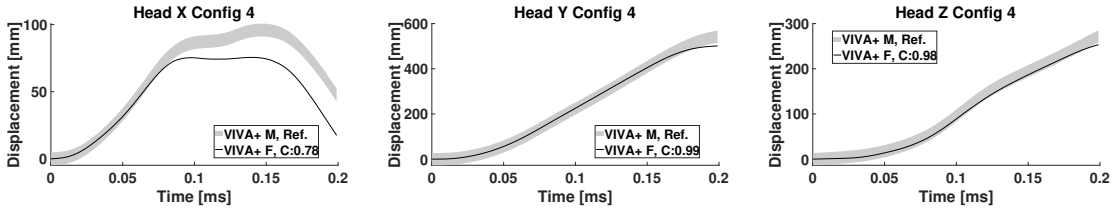

Figure D.64: Displacement of head, Configuration 4

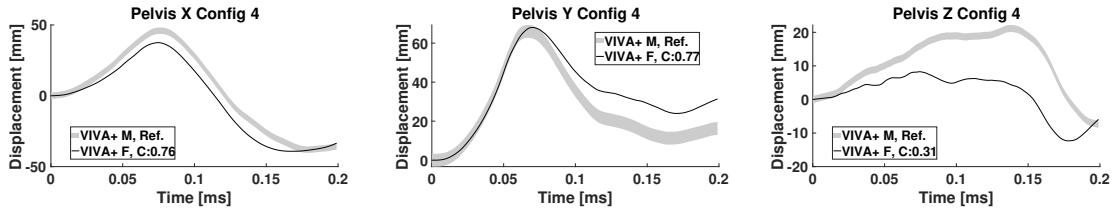

Figure D.65: Displacement of pelvis, Configuration 4

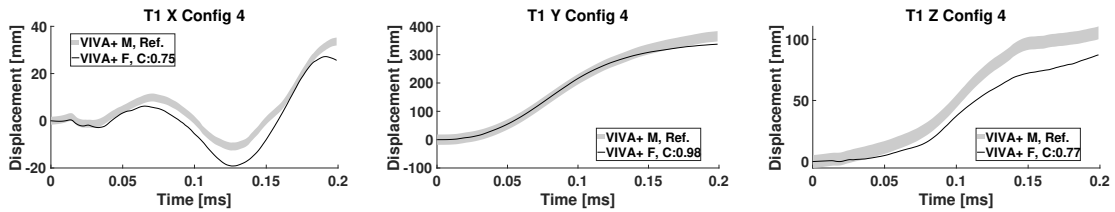

Figure D.66: Displacement of T1, Configuration 4

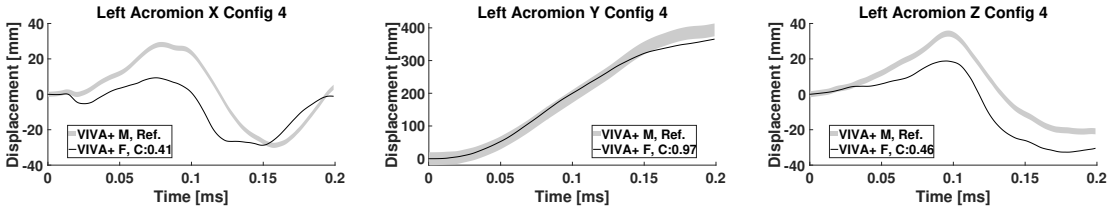

Figure D.67: Displacement of left acromion, Configuration 4

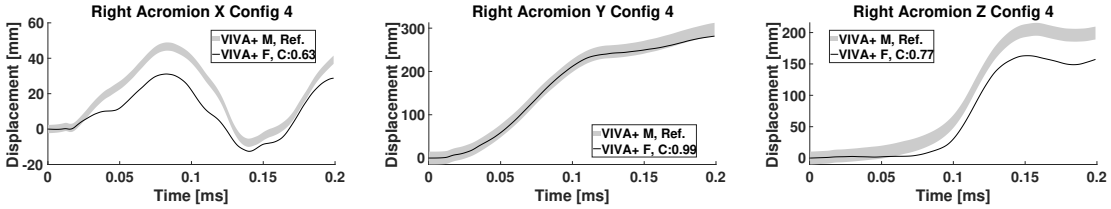

Figure D.68: Displacement of right acromion, Configuration 4

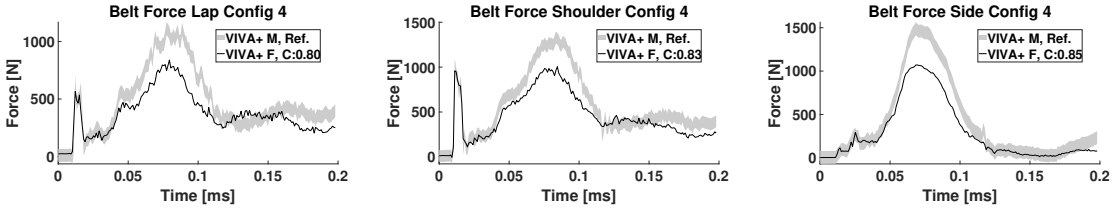

Figure D.69: Belt forces, Configuration 4

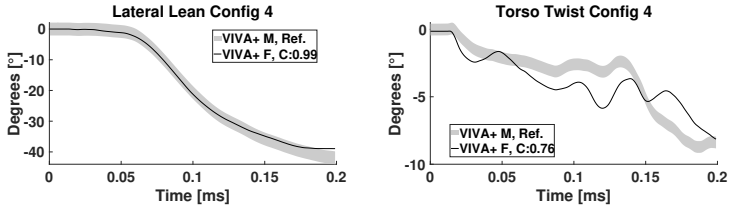

Figure D.70: Motion of thorax, Configuration 4

D.2.5 Configuration 5

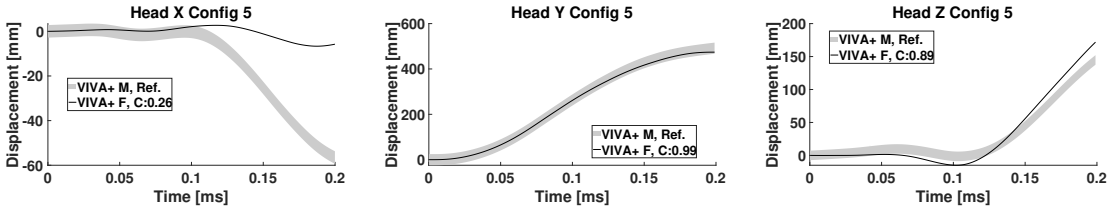

Figure D.71: Displacement of head, Configuration 5

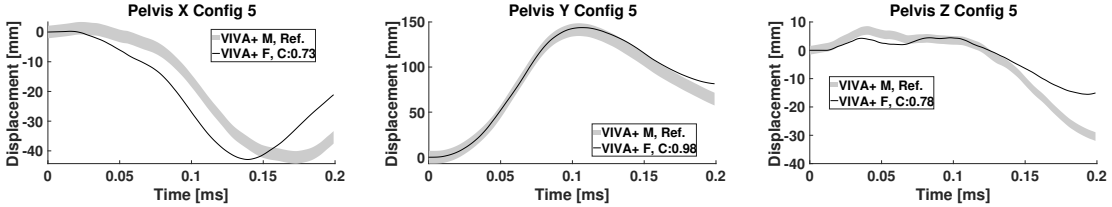

Figure D.72: Displacement of pelvis, Configuration 5

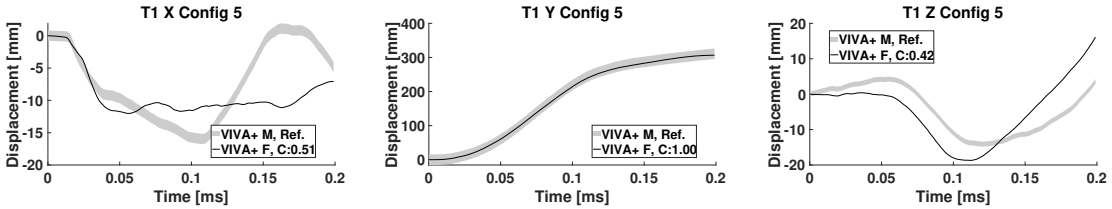

Figure D.73: Displacement of T1, Configuration 5

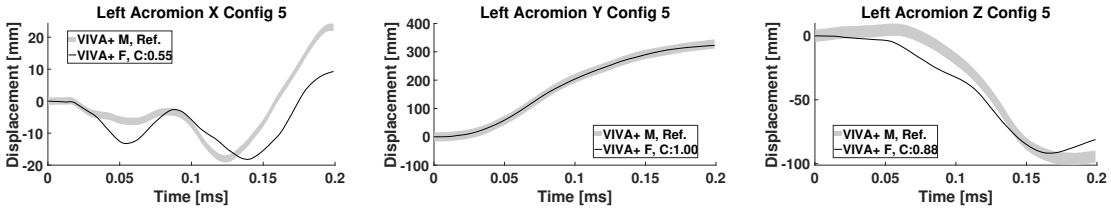

Figure D.74: Displacement of left acromion, Configuration 5

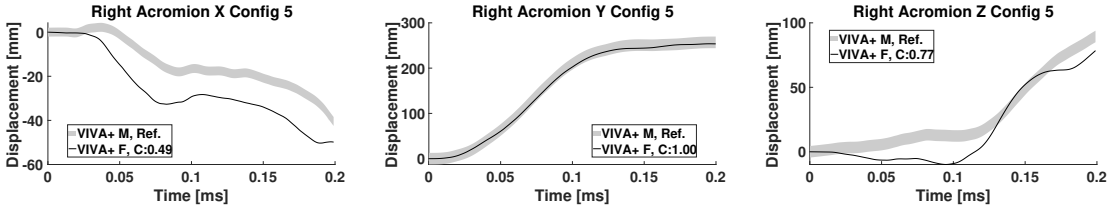

Figure D.75: Displacement of right acromion, Configuration 5

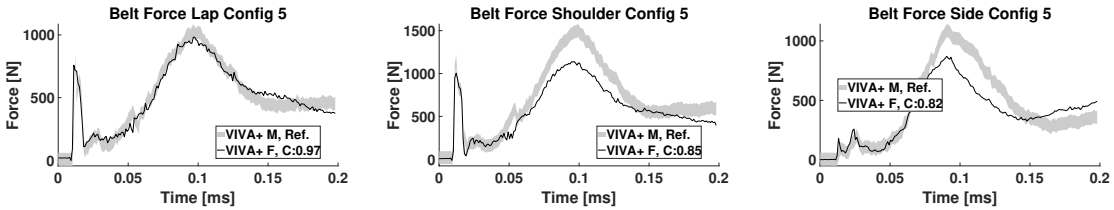

Figure D.76: Belt forces, Configuration 5

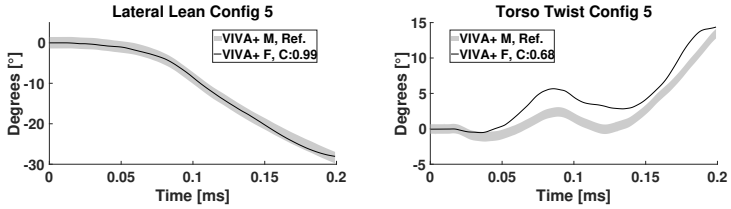

Figure D.77: Motion of thorax, Configuration 5

D.2.6 Configuration 6

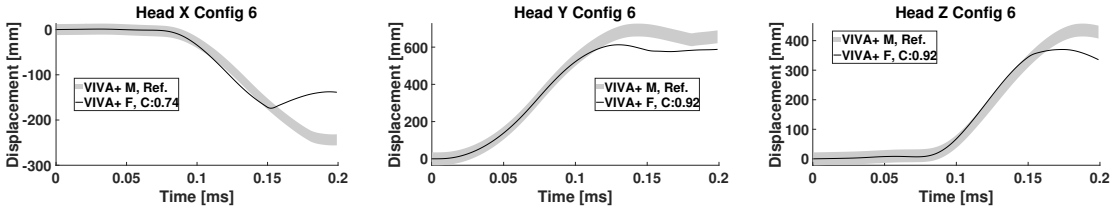

Figure D.78: Displacement of head, Configuration 6

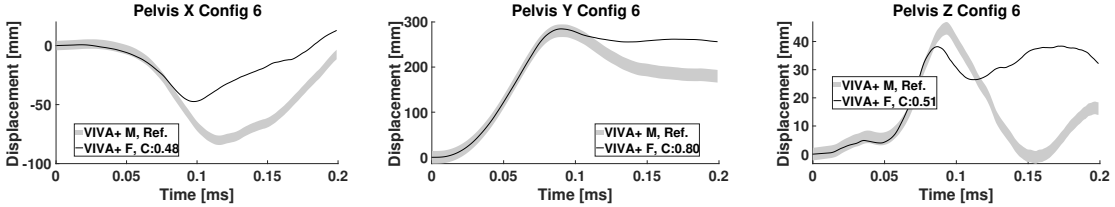

Figure D.79: Displacement of pelvis, Configuration 6

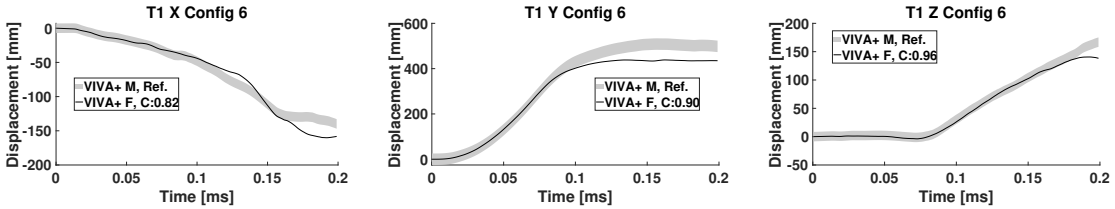

Figure D.80: Displacement of T1, Configuration 6

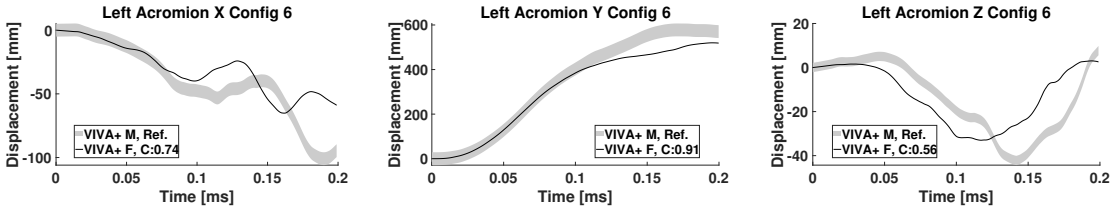

Figure D.81: Displacement of left acromion, Configuration 6

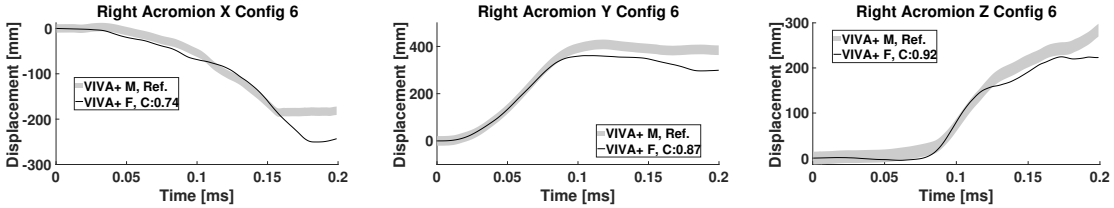

Figure D.82: Displacement of right acromion, Configuration 6

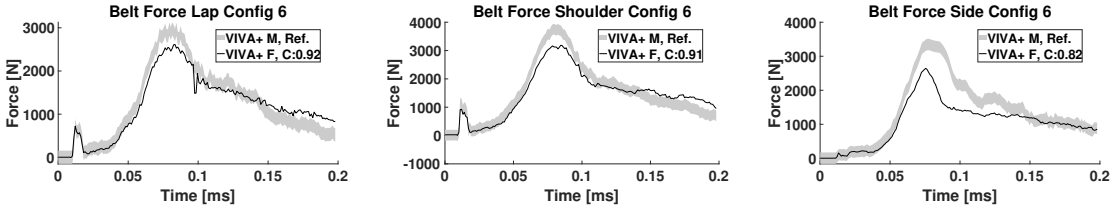

Figure D.83: Belt forces, Configuration 6

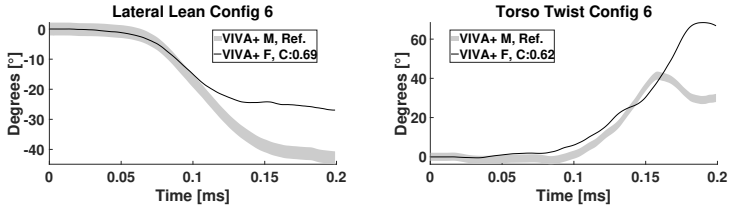

Figure D.84: Motion of thorax, Configuration 6

E

Snapshots From Sled Simulations

E.1 Male VIVA+ HBM Sled Configurations

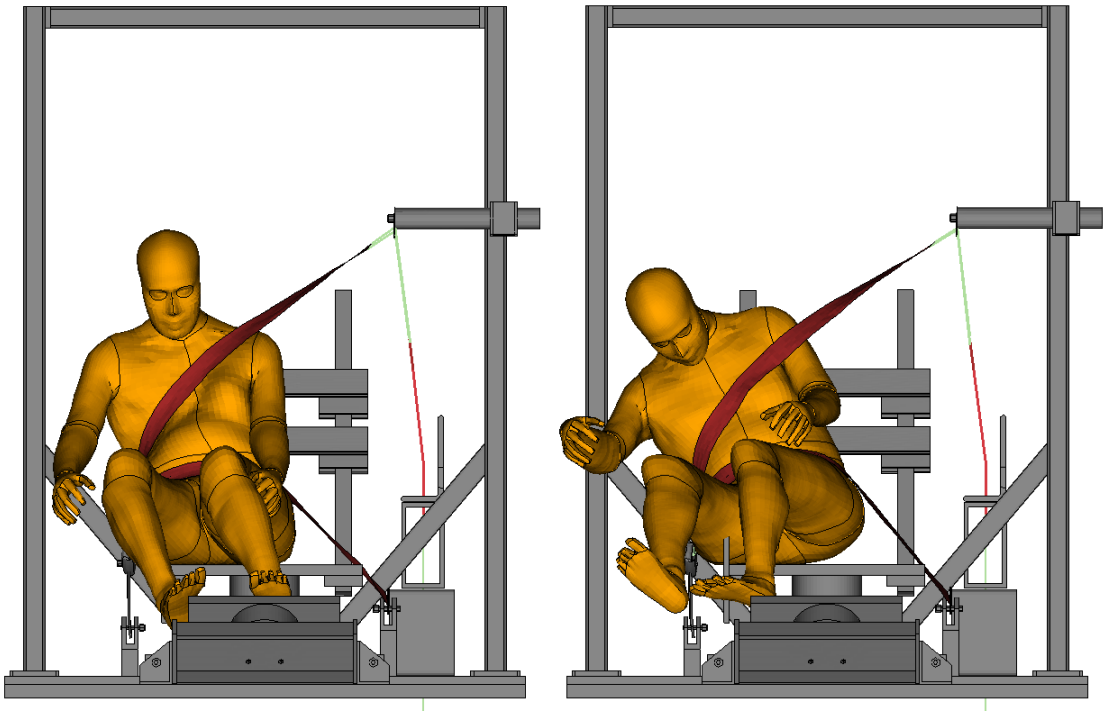

Figure E.1: Snapshot of a male VIVA+ HBM in Configuration 2, just before and after the seat belt has slipped off. Taken at 100 ms and 150 ms respectively, after the pulse was applied

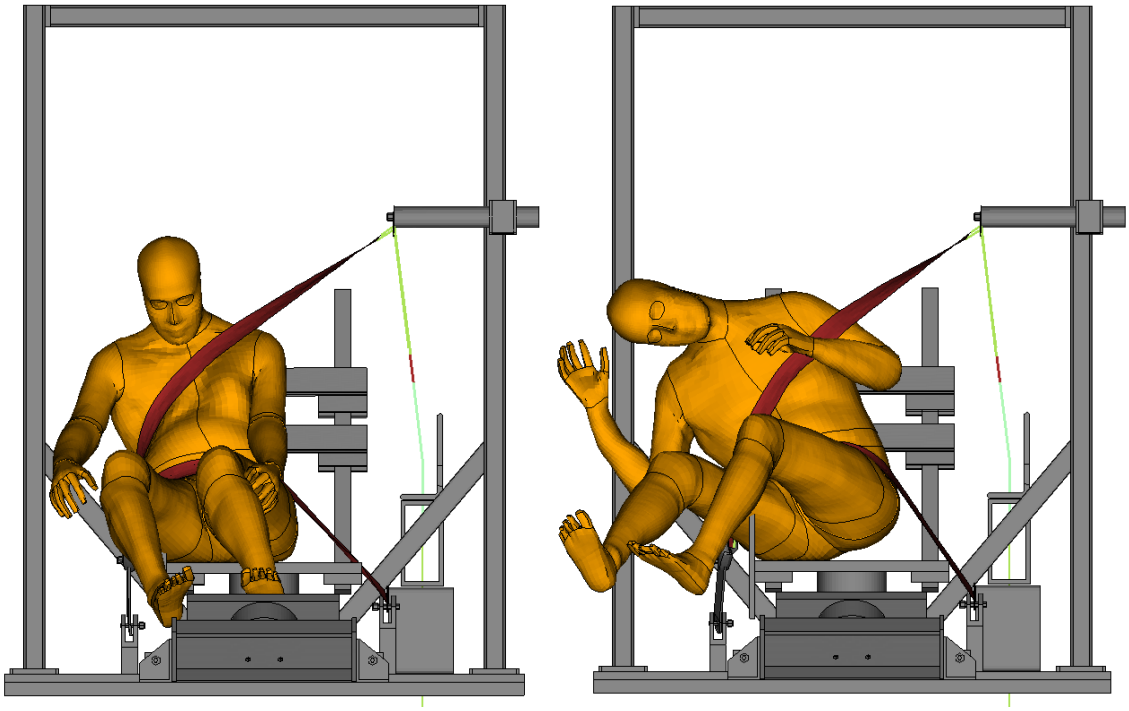

Figure E.2: Snapshot of a male VIVA+ HBM in Configuration 3, just before and after the seat belt has slipped off. Taken at 100 ms and 200 ms respectively, after the pulse was applied

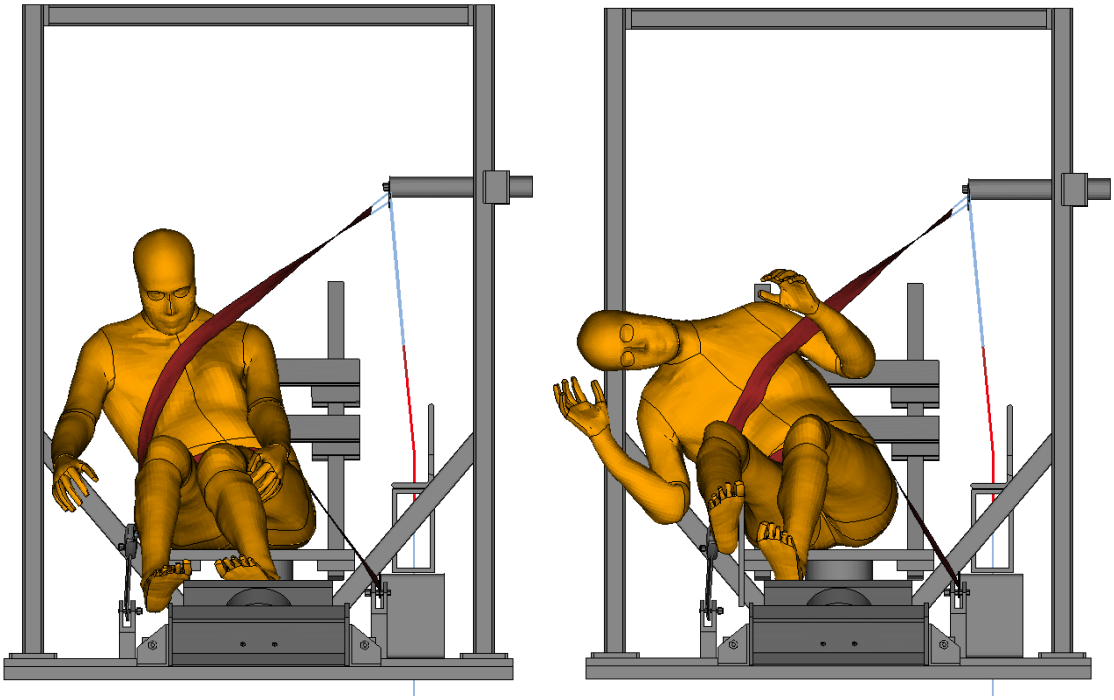

Figure E.3: Snapshot of a male VIVA+ HBM in Configuration 4, just before and after the seat belt has slipped off. Taken at 100 ms and 200 ms respectively, after the pulse was applied

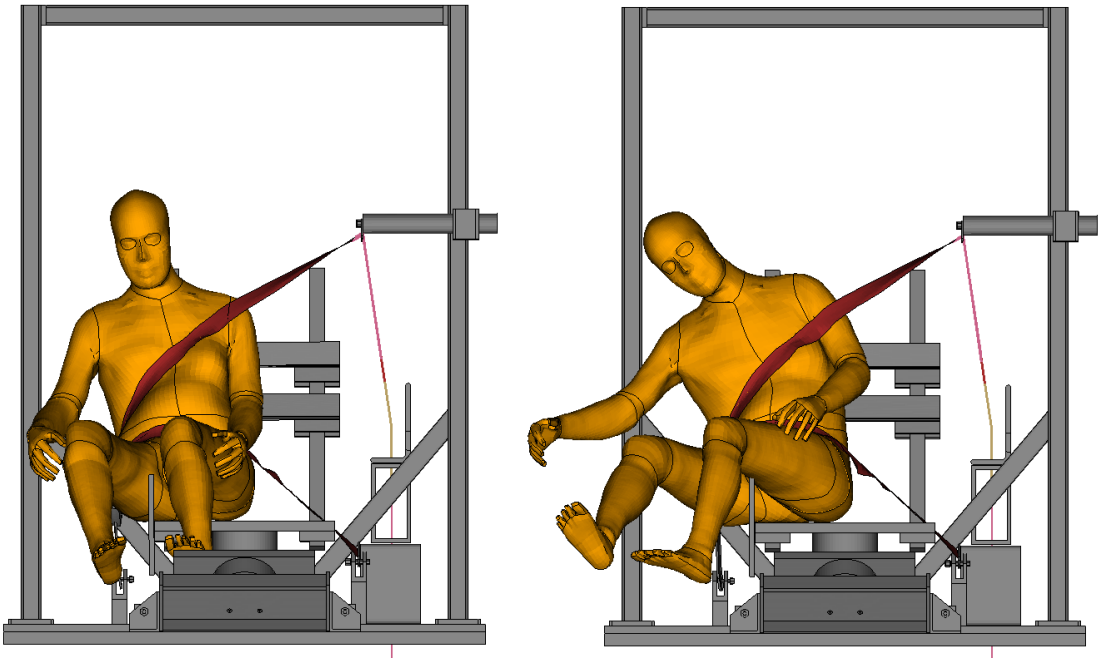

Figure E.4: Snapshot of a male VIVA+ HBM in Configuration 5, just before and after the seat belt has slipped off. Taken at 100 ms and 150 ms respectively, after the pulse was applied

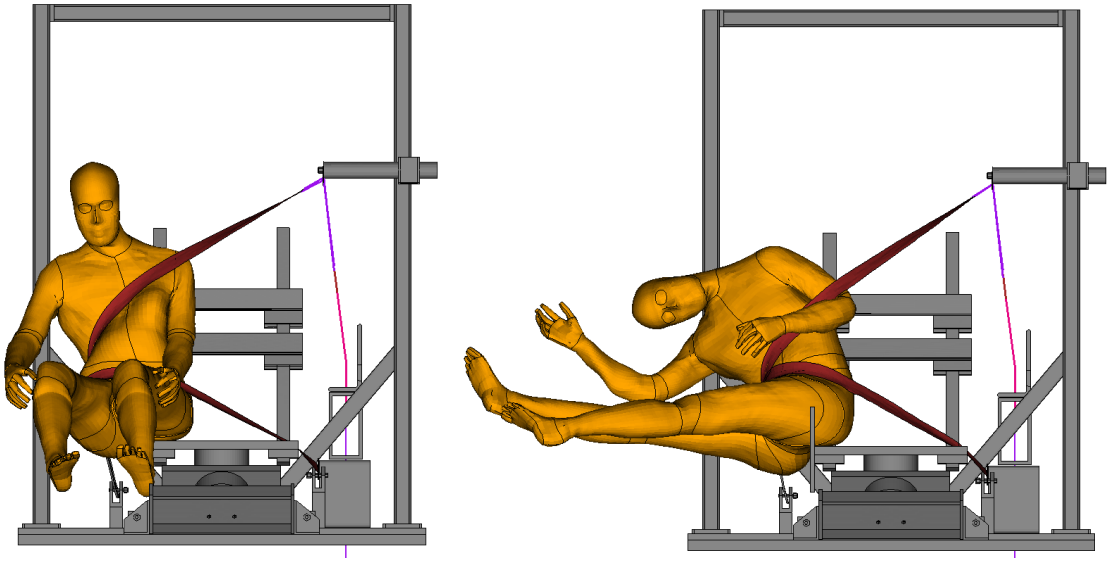

Figure E.5: Snapshot of a male VIVA+ HBM in Configuration 6, just before and after the seat belt has slipped off. Taken at 80 ms and 150 ms respectively, after the pulse was applied

E.2 Female VIVA+ HBM Sled Configurations

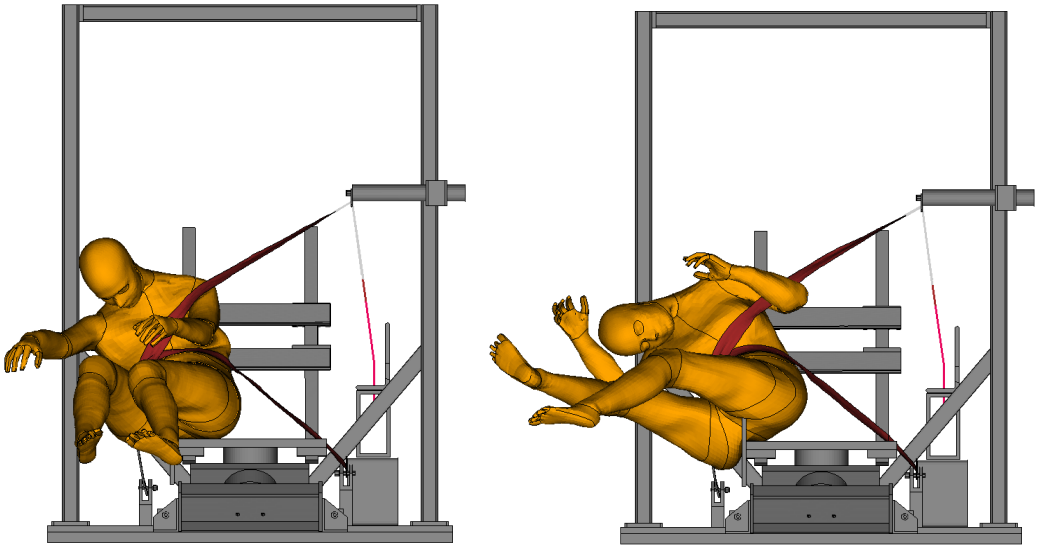

Figure E.6: Snapshot of a female VIVA+ HBM in Configuration 1, just before and after the seat belt has slipped off. Taken at 100 ms and 150 ms respectively, after the pulse was applied

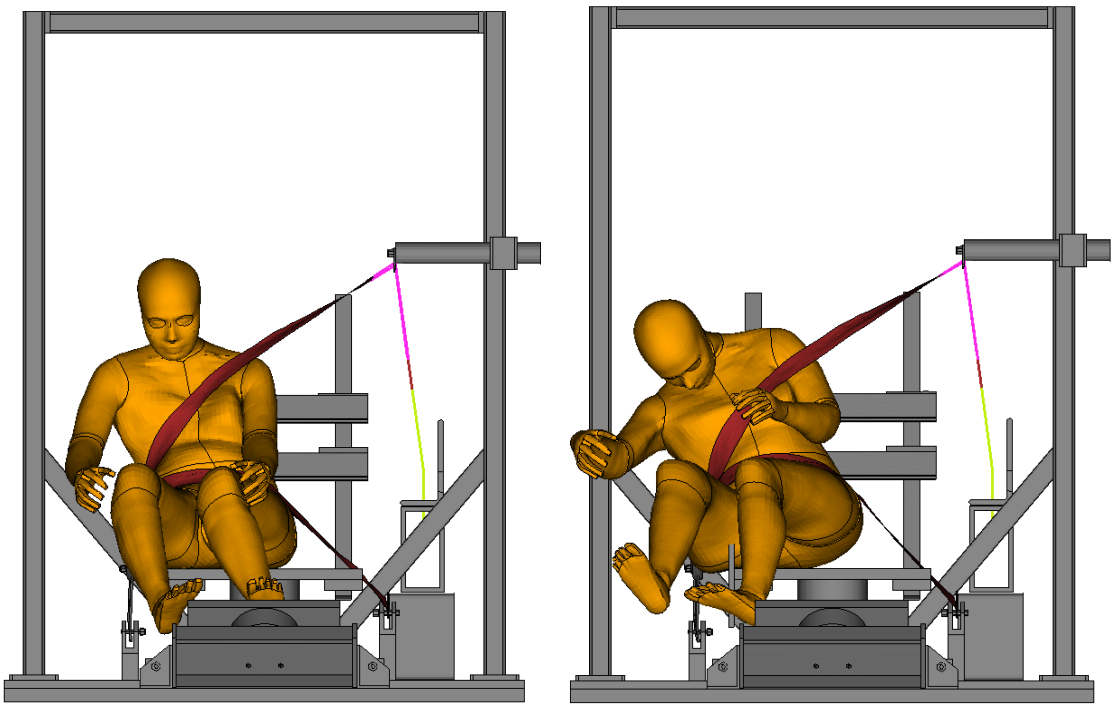

Figure E.7: Snapshot of a female VIVA+ HBM in Configuration 2, just before and after the seat belt has slipped off. Taken at 100 ms and 150 ms respectively, after the pulse was applied

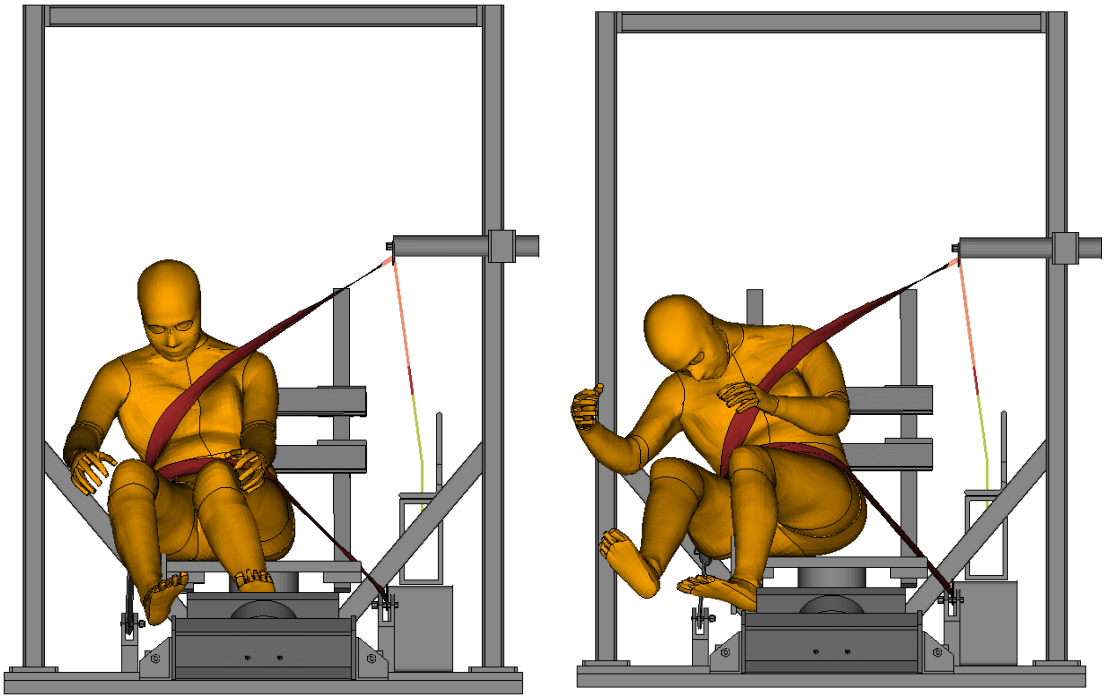

Figure E.8: Snapshot of a female VIVA+ HBM in Configuration 3, just before and after the seat belt has slipped off. Taken at 100 ms and 150 ms respectively, after the pulse was applied

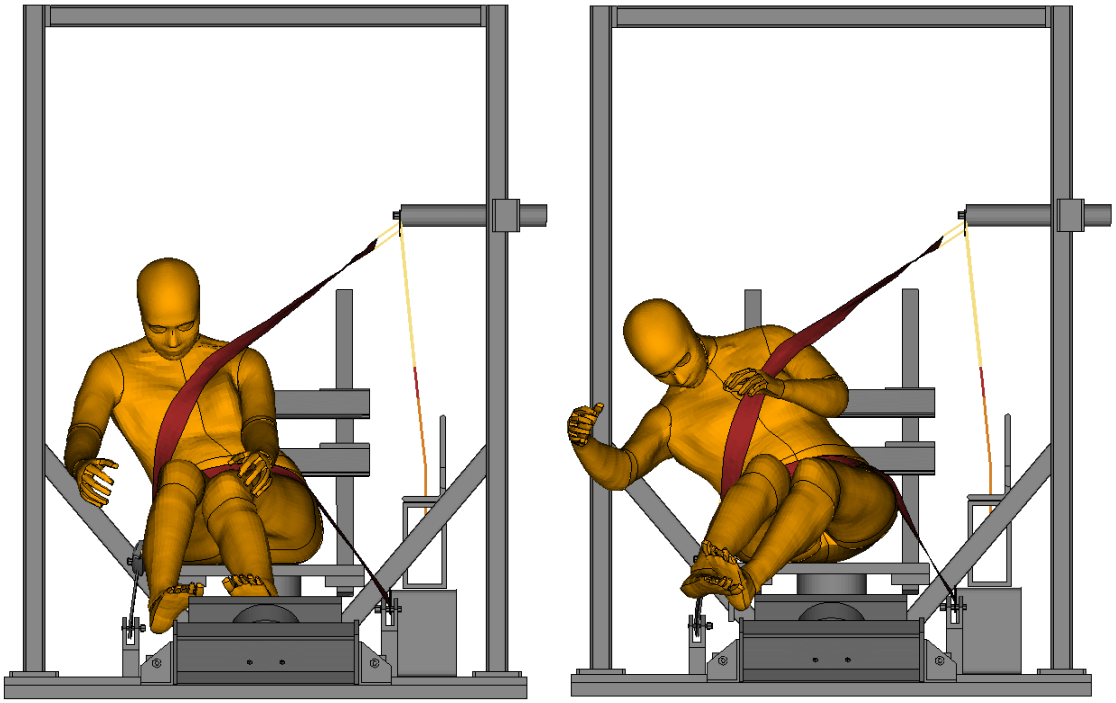

Figure E.9: Snapshot of a female VIVA+ HBM in Configuration 4, just before and after the seat belt has slipped off. Taken at 100 ms and 150 ms respectively, after the pulse was applied

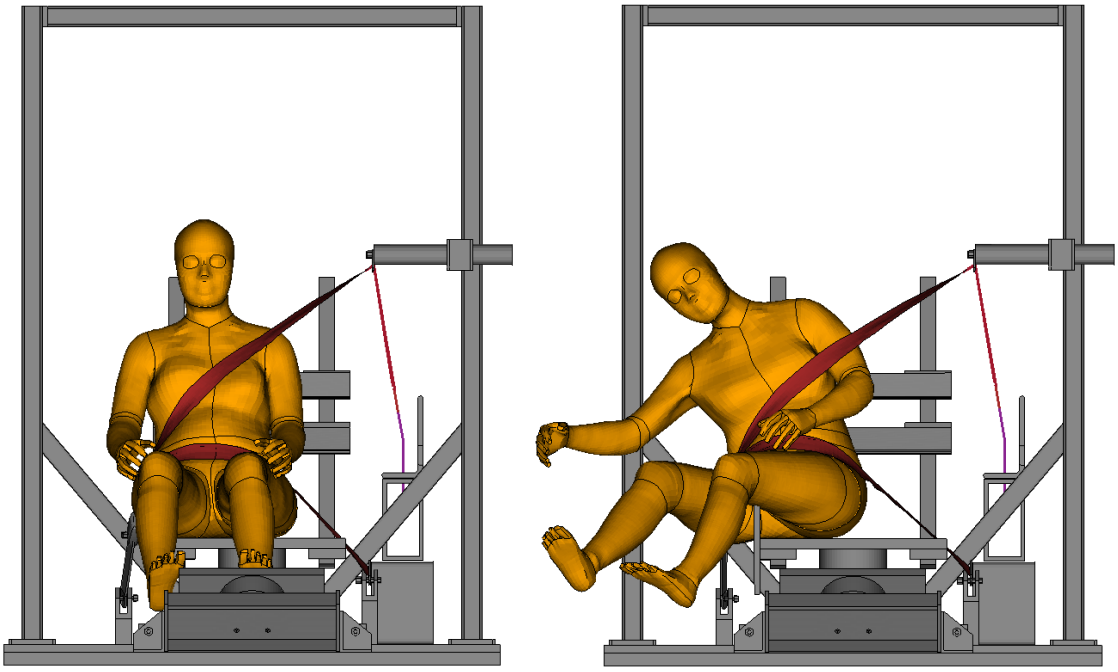

Figure E.10: Snapshot of a female VIVA+ HBM in Configuration 5, just before and after the seat belt has slipped off. Taken at 65 ms and 150 ms respectively, after the pulse was applied

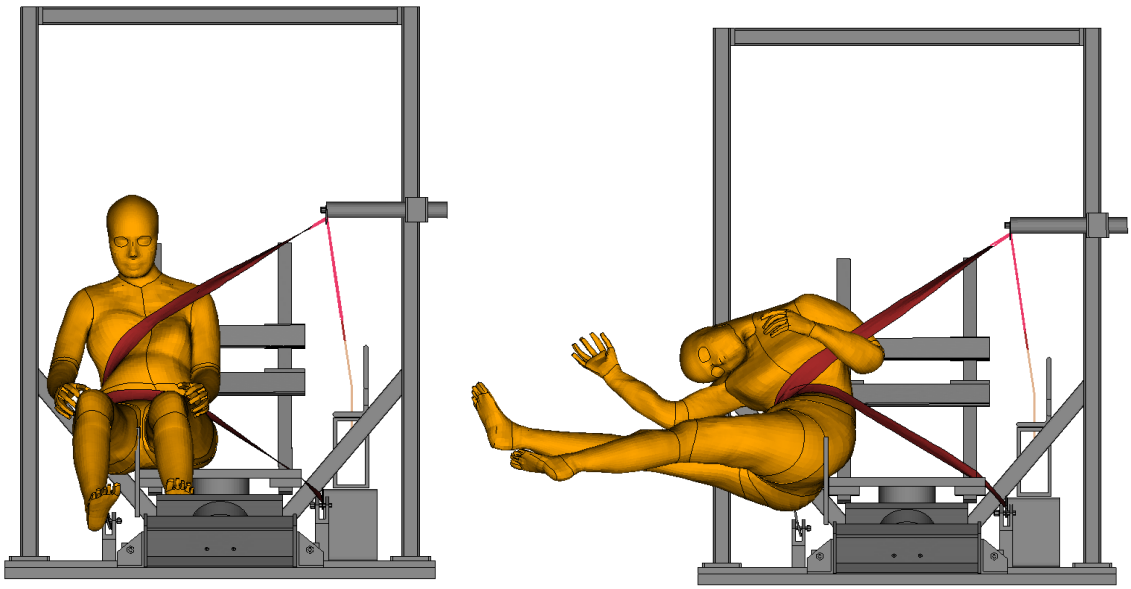

Figure E.11: Snapshot of a female VIVA+ HBM in Configuration 6, just before and after the seat belt has slipped off. Taken at 65 ms and 150 ms respectively, after the pulse was applied

F

HIC_{15} Curves

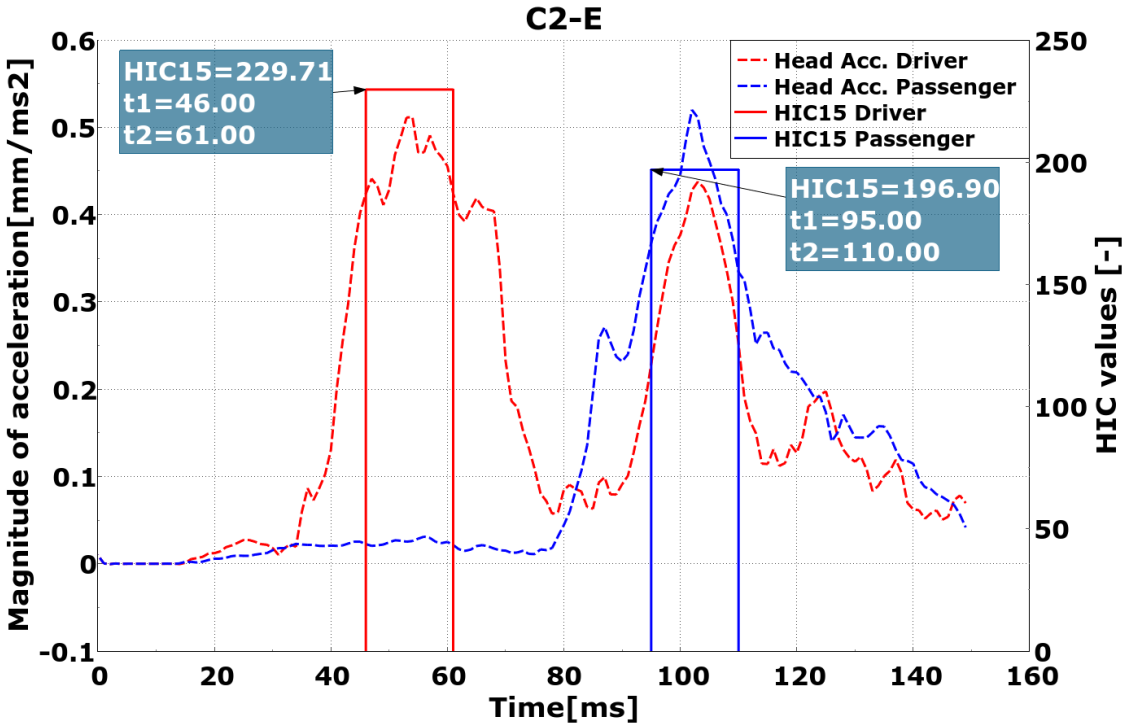

Figure F.1: Head accelation and HIC_{15} values of the occupants in configuration C2-E

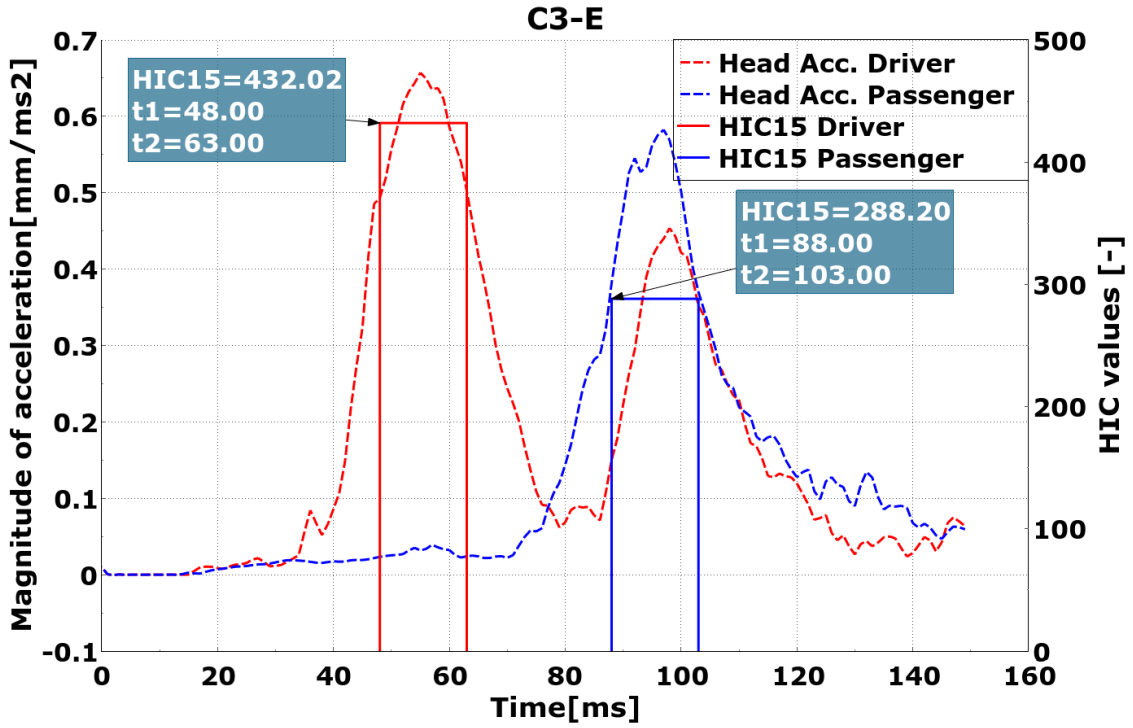

Figure F.2: Head accelation and HIC_{15} values of the occupants in configuration C3-E

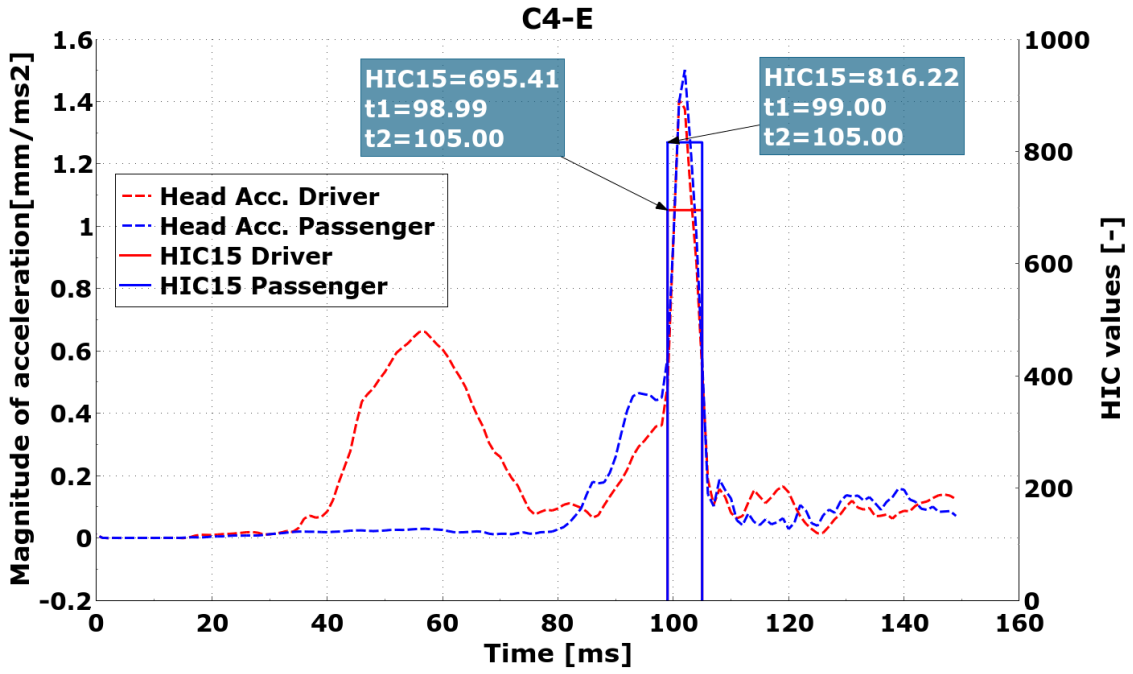

Figure F.3: Head accelation and HIC_{15} values of the occupants in configuration C4-E

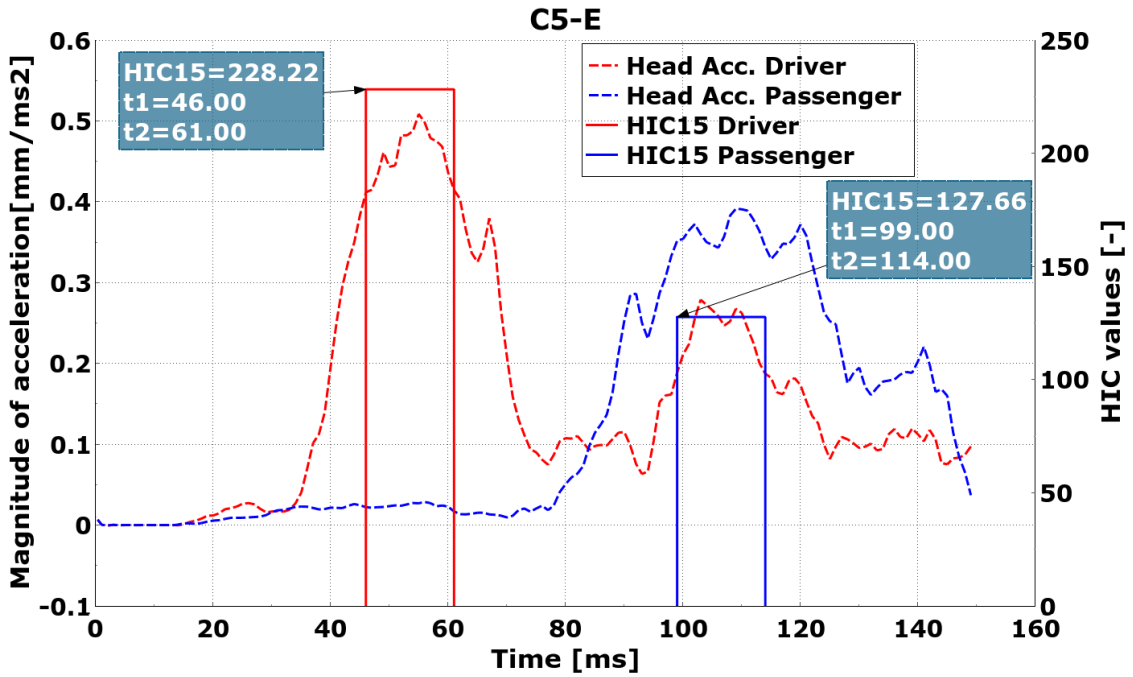

Figure F.4: Head accelation and HIC_{15} values of the occupants in configuration C5-E

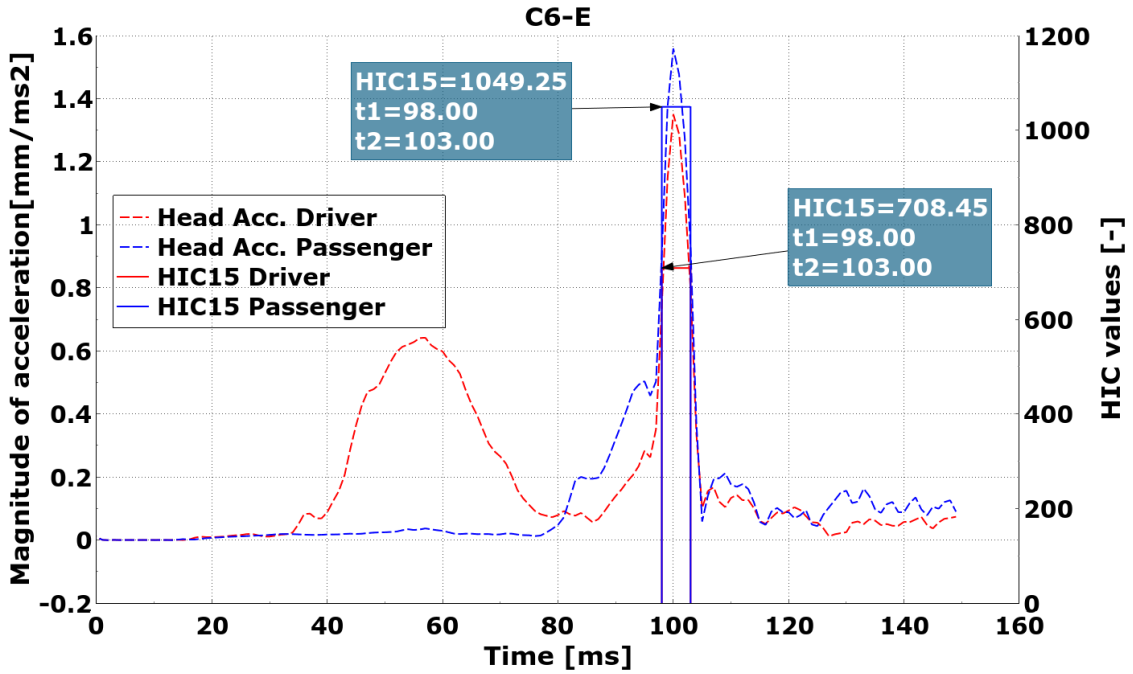

Figure F.5: Head accelation and HIC_{15} values of the occupants in configuration C6-E

G

Rib Strains

Table G.1: All maximum first principal strains in each configuration from the evaluation phase

	C1-E Driver	C1-E Pass	C4-E Driver	C4-E Pass
Left Rib 1	0.00709	0.00561	0.00797	0.00601
Left Rib 2	0.0108	0.00585	0.00981	0.00584
Left Rib 3	0.0175	0.0132	0.019	0.0116
Left Rib 4	0.0176	0.0109	0.016	0.012
Left Rib 5	0.013	0.00812	0.013	0.00789
Left Rib 6	0.0173	0.00723	0.0169	0.00715
Left Rib 7	0.0136	0.00581	0.0129	0.00574
Left Rib 8	0.0105	0.00607	0.0102	0.00693
Left Rib 9	0.0101	0.00976	0.00995	0.0127
Left Rib 10	0.00838	0.0265	0.00815	0.0301
Left Rib 11	0.00881	0.0229	0.00899	0.0241
Left Rib 12	0.00463	0.0131	0.00449	0.0142
Right Rib 1	0.0164	0.0204	0.0154	0.023
Right Rib 2	0.00356	0.00377	0.00335	0.00392
Right Rib 3	0.00532	0.00369	0.00509	0.00394
Right Rib 4	0.00797	0.00586	0.00749	0.00556
Right Rib 5	0.0067	0.00461	0.00743	0.00591
Right Rib 6	0.00642	0.00406	0.00539	0.00442
Right Rib 7	0.00699	0.00439	0.00561	0.00439
Right Rib 8	0.00775	0.00494	0.00678	0.00515
Right Rib 9	0.00797	0.0062	0.00755	0.00623
Right Rib 10	0.00458	0.00657	0.00488	0.00619
Right Rib 11	0.00471	0.01	0.00501	0.0115
Right Rib 12	0.00101	0.0125	0.00872	0.013

	C2-E Driver	C2-E Pass	C5-E Driver	C5-E Pass
Left Rib 1	0.00705	0.00482	0.00652	0.00581
Left Rib 2	0.00486	0.00564	0.00486	0.00464
Left Rib 3	0.00934	0.00772	0.00959	0.00631
Left Rib 4	0.0104	0.00771	0.0104	0.00787
Left Rib 5	0.0096	0.00549	0.0099	0.00617
Left Rib 6	0.0103	0.00549	0.0103	0.00529
Left Rib 7	0.011	0.00419	0.0114	0.00456
Left Rib 8	0.0091	0.00666	0.00926	0.00706
Left Rib 9	0.00671	0.0103	0.00656	0.0127
Left Rib 10	0.00752	0.0264	0.00691	0.0272
Left Rib 11	0.00764	0.0217	0.00765	0.0234
Left Rib 12	0.00435	0.0131	0.00435	0.0138
Right Rib 1	0.00571	0.0188	0.00583	0.0176
Right Rib 2	0.00273	0.00407	0.00285	0.0035
Right Rib 3	0.00351	0.00379	0.00351	0.00362
Right Rib 4	0.00359	0.00504	0.00344	0.00478
Right Rib 5	0.0396	0.00411	0.00419	0.00421
Right Rib 6	0.00462	0.00439	0.00467	0.00442
Right Rib 7	0.00561	0.00427	0.00476	0.00439
Right Rib 8	0.00524	0.00543	0.0047	0.00497
Right Rib 9	0.00554	0.00602	0.00483	0.00602
Right Rib 10	0.00468	0.00598	0.00381	0.00598
Right Rib 11	0.00567	0.0102	0.00569	0.0112
Right Rib 12	0.00694	0.0114	0.00751	0.0124

	C3-E Driver	C3-E Pass	C6-E Driver	C6-E Pass
Left Rib 1	0.00631	0.00765	0.0058	0.00524
Left Rib 2	0.00975	0.00684	0.0258	0.00591
Left Rib 3	0.0179	0.00877	0.0195	0.00736
Left Rib 4	0.0176	0.00837	0.0171	0.00834
Left Rib 5	0.013	0.00601	0.013	0.00608
Left Rib 6	0.0168	0.00549	0.0168	0.00549
Left Rib 7	0.00135	0.00419	0.013	0.005
Left Rib 8	0.0103	0.00525	0.0102	0.00612
Left Rib 9	0.00995	0.00642	0.00995	0.00776
Left Rib 10	0.00838	0.0132	0.00815	0.0141
Left Rib 11	0.00881	0.0126	0.00881	0.013
Left Rib 12	0.00463	0.00906	0.00442	0.00939
Right Rib 1	0.0149	0.0167	0.0155	0.0143
Right Rib 2	0.00343	0.00406	0.00335	0.00358
Right Rib 3	0.00462	0.00312	0.00446	0.00286
Right Rib 4	0.00797	0.0042	0.00735	0.00392
Right Rib 5	0.00708	0.00365	0.00789	0.0036
Right Rib 6	0.00562	0.00438	0.00514	0.00419
Right Rib 7	0.00693	0.00409	0.00519	0.00439
Right Rib 8	0.00717	0.00509	0.00603	0.00488
Right Rib 9	0.00795	0.00827	0.00714	0.0085
Right Rib 10	0.00488	0.00571	0.00443	0.00594
Right Rib 11	0.00442	0.00961	0.00495	0.00952
Right Rib 12	0.00869	0.00839	0.00966	0.00875

H

Head2Head Snapshots

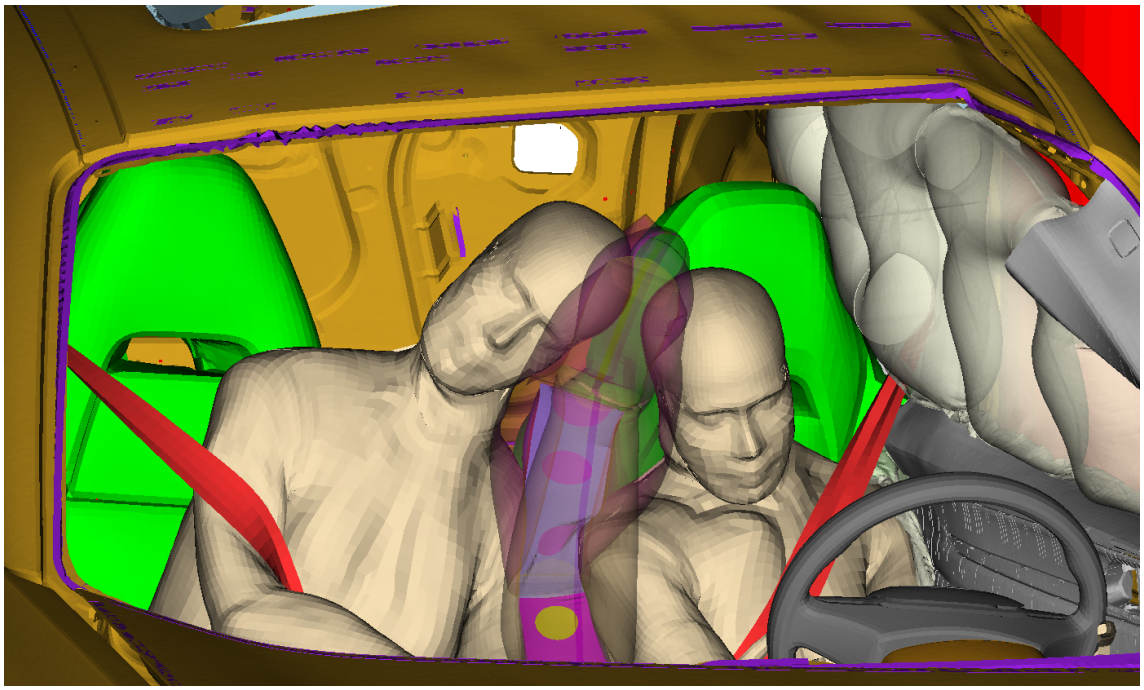

Figure H.1: A snapshot at 105 ms of the minimum Head2Head distance in configuration C1-E

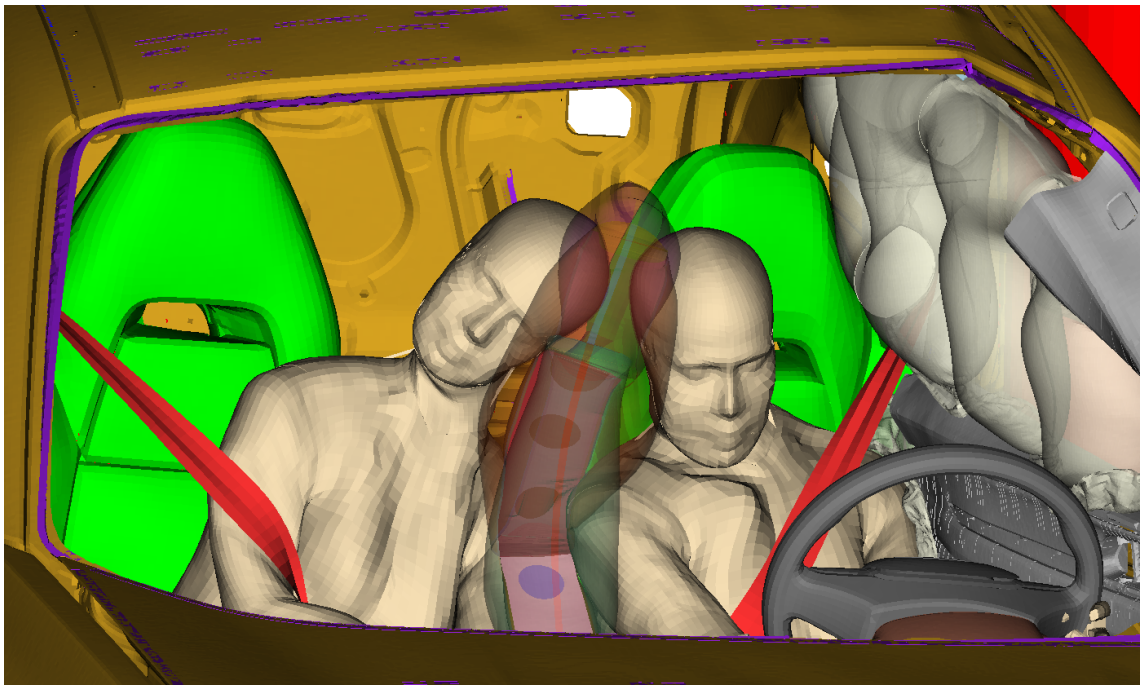

Figure H.2: A snapshot at 102 ms of the minimum Head2Head distance in configuration C3-E

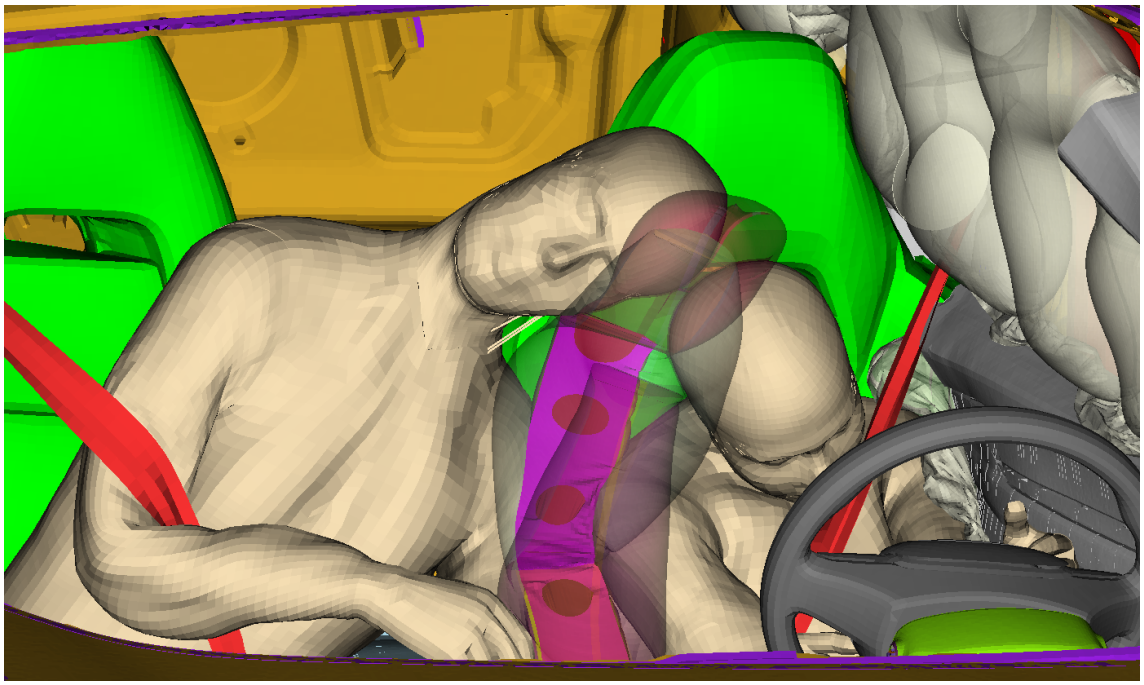

Figure H.3: A snapshot at 117 ms of the minimum Head2Head distance in configuration C5-E

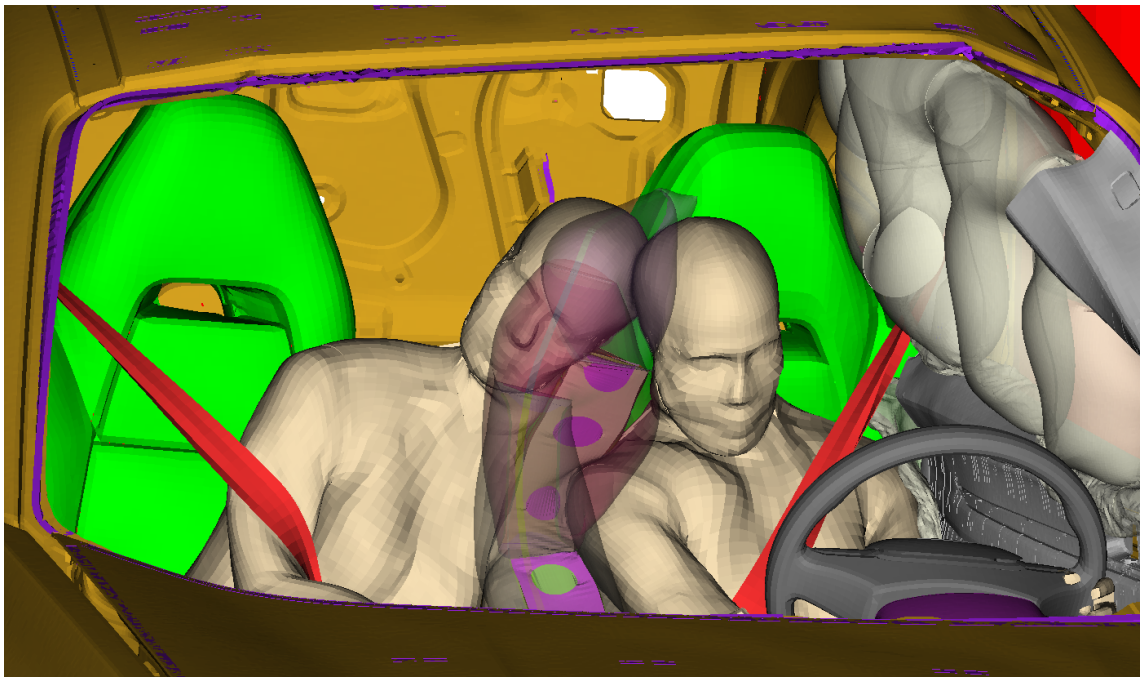

Figure H.4: A snapshot at 102 of the collision between the heads in configuration C6-E

DEPARTMENT OF MECHANICS AND MARITIME SCIENCES
CHALMERS UNIVERSITY OF TECHNOLOGY
Gothenburg, Sweden
www.chalmers.se

CHALMERS
UNIVERSITY OF TECHNOLOGY